

THESIS ON POWER ENGINEERING,  
ELECTRICAL ENGINEERING, MINING ENGINEERING D49

**Research and Development of Control  
Methods for Low-Loss IGBT Inverter-Fed  
Induction Motor Drives**

MIKHAIL EGOROV

**TUT**  
**PRESS**

TALLINN UNIVERSITY OF TECHNOLOGY  
Faculty of Power Engineering  
Department of Electrical Drives and Power Electronics

Dissertation was accepted for the defence of the degree of Doctor of Philosophy on June 21, 2011.

**Supervisor:** Professor Ph.D. Valery Vodovozov, Department of Electrical Drives and Power Electronics, Tallinn University of Technology

**Opponents:** Professor Dr. Sc. Ing. Ilja Galkin, Riga Technical University, Latvia

D.Sc. Jüri Joller Tallinn, Estonia, Energiatehnika OÜ

Defence of the thesis: September 5, 2011, 14:00, room VII-430 at Tallinn University of Technology, Ehitajate tee 5, Tallinn, Estonia.

Declaration:

Hereby I declare that this doctoral thesis, my original investigation and achievement, submitted for the doctoral degree at Tallinn University of Technology has not been submitted for any academic degree.

Mikhail Egorov, .....

Copyright Mikhail Egorov 2011  
ISSN 1406-474X  
ISBN 978-9949-23-145-4 (publication)  
ISBN 978-9949-23-146-1 (PDF)

ENERGEETIKA. ELEKTROTEHNIKA. MÄENDUS D49

**Energiatõhusa IGBT transistor-vaheldiga  
asünkroonajami juhtimismeetodite  
uurimine ja väljatöötamine**

MIKHAIL EGOROV



# Contents

<b>INTRODUCTION</b> .....	8
<b>ABBREVIATIONS</b> .....	15
<b>SYMBOLS</b> .....	16
<b>1. STATE OF THE ART AND RECENT ADVANCES IN POWER ELECTRONICS TECHNOLOGY FOR INDUCTION MOTOR DRIVES</b> .....	18
1.1 Analysis of Contemporary Motor Drive Technology Issues .....	18
1.1.1 Progress in Electrical Motors.....	18
1.1.2 Motor Drive Implementation and Packaging.....	20
1.1.3 Advances in Power Electronics .....	21
1.1.4 IGBT Inverters of Motor Drives.....	23
1.2 Power Losses of IGBT Inverters .....	26
1.2.1 Figure-of-Merit for Economical Power Converter .....	26
1.2.2 Reducing of Converter Size and Power Consumption.....	29
1.2.3 Power Quality Improvement.....	31
1.2.4 Influence of Switching Frequency on the Drive Components .....	33
1.3 Regimentation of Control Systems for Inverter-Fed Induction Motor Drives.....	36
1.3.1 Overview of Control Methods .....	36
1.3.2 Control Arrangement of Induction Motor Drives .....	37
1.3.3 Common Control and Protection Architecture .....	38
1.4 Analysis of Switching Patterns for IGBT Inverters.....	40
1.4.1 Six-Step Modulation.....	40
1.4.2 PWM Switching Pattern .....	43
1.4.3 SVM Switching Patterns.....	47
1.5 Conclusions .....	52
<b>2. SIMULATION STUDY OF INDUCTION MOTOR DRIVES WITH IGBT INVERTERS</b> .....	54
2.1 Comparative Analysis of Power Converter and Motor Drive Simulators ...	54
2.1.1 Role of Simulation in Motor Drive Design and Study.....	54
2.1.2 Overview of Toolboxes Used in Power Electronics and Motor Drives..	55
2.1.3 Comparison of Toolboxes in View of the Drive Application .....	58
2.2 Physical Prototypes for Validation of Motor Drive Models .....	60
2.2.1 Requirements to Physical Prototyping.....	60
2.2.2 ABB Setup for Motor Drive Identification .....	61
2.2.3 TUT Experimental Setup.....	64
2.3 Modelling of Inverter-Fed Induction Motor Drives in Matlab/Simulink ....	73
2.3.1 Basic Circuit Topology and Specification .....	73
2.3.2 Simulation Study of Inverter-Fed Drive with Six-Step Modulation .....	74
2.3.3 Simulation Study of PWM Patterns.....	77
2.3.4 Simulation Study of SVM Patterns.....	80
2.4 Vendor's Software to Explore IGBT with Power Loss and Heating.....	85
2.4.1 Problems of IGBT Modelling.....	85
2.4.2 IGBT Simulators of International Rectifier .....	87
2.4.3 IGBT Loss Simulator Melcosim from Mitsubishi Electric.....	88

2.4.4	Semiconductor Selector SemiSel from Semikron.....	89
2.5	Conclusions .....	92
<b>3.</b>	<b>IMPLEMENTATION AND PERFORMANCE EVALUATION OF LOAD-DEPENDENT SWITCHING PATTERNS .....</b>	<b>94</b>
3.1	Load-Dependent Control of Motor Drive Inverters.....	94
3.1.1	A Problem of Current, Voltage, and Frequency Restrictions .....	94
3.1.2	Relationship Between the Inverter and Electromagnetic Motor Models	95
3.1.3	Correlation Between the Inverter and Electromechanical Motor Models.....	96
3.1.4	Loss Analysis.....	98
3.2	Current-Dependent Clamping of Inverter Legs.....	100
3.2.1	Principle of Current-Dependent Clamping of Inverter Legs.....	100
3.2.2	Simulation.....	103
3.2.3	Experimentation.....	104
3.3	Elimination of Short Pulses from Switching Patterns .....	106
3.3.1	Principle of Elimination of Short Pulses.....	106
3.3.2	Simulation.....	108
3.3.3	Experimentation.....	110
3.4	Concluding Remarks on Load-Dependent Control .....	112
3.4.1	Comparison of THD .....	112
3.4.2	Comparison of Heat.....	114
3.4.3	Comparison of Motor Speed and Torque Ripples .....	115
3.5	Conclusions .....	116
<b>4.</b>	<b>COMPUTER AIDED DESIGN OF LOW-LOSS INVERTER-FED INDUCTION MOTOR DRIVES .....</b>	<b>118</b>
4.1	Advancement in Motor Drive Design.....	118
4.1.1	Requirements to Motor Drive Designs .....	118
4.1.2	Review of Contemporary Motor Drive CAD Systems .....	121
4.1.3	eDrive Toolkit as the Core of CAD .....	122
4.1.4	Advanced Design Technology.....	126
4.2	New Toolbox for Switching Patterns Optimization .....	129
4.2.1	Description of the Developed Toolbox.....	129
4.2.2	Built-in Models of Inverter and Induction Motor .....	132
4.2.3	User Interface of the Toolbox.....	133
4.3	Design Example of Inverter-Fed Motor Drive for a Vehicle Application.	135
4.3.1	Aim and Load Object.....	135
4.3.2	Gear and Motor Selection .....	136
4.3.3	Inverter Design .....	137
4.4	Future Research Scenario .....	141
4.4.1	Involvement of a PWM Rectifier to Decrease Power Losses .....	141
4.4.2	Adaptive SVM as a Universal Tool to Decrease Power Losses .....	144
4.5	Conclusions .....	145
	<b>CONCLUSIONS.....</b>	<b>146</b>
	<b>REFERENCES .....</b>	<b>148</b>
	<b>ABSTRACT .....</b>	<b>154</b>
	<b>KOKKUVÕTE .....</b>	<b>155</b>

**AUTHOR'S MAIN PUBLICATIONS.....156**  
**LISA 1 / ANNEX 1 .....158**  
**LISA 2 / ANNEX 2 .....160**

# INTRODUCTION

## Motivation

The induction motor drive is by far the most widely used electromechanical system and well-known today as the workhorse of industry. Traditionally, induction motor has been used in constant and variable-speed applications that do not cater for fast dynamic processes. Because of the recent development, this situation is changing rapidly. The underlying reason for this is the fact that the cage induction machines are much cheaper and more rugged than their competitors, the synchronous and dc motors. Their sophisticated closed-loop systems are the result of extensive research and development.

Over the last decades, computer aided design of induction motor drives fed by power inverters has become a major research topic. Although there has been much progress in this area and the novel control systems have been developed, they stay often restricted by design because of focus on those converters that concern particular applications.

Almost from inception, power dissipation and its adverse impact on electronics and electromechanical equipment has been a point of concern for the industry. An integral part of the design cycle has always been the consideration of power dissipation and consumption issues. Although the level of attention paid to thermal matters has been inconsistent, the reality is that the role of thermal management of power converters in the ultimate success of motor drives has never diminished. Converter-level power dissipation remains a point of contention for equipment manufacturers and will impose larger challenges as the years pass.

The main efforts to decrease power dissipation of inverters in the scope of motor drive performance are addressed for searching the best relation between the switching frequency, duration of transition intervals, and switched powers. Based on such standpoint, the following two approaches called hardware way and software way are distinguished:

- optimization of power converter circuits (development of new power circuit topologies, search of effective electronic components, and enhancement of cooling methods);
- improvement of control principles (design of new control system topologies and modulation techniques).

The first group of approaches relates to the inverter build-up based on the various associations of semiconductor devices and reactive components. The typical drawbacks of the designs obtained in this direction are as follows:

- they are often bulky in size, weight, and housing;
- expensive in cost, maintenance, and special control needs;



- slow in operation due to the presence of the charge/discharge intervals, phase delays and amplitude distortions;
- load/supply dependent (unstable under variable supply and load) and parametrically sensitive in rebuilding and tuning.

The second group relates to control schemes that minimize the negative effect of the switching principle of inverter operation. This approach has such benefits as:

- software based easy programming and tuning;
- suitability for parametric and algorithmic rebuilding;
- variety of ways for the switching frequency and switching pattern optimization;
- flexibility in improving the switch on/off transitions;
- availability of multiple open-ended and closed loop load-dependent solutions.

This work follows the software approach. It aims to improve the control methods and techniques that provide power economical benefits across the broad design area.

Previous research on IGBT-fed motor drives was carefully examined through the literature survey enveloped by the Reference list to compare this thesis with the recent studies. Because of the overwhelming breadth of published material, the review was limited by inverters for induction motor drives and their modulation techniques, as well as motor drive design and simulation, because these topics are closely related to the work.

At the present time, the majority of research and development effort in the field of power converters for motor drives concentrates on the non-expensive power economical variable-speed open-loop drives and high-precision closed-loop torque and power adjustable drives. The most comprehensive review in these fields may be found in [1] [2] [3] [4] [5] [6]. Theoretical grounding of the drive supply systems is given in [7] [8] [9] [10] [11] [12] [13]. These researches were used as the basis of this study.

Multiple topologies of IGBT inverters are discussed in [14] [15] [16] [17] [18] [19] [20] [21]. Advanced solutions of power economical problems are proposed in [2] [22] [23] [24] [25] [26] [27]. In contrast to the mentioned works, the major attention is paid here to inverters supplying the motor load having variable inductive character with counter-electromotive force.

Modulation theory of power converters is strongly based in [28] [29]. The most effective space vector modulation algorithms are proposed by [30] [31]. They are developed and improved in this study.

Power converter design and simulation problems are observed in [32] [33] [34] [35] [36] [37] [38] [39]. Special attention concerning motor drive supply was paid in this work to the studies of [28] [40] [41] [42].

### **Thesis objectives and tasks**

The first objective of this study is to develop and explore the control methods for inverters that supply low-loss variable-speed induction motor drives. Importance of this problem is pointed by the fact that IGBT control governs the voltage and current harmonics, torque ripple, acoustic noise, and electromagnetic interference. A significant feature of the proposed technique is adaptation of the inverter control to the load parameters.

The second objective of the thesis is to improve the computer aided design methodology for variable-speed induction motor drives aiming power economical combined inverter and motor performance. The proposed approach focuses on the converter composition that provides minimization of the drive power losses.

The main research tasks to be solved are as follows:

1. development of simulation and experimental tools to study the major techniques of inverter control in induction drive applications;
2. exploration of the IGBT modulation methods from the viewpoint of loss reduction;
3. proposition, examination, and implementation of the new switching patterns for the modulation systems of motor drive inverters;
4. improvement in the methodology of computer aided motor drive design basing on the new IGBT switching patterns.

### **Major results**

The scientific contribution of the thesis, which is considered as new, can be summarised as follows:

1. classification criteria for the power converters design, study, and comparison, focused on the motor drives;
2. comparative analysis of the main toolkits used in the world-wide power electronic practice from the viewpoint of motor drive characteristics;
3. an original experimental setup for the verification of the developed models;
4. methodology of experimentation on the steady-state and dynamical operation modes using the developed physical prototypes;
5. library of the motor drive models developed in the *Matlab/Simulink* environment, which supports the six-step modulation, PWM, and multiple SVM techniques;

6. methodology of combined using both the traditional simulation packages and marketable toolkits in the motor drive design;
7. concept of the load-dependent control of an inverter based on the built-in motor model;
8. method of current-dependent clamping of inverter legs which decreases the losses and temperature of inverter-fed drive components;
9. principle of the elimination of short pulses from the switching pattern which opens a way to choose the optimal switching frequency in respect to the particular application performance;
10. computer aided motor drive design methodology which includes an additional stage for IGBT switching patterns and frequency optimization;
11. toolbox for analyzing and exploring switching patterns of three-phase inverter-fed induction motor drives;
12. recommendations on applying a PWM front-end and adaptive control for both the power loss decrease and the THD level stabilization.

#### **Practical novelty of the thesis**

1. The work opens new possibilities in the analysis and comparison of multiple power electronics converters from the viewpoint of their power economical performance.
2. Developed models are suitable for exploring different steady-state and dynamic modes of the power converter performance in motor drive applications.
3. Proposed category of the simulation and experimental techniques can be effectively applied in drives working in open-ended voltage/frequency and close-loop control modes.
4. Using the developed ware, the new modulation systems of low-loss motor drive inverters can be designed and described.

#### **Direct practical output of the thesis**

Two novel switching patterns were implemented in the experimental laboratory setup developed by the author. An improved computer aided motor drive design methodology and a toolbox for analyzing and exploring power inverter control systems were implemented in Tallinn University of Technology.

#### **Confirmation and dissemination of results**

The thesis involves both the theoretical and practical investigations. Novelty and profitability of the work have been confirmed by analytical and simulation based results, as well as experimental verification and result dissemination.

On the theoretical stage, mathematical description based on space vector notation, numerical spectral analysis, and digital computation was applied.

All the results have been experimentally validated using the developed physical prototype of the IGBT converter-fed motor drive.

The author has 19 international scientific publications, 8 of which are directly associated with the thesis. 11 author's papers are included in the collections indexed by ISI-Thomson Reuters.

### **Thesis outline**

The contents of the thesis are divided into four chapters, introduction, and conclusions.

Chapter 1 provides an analysis of contemporary motor drive technology issues. It describes the progress in electrical motors, specific features of the drive implementation and packaging, advances in power electronics and in power semiconductor devices, and progress in power converters. Then, the figures-of-merit of IGBT inverters are proposed in view of power losses in IGBTs and inverters, converter size, power consumption, power quality, and switching frequency. Next, the regimentation of the control systems for inverter-fed motor drives is presented based on the overview of control methods, general-purpose control arrangement of industrial motor drives, and common control and protection architecture. The chapter is completed by the analysis of switching patterns for IGBT inverters, such as six-step modulation, pulse-width modulation, and space vector modulation.

Chapter 2 is devoted to the simulation study of IGBT inverters for induction motor drives. First, the comparative analysis and categorization of power converter simulators is performed including understanding of designed system via simulation, overview of toolboxes used in power converter design, and comparison of toolboxes in view of the drive application. Following the requirements to physical prototyping, the developed physical prototypes for model validation, such as ABB experimental setup and the new TUT experimental setup, are described. The core of this chapter is presented by the new models of inverter-fed induction motor drives implemented in *Matlab/Simulink*. They provide the basic circuit topology and specification, simulation study of the inverter-fed drive with six-step control, pulse-width modulation, and space vector approach. Additionally, vendor's software to explore IGBT with power loss analysis is involved. Among them, IGBT simulators of International Rectifier, IGBT loss simulator *Melcosim* from Mitsubishi Electric, and semiconductor selector *SemiSel* from Semicron are described.

Chapter 3 relates to the implementation and performance evaluation of new switching patterns. First, the load-dependent control of motor drive inverters is explained. To show the benefits of the proposed approach, correlation between inverter and motor performances is analytically examined with focus on the loss

minimization. The current-dependent clamping modulation principle is provided including mathematical, simulation, and experimental study. Further, some algorithms of the short pulse elimination from the switching patterns are discussed. Again, they are grounded analytically, by simulation, and by experimentation. Both methods are compared with traditional ones and with each other.

In the last chapter, the advanced methodology of computer aided design of low-loss inverter-fed induction motor drives is described. Following the requirements to motor drive designs and review of contemporary design tools, the proposed technological flowchart is explained. The description of the new toolbox to explore modulation techniques envelops its properties and possibilities, the electromagnetic model of the induction motor, and the user interface. Next, the design example of inverter-fed motor drive for a vehicle application is provided, including the design aim and the load object description, the gear and motor selection process, and the actual inverter design procedure. Finally, the principles of active rectification and adaptive modulation are suggested to further decrease power losses.

The conclusive list of references consists of 80 external published works and 19 author's papers.

## **Acknowledgements**

First of all, I would like to express my sincere gratitude to my supervisor, Professor Ph.D. Valery Vodovozov, for his skilful guidance, encouragement, and patience during this work.

I warmly thank my parents for all their love and support during my studies.

I want to express my gratitude to the deceased Professor Juhan Laugis.

I wish to thank my colleagues I have worked with over the years: Ph.D., professor Tõnu Lehtla, D.Sc. Endel Risthein, Ph.D. Rain Lahtmets, Ph.D. Elmo Pettai, Ph.D. Raivo Teemets, D.Sc. Dmitri Vinnikov, D.Sc. Madis Lehtla, D.Sc. Raik Jansikene, D.Sc. Argo Rosin, for enlightening discussions and constructive feedback.

I am grateful to Ph.D. Indrek Roasto, Ph.D. Tanel Jalakas, Ph.D. Hardi Hõimoja, D.Sc. Jānis Zaķis, M.Sc. Margus Müür, M.Sc. Taavi Möller for their outstanding help and companionship during my work.

I am deeply indebted to Ms. Mare-Anne Laane for checking the language used in this thesis.

I am also grateful to Mr. Ants Rööp, Mr. Raul Aarpuu, Ms. Zoja Raud, Ms. Tuuli-Piret Kõuts, Ms. Ann Gornischeff, Ms. Ilda Timmerman for kindly handling not only all the administrative issues but also many other cases.

This work was financially supported by the Archimedes Foundation.

Tallinn  
September 2011

Mikhail Egorov

## **ABBREVIATIONS**

A/D – analog to digital

ac – alternating current

BJT – bipolar junction transistor

CAD – computer aided design

D/A – digital to analog

dc – direct current

IEC – International Electrotechnical Commission

IEEE – Institute of Electrical and Electronics Engineers

IGBT – insulated gate bipolar transistor

JFET – junction field-effect transistor

MOSFET – metal-oxide semiconductor field-effect transistor

OPD – output power density

PWM – pulse-width modulation

rms – root mean square

SQL – structured query language

SVM – space vector modulation

THD – total harmonic distortion

TUT – Tallinn University of Technology

## SYMBOLS

$A_k$	amplitude of $k^{\text{th}}$ harmonic
$a_k$	Fourier coefficient of $k^{\text{th}}$ harmonics
$b_k$	Fourier coefficient of $k^{\text{th}}$ harmonics
$C$	complex constant
$E_{\text{on}}$	turn-on energy
$E_{\text{off}}$	turn-off energy
$E_{\text{sw}}$	common loss energy
$f_c$	carrier frequency
$f^*$	modulation frequency
$f_{\text{sw}}$	switching frequency
$I_{(1)}$	fundamental current amplitude
$I_{\text{av}}$	average current of IGBT
$I_c$	IGBT collector current
$I_{\text{fd}}$	freewheeling diode current
$I_L$	phase current of the load
$I_{\text{max}}$	maximum value of the phase current of the inductive load
$I_{\text{rms}}$	rms current of IGBT
$I_{\text{rrD}}$	reverse recovery pick current
$J$	moment of inertia of motor shaft
$J'$	moment of inertia of the driven wheels
$k_{\text{cond1}}$	manufacture correction factor 1
$k_{\text{cond2}}$	manufacture correction factor 2
$k_{\text{mod}}$	modulation index
$L_1$	stator inductance
$L_2$	rotor inductance
$L_{12}$	mutual inductance
$m$	mass
$M_s$	static load torque
$M_e$	electromagnetic torque
$M_d$	dynamic torque of the load
$\Delta M$	friction and windage losses
$p$	pole pair number
$P_{\text{LOAD}}$	output power of the motor drive
$P_s$	supply power
$\Delta P$	power losses in the motor components
$\Delta P_c$	power converter losses
$\Delta P_{\text{cond}}$	conduction losses
$\Delta P_{\text{condD}}$	conduction losses of the feedback diode
$\Delta P_{\text{sw}}$	switching losses
$\Delta P_{\text{swD}}$	diode switching losses
$q$	duty cycle
$R_1$	stator resistance of the motor
$R_2$	rotor resistance of the motor
$t$	time
$T_e$	electromagnetic time constant of the motor drive
$t_{\text{rrD}}$	reverse recovery time



$T_m$	modulation period
$U_d$	dc link voltage
$U_F$	mean IGBT voltage drop
$U_{FD}$	diode voltage drop
$U_s$	supply voltage
$y_k$	spectrum characteristics of signals
$\eta_c$	efficiency of the converter
$\eta_{MG}$	efficiency of the motor-gear system
$\varphi$	phase shift between the current and voltage waves
$\varphi_k$	phase spectrum of signals
$\psi$	flux linkage
$\omega$	angular frequency of motor shaft

# **1. STATE OF THE ART AND RECENT ADVANCES IN POWER ELECTRONICS TECHNOLOGY FOR INDUCTION MOTOR DRIVES**

This chapter examines the key development trends including the dominance of ac adjustable speed drives in new applications, with the squirrel-cage induction machine as the preferred motor in most cases. Particularly striking has been the rapid ascendance of the insulated-gate bipolar transistor (IGBT) as the preferable power switch in different driving applications ranging from fractional kilowatts to megawatts. Important current issues such as drive power loss as well as power quality and the effects of fast IGBT switching transients on the converters, machines, and electromagnetic interference production are studied. The last section of this chapter presents an analysis of the major discrete pulse modulation strategies.

## **1.1 Analysis of Contemporary Motor Drive Technology Issues**

### **1.1.1 Progress in Electrical Motors**

The growth in industrial motor drives over the past 10 years has exceeded 25 %, a rate far exceeding the previous 30 years. Such an unprecedented expansion results from the increased demand for efficient reliable supervising, power flexibility, process improvement, and control complexity. This progress requires significant effort in mitigating numerous technical problems associated with new technologies [1].

An electrical machine, the workhorse of modern motor drive, has gone through slow but sustained evolution during the past century that has resulted in higher power density, higher efficiency, and many performance enhancements. Although, traditionally, ac machines have been used for constant-speed applications and dc machines for variable speed drives, the advent of power semiconductor devices, various converter topologies, advanced control techniques, and improved adaptive and estimation methods gradually brought high-performance ac drives of varied types in the market place, pushing the dc drives toward obsolescence. Both induction and synchronous ac machines are extensively used in contemporary motor drives [3].

The cage-type induction motors are universally popular [12]. Squirrel-cage machines dominate for both new and retrofit industrial drive applications around the world. Three-phase ac motor drives are employed now in different areas of wide power ranges starting from few watts to several megawatts. The majority of domains, about 80-90 % of the market, are satisfied with general-purpose induction motor drives having simple voltage-frequency control [4]. According to the estimate of Electric Power Research Institute, around 60 to

65 % of grid energy in the USA is consumed by motor drives, and 75 % of these are pump-, fan-, and compressor-type asynchronous drives, majority of them being used in the industrial environment for the fluid flow control. It was reported that currently around 97 % of medium and high-power drives for such applications operate at fixed speed, where flow is controlled by mechanical methods, such as throttling control, dampers, or flow control valves, resulting in a substantial amount of energy loss. Only 3 % of these drives are operated at variable speed control, thus improving efficiency up to 30 % at light load. Power electronics-based load-proportional speed control in air-conditioning saves as much as 30 % energy compared to the traditional thermostatic control [6]. Along with that, more sophisticated adjustments are used for the drives that require high dynamic speed regulation or high torque accuracy. Therefore, vector methods including the direct torque control opened the door for the researchers aiming to enhance motor performance.

Other types of brushless machines account for only a small fraction of new industrial drive applications. Among the constant-speed applications of induction motors, the variable-frequency starters have the advantages of full torque starting, sinusoidal line current, and reduced-flux efficiency-optimal control. Wound-rotor induction motor drives with slip power recovery are used in a limited speed range for large pumps, compressors, variable-speed hydro-systems, flywheel energy storage, and modern wind generation systems. Although the machine cost is somewhat higher along with the disadvantages of slip rings and brushes, the converter cost is enough economical in such cases. In a very high-power range, wound-field synchronous motor drives are yet very popular, although the machine cost is somewhat higher.

Permanent magnet synchronous machines, particularly brushless dc drives, are more popular in the lower end of power. Generally, they are more expensive than cage-type motors, but have the advantages of higher efficiency, lower life-cycle cost, and rotor inertia. These machines are increasingly popular choices for high-performance servo applications because of their high power density. However, these represent only a small fraction of the total number of industrial drive applications. As a major hallmark of the unfolding drive development history has been an accelerating trend away from dc commutator machines toward various types of ac brushless machines, markets for adjustable-speed drives continue to expand steadily in response to the well-recognized opportunities for major efficiency and cost improvements.

Though in today's automation area the stand-alone drives dominate, at an increasing rate they are being replaced with intricately controlled drive systems using a computer based control platform with a multitude of drives, motors, sensors, and processing equipment. Automation has placed increasing demands on the industrial drive market regarding volume, functionality, configurability, and cost. The real estate requires to mount the drives that has forced suppliers to decrease the drive size, but with better functionality.

The underlying strategic tendency for electrical machines of all types is increasing high value-added functionality without adding cost. This benefit includes reliability in the presence of unknown loading, continuous energy loss minimization, integrated sensing suitable for application specific diagnostics, and permanently optimized thermal utilization of full drive capacity.

### 1.1.2 Motor Drive Implementation and Packaging

The common block circuit diagram of an electric drive is given in Fig. 1.1. Power supplies the circuit from the mains or from an on-board battery. The power converter transforms energy of power supply into energy feeding the motor. In turn, the motor converts electrical energy into mechanical work by transmitting energy induced in the motor gap onto the output shaft. Usually, the gear steps down the motor shaft angular speed and steps up the rotational torque at the same time. The required velocity or angle value and the motion law come to the controller inputs. Other inputs acquire the sensor information about the speed, current, etc. Using these data, the controller generates the references to the gate circuit which controls the power converter.

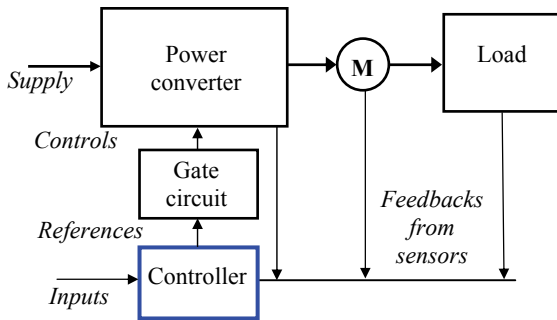


Fig. 1.1 Block diagram of a motor drive

Industrial drives generally fall into one of the three categories based on their power ratings. Although standard terminology is lacking, these three drive classes may be referred to as low-power package drives (<20 kW), medium-power chassis drives (20 to 500 kW) and high-power cabinet drives (>500 kW). The power rating boundaries between these drive classes are only approximate and vary from a manufacturer to a manufacturer with considerable overlap [43].

Low-power package drives are manufactured in the largest numbers and have achieved the highest levels of design integration and automated manufacturing. Power and current levels are low enough for these drives to be designed onto a single printed-circuit board. All the components are packaged into few power modules that can be mounted directly on the board together with the necessary control circuitry. Manufacturing of this type of drive is highly automated using extensions of techniques developed for signal-level construction. As such, these drives are typically the catalog items with a defined set of options, unless they are being built to order for an original equipment manufacturer application. Most of these package drives use simple voltage-frequency control appropriate

for general-purpose adjustment of fans and pumps, though the available operating modes and user interface can be quite sophisticated.

A major distinguishing factor of medium-power chassis drives is that the power levels are high enough that dedicated bus work is generally required to interconnect the power stage components. The switch modules, typically in dual-switch phase-leg configurations for this power range, are mounted on an aluminum heat sink and connected into bridge configurations using laminated bus-bar structures designed to minimize parasitic inductances. Power modules with six switches in the same package are becoming increasingly available for this power range, simplifying the external interconnection requirements. Cooling is usually accomplished by forced air over finned heat sinks, sometimes assisted by sink-mounted pipes to efficiently extract the heat from the compact power stage section where the losses are concentrated. The control functions of the chassis drives are typically partitioned into two or more cards and the drive components are then assembled manually into a steel enclosure. Much of the customization for these drives is typically accomplished during the final assembly stages by mounting the completed drive onto a flat panel that subsequently receives the desired auxiliary components including circuit breakers, contactors, and reactors.

The basic drive partitioning and construction techniques used in high-power cabinet drives are similar to those used for the chassis drives, although the power stage is physically larger and the power switches are typically packaged as single-switch modules. As power ratings climb above 1 MW, competition between power transistors and thyristors intensifies. Thyristors are used in large current-source inverters with induction machines, and also in load-commutated inverters with overexcited synchronous machines. Forced air is the standard cooling technique for these drives, often in combination with heat pipes to efficiently extract the heat from the compact power stage. Water-cooled heat sinks are also available when required by the application. A major distinguishing feature of these large drives is that they are individually built to order in large steel cabinets that are often large enough for maintenance workers to step inside. All of the necessary drive components, including auxiliary transformers, circuit breakers, etc., are mounted inside the cabinet.

### **1.1.3 Advances in Power Electronics**

Resulting from advances in the power technologies it is estimated that about 50 to 60 % of electric power in industrialized countries is flowing through electronic systems and the percent is growing.

Power semiconductors play a leading role in the progress of power electronics since they are essential to satisfy the constantly growing demands on cost, performance, and reliability. Silicon as a well-established starting material that has met these requirements already for 50 years. Solid-state power semiconductor devices constitute the heart of modern power electronic

apparatus, and today's power electronics development has been possible primarily due to device evolution.

The advances in power devices follow the growth of the manufacturing, particularly the technology of large-scale integrated circuits. Power semiconductor evolution has closely followed the evolution of microelectronics. The researchers in microelectronics have worked relentlessly to improve semiconductor processing, device fabrication and packaging, and these efforts have contributed to the successful development of so many advanced power devices available today. The most noticeable directions are as follows:

- improvement of the ratings of the classical power semiconductor devices (diodes, thyristors, and transistors);
- increase of the voltage that can be sustained by action on the thickness and the doping of the silicon wafer;
- increase of the current that can be handled by increasing the chip size;
- reduction of the switching time by using an appropriate device geometry;
- reduction of the reverse recovery charge by controlling the carrier lifetime;
- integration on the same chip both the power device and the control and protection circuitry in the frame of smart power devices.

Large transistors of BJT type, once so popular device in the 1970s, have now become obsolete. For the lower end of power, they have been replaced by power MOSFETs that dominate in the low-voltage (< 300 V) sector. For the high end, the high-voltage semiconductor devices are now the critical components in a wide variety of power electronics applications [44]. Along with usual thyristors, the new high-power (6.5 kV, 4 kA) integrated gate-commutated thyristors have been introduced in recent years that are available with forward and reverse blocking capabilities. In the meantime, their scalability has increased up to 10 kV and several kiloamperes. The maximal turnoff current of a 4.5 kV device has increased towards 7 kA and blocking voltages at 10 kV have been achieved. A 100 MVA class thyristor inverter is also now in the market. This means that the thyristors will remain the switches with the highest power rating also in the future.

An IGBT combines the advantages of MOSFETs and BJTs. During 25 years, the IGBTs have systematically pushed the application of bipolar devices towards the highest voltage classes and current ratings. The IGBT is becoming the power switch of choice for many motor drive applications because it offers a good compromise between on-state loss, switching loss, and ease of use. Today, the range 0.8 to 3.3 kV belongs to the IGBT, which has also penetrated into the 4.5 and 6.5 kV classes, the traditional domain of thyristors. Typical example is

the medium-voltage drives, where the region below 10 MVA is covered rather by IGBTs while above this level - by the thyristors.

IGBT voltage and current ratings increase along with the improvement of electrical characteristics and their application range is extending to high power applications. Fabrication of 3.3, 5.0, and 6.5 kV, 700 A devices has been reported and 10 kV, 1200 A IGBTs are also commercially available. Structure design improvements of medium power IGBTs enable operation at higher frequencies. 600 V, 50 A devices capable of hard-switching at 150 kHz are also available. New IGBT generations are characterized by short switching times lower than 100 ns. This fact has led to a progressive increase in the switching frequency and improvement in their switching laws.

#### **1.1.4 IGBT Inverters of Motor Drives**

Power converters are the major components of the contemporary industrial systems due to their universal application range. In many semiconductor-controlled systems, especially electrical drives, the cost of power electronics and associated auxiliary and protection circuits exceeds the cost of mechanical parts. The influence of their design and functionality on the reliability of applications is increasing because they require less maintenance than other equipment that incorporates sliding and moving parts. In addition, power converters are acknowledged for the robustness that is derived from their fuzzy construction.

The set of requirements that the converters can fit is very diverse due to a wide range of applications. In addition, the relative weighting of importance of different features should vary between particular applications. As power converters are used differently in different areas, the requirements to their static and dynamic precision, frequency and time responses, as well as surge withstand capability, and electrical parameters suitable for a consumer are often themselves the decisive properties.

Industry has settled into several basic topologies for a majority of drive applications [14]. Figure 1.2 sketches the approximate range of usage for these topologies. The boundaries are determined primarily by the amount of stress the power switches must endure and still provide reliable performance. The flyback configuration is used predominantly in low to medium power drives because of its simplicity and low cost. This topology exhibits much higher peak currents than do the forward-mode supplies, so at the higher output powers it quickly becomes an unsuitable choice. For medium-power applications, the half-bridge topology becomes the predominant choice. As the half-bridge does not effectively utilize the full power capacity of the input source, above 0.5 kW the dominant topology is the full-bridge, which offers the most effective utilization of the input power source. It is the most expensive to build, but for those power levels the additional cost becomes a trivial matter.

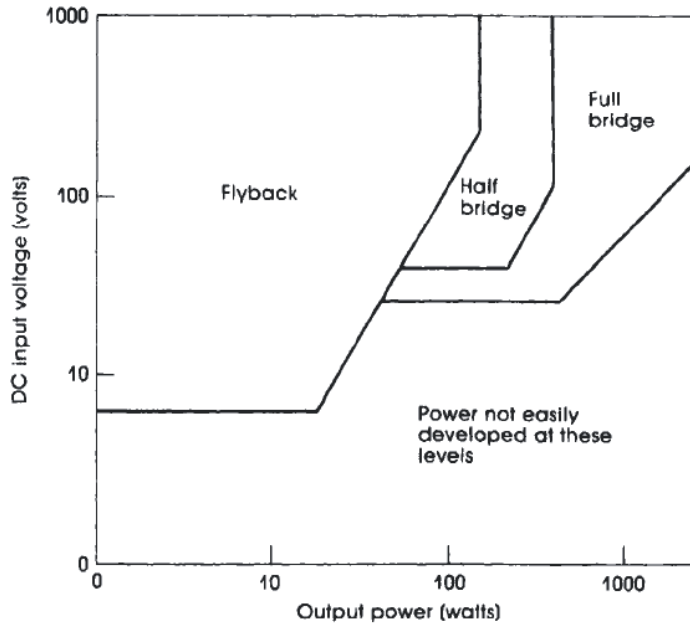


Fig. 1.2 Favorite industrial converter configurations and their areas of usage in motor drives

Today's power conversion technology is mainly based on the two traditional converter topologies: voltage source and current source converters (or inverters, depending on power flow directions and source and load types, ac or dc) [11]. A voltage source converter is fed from a power grid with relatively constant voltage that is generally supported with capacitors. Among the converters that supply an ac drive, the three-phase voltage source inverters have become the overwhelming favorite for industrial drive applications less than 2 MW [5]. Commonly, they have the basic six-switch bridge topology shown in Fig. 1.3. For the voltage dc link, the mains coupling could be implemented by a diode bridge.

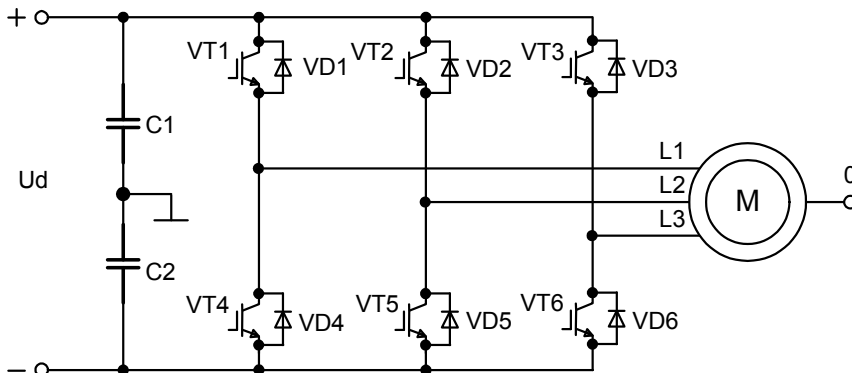


Fig. 1.3 Voltage source inverter-fed motor drive



This class of converters has been accepted almost universally for general power processing applications. An overview given in [45] shows that inverters realized with the three-phase architecture as compared to single-phase bridges yield the following benefits:

- lower rms current through the inverter and rectifier switches (higher power transfer through the switch with the same level of switch current and voltage stress);
- reduced transformer volume and weight due to lower overall volume, voltage, and magnetic stress;
- generally smaller, for the same processed power, energy losses in three-phase transformers and inductors;
- reduced size of the output filter due to a dramatic increase of ripple frequency of the dominant harmonic.

Each main switch used in a voltage source converter must carry bidirectional current and block unidirectional voltage, thus the anti-parallel combination of a transistor and diode is normally used.

However, the voltage source converters have the following conceptual and theoretical limitations:

- inductive load (or source) is required for proper operation;
- output voltage is limited below the dc rail voltage or the dc rail voltage has to be greater than the input voltage;
- dead time is required for the upper and lower devices of each phase leg;
- electromagnetic noise can cause a shoot-through and destroy the devices.

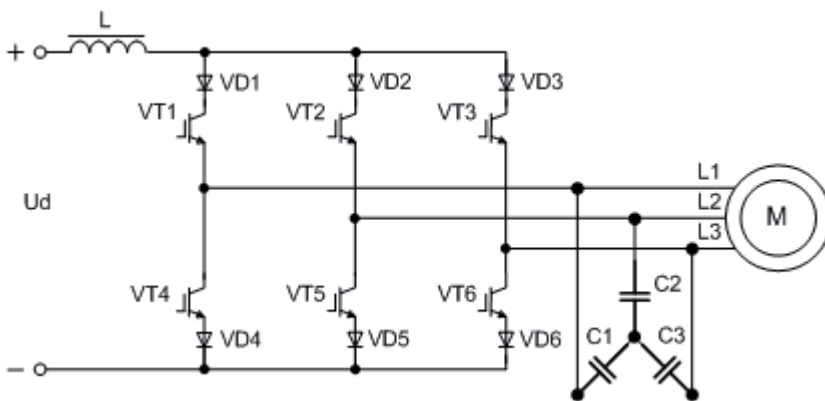


*Fig. 1.4 Current source inverter-fed motor drive*

A current source converter (Fig. 1.4) is fed from a power source with relatively constant current that is generally smoothed through an inductor. For a current

source converter, the main switch has to block bidirectional voltage and only carry unidirectional current, thus a reverse blocking device or the series combination of a transistor and a diode is used. The traditional current source converter has the following conceptual and theoretical barriers:

- capacitive load (or source) is required for proper operation;
- output voltage has to be greater than the original dc voltage or the dc voltage is always smaller than the input voltage;
- for variable-speed motor drive applications, a variable dc source is thus needed;
- overlap time for at least one of the upper devices and one of the lower devices to be gated is needed, otherwise, an open circuit of the dc inductor would occur and destroy the devices.

Due to these limitations, current source inverters have rare practical use in motor drives.

### **Resume of 1.1**

Fast growth of motor drive applications results from the increased demand for efficient reliable process adjustment, power flexibility, technology improvement, and control complexity. The great part of the modern industry market is represented by induction drives with low dynamic and simple control laws. Power converters of ac motor drives are improved regularly, though their basic topology keeps stable on the basis of the dc link supplied three-phase bridge inverter. At the same time, their power economic requirements grow along with increasing consumption and diminishing resources of power energy. This is the reason why the new ways to build economic inverters are to be found.

## **1.2 Power Losses of IGBT Inverters**

### **1.2.1 Figure-of-Merit for Economical Power Converter**

First ten years of the new millennium have acknowledged correctness of the forecasts that the most serious problem of the 21<sup>st</sup> century will be the lack of energy. Continuously growing consumption and diminishing resources of electric power increase its price and stimulate the market growth and technical development on the side of transmission and distribution of electric energy. The same is stimulated by the profit from huge energy savings when modern power electronics is being applied [27]. The fastest growing are the energy sources with the ultimate generation resource, such as solar and wind. The imperative need for their cost reduction represents further stimulus for technical development in power electronics.

There is an extra degree of freedom to fulfill the function of motor drive operation, namely the choice of the motor flux level that influences the generated losses. As the motor drive is an electromechanical system, its efficiency is derived as the product of power efficiencies of the converter ( $\eta_C$ ) and the motor-gear system ( $\eta_{MG}$ ):

$$\eta_{\Sigma} = \frac{P_{LOAD}}{P_s + \Delta P} = \eta_C \eta_{MG}, \quad (1.1)$$

where  $P_{LOAD}$  is the output power of the motor drive usually counted on the gear shaft,  $P_s$  is the supply power, and  $\Delta P$  represents the power losses in the motor drive components.

The full spectre of motor drive losses  $\Delta P$  includes both electrical and mechanical fractions. These loss components are interconnected with each other, therefore to build an economical system both parts should be considered together. A comprehensive discussion of the methods of loss minimization by motor flux adaptation may be found in [41]. However, the converter losses are not considered there.

Vice versa, in this thesis the main attention is paid to the power converter losses, an influence of which on the motor-gear unit is also taking into account.

Additional cost of power electronics can be recovered by saving energy. According to the estimation [6], 15 % of grid energy can be saved easily by widespread but economical applications of power electronics. Saving energy not only provides the direct economic benefit, but helps preserving the dwindling fossil and nuclear fuel reserves. Indirectly, it helps mitigation of environmental pollution, such as global warming problems.

In the development of power electronics, power conversion efficiency has been steadily increasing in the last 30 years, corresponding to the progress in power devices. Efficiency of small power converters such as switching power supplies was at a level of 60 % at the beginning of 1970 and is now more than 90 %. Efficiency of high power converters including motor drive systems and thyristor transmissions exceeds the level of more than 98 %. Therefore, the progress seems to be saturated recently, approaching efficiency to 100 % along with the smallest converter inner power losses. This means that it is gradually becoming difficult to predict future development of power electronics from an efficiency point of view. The technical approaches to meeting these challenges fall into three broad categories of development [46]:

- new power switching devices with reduced power losses;
- effective power converter topologies;
- progressive control strategies.

As power devices are still making substantial progress, by use of novel structures and wide bandwidth of semiconductor materials, all these directions relate to the implementation of economical low-loss power converters.

Today, besides efficiency, power losses affect other converter parameters, like weight, size, cost, power quality, power consumption, transient responses, etc. Because of this, an output power density (OPD) was taken by electronics community as an effective figure of merit, instead of efficiency. The OPD is defined in [22] as output power per unit volume of a converter. Its level of 20 to 30 W/cm<sup>3</sup> is predicted to 2015.

Increase of OPD to decrease power losses means:

- reduction of converter size and power consumption;
- improvement of power quality;
- increase of the switching frequency.

Commonly, the power converter losses are defined as a time integral of the power module current times the voltage:

$$\Delta P_c = \int U_c I_c dt. \quad (1.2)$$

They may be contingently divided between the conduction losses and the switching ones:

$$\Delta P_c = \Delta P_{cond} + \Delta P_{sw}. \quad (1.3)$$

In the case of IGBT bridge inverters with freewheeling diodes, the conduction losses have as a minimum the following three components:

$$\Delta P_{cond} = k_{cond1} U_f I_{av} + k_{cond2} R_f I_{rms}^2 + \Delta P_{condD}, \quad (1.4)$$

where  $I_{av}$ ,  $I_{rms}$  - average and rms currents of IGBT,  $R_f$  - forward IGBT impedance,  $U_f$  - forward IGBT voltage drop equals the saturation voltage,  $k_{cond1}$  and  $k_{cond2}$  - manufacturer correction factors,  $\Delta P_{condD}$  - conduction losses of the feedback diode. Because of non-linear properties of the semiconductor devices this formula is modulation- and load-dependent, and in the case of sine wave operation it is as follows [47]:

$$\Delta P_{cond} \cong \left( \frac{1}{2\pi} + \frac{k_{mod} \cos \varphi}{8} \right) U_f I_{(1)} + \left( \frac{1}{8} + \frac{k_{mod} \cos \varphi}{3\pi} \right) R_f I_{(1)}^2 + \Delta P_{condD}, \quad (1.5)$$

where  $k_{mod}$  is the modulation index,  $\varphi$  is the phase shift between the current and voltage waves,  $I_{(1)}$  is the fundamental current amplitude,  $U$  and  $R$  are the IGBT voltage drop and dynamic resistance.

The switching losses are defined primarily by the switching frequency  $f_{sw}$  as well as the switching on and off energies  $E_{on}$ ,  $E_{off}$  dissipated during the transition intervals:

$$\Delta P_{sw} = f_{sw} (E_{on} + E_{off}). \quad (1.6)$$

As the time integral is a complex value of many parameters, the simplified formula is somewhere used:

$$\Delta P_{sw} = k_{sw1} f_{sw} E_{sw} (I_c, R_{gate}) + \Delta P_{swD}. \quad (1.7)$$

It is defined through the common loss energy  $E_{sw}$  counted by the collector current  $I_c$ , an impedance of the gate circuit given by the manufacturer diagrams  $E_{sw}(R_{gate})$  and  $E_{sw}(I_c)$ , as well as the diode switching losses  $\Delta P_{swD}$ . Although an accurate description of the switching energy is a complex function, it is shown in [41] that the total inverter switching loss can approximately be considered as a linear function of the stator current and switching frequency:

$$\Delta P_{sw} \cong C_{sw} I_{sw} f_{sw}, \quad (1.8)$$

where  $C_{sw}$  is an empirically determined constant.

The feedback diode dissipates additional powers,  $\Delta P_{condD}$  and  $\Delta P_{swD}$ , that must be calculated separately because the IGBT and the diode pass the current in different time instants:

$$\Delta P_D = \int U_{jD} I_{jD} dt, \quad (1.9)$$

where  $U_{jD}$  and  $I_{jD}$  - diode voltage drop and current. In [47], the simplified formulae for the case of sine-wave operation are given:

$$\Delta P_{condD} \cong U_{jD} I_{jD} \left( \frac{1}{8} + \frac{k_{mod} \cos \varphi}{3\pi} \right), \quad (1.10)$$

$$\Delta P_{swD} \cong \frac{1}{8} U_s I_{rrD} t_{rrD} f_{sw}, \quad (1.11)$$

where  $U_s$  - supply voltage of the power cascade,  $I_{rrD}$  - reverse recovery pick current,  $t_{rrD}$  - reverse recovery time.

Commonly, [41] and other authors link both equations, thus showing that the inverter loss is a function of the stator current and voltage amplitudes, phase shift, switching frequency, and modulation index:

$$\Delta P_c = 3\Delta P_{cond} + \Delta P_{sw}. \quad (1.12)$$

## 1.2.2 Reducing of Converter Size and Power Consumption

A survey of three-phase industrial drives over the last 20 years indicates the volume of their packages has dramatically decreased, primarily due to faster rise-times leading to reduced power losses. Simultaneously, the cost of these drives has dropped over time. The major driving force in this field is the need for increased power density. This is explained by currently enlarging

requirements for higher power output along with simultaneous reducing of system size and maintaining of low system cost.

There are two main factors, which determine the size of a power electronics apparatus, mainly the volume of heat sinks and passive components such as capacitors and inductors. Future emphasis on power electronic industry exerts integration of the converter building blocks, which is somewhat similar to the trends of very large scale integration. IGBT power modules are available now with built-in gate drivers, control, and protection for up to several hundred horsepower motor drives. It appears that in future these modules will continue to dominate in power electronic applications [21].

During the past decade, IGBTs packaged in compact plastic power modules have rapidly expanded their voltage and current ratings so that they now dominate nearly in all of the new industrial drive inverter designs. Power modules are supplied by several manufacturers with 1200 V IGBTs (appropriate for 460 V motors) that are packaged either as single-switches (400 A), dual-switch phase legs (800 A), or complete six-switch bridges (2400 A) depending on the required current ratings [44].

In modules, the assemblies of power semiconductor switches and their associated drive circuits are presented. Upward into the multi-kilowatt range, mixed module constructions are used. They incorporate monolithic, hybrid, surface-mount, and wire-bond technologies. However, a close examination of the applications in motor drives and power supplies indicates that there has been no dramatic volume reduction of the subsystem. The power semiconductor modules have shrunk the power switching part of the converter, but the bulk of the subsystem volume still comprises the associated control, sensing, electromagnetic power passives (inductors, transformers, capacitors) and interconnects [23].

As power devices consume the most part of total power loss of converters, reduction of their dissipation represents a crucial problem to be solved. Traditionally, converters with self-controlled switches use simple hard-switching principle. However, hard switching has the inherent disadvantages of high switching loss that decreases the converter efficiency and burdens the cooling system, stress on the devices, and electromagnetic interference problems.

To overcome the loss problems, soft-switched converters have been proposed. As the literature on soft-switched converters is voluminous, a comprehensive review has been made in [48]. One popular application area of soft-switched converters is the resonant and quasi-resonant dc/dc converters [45]. Soft-switching is justified in high-frequency link power conversion, where the load requires galvanic isolation from the source through a transformer. Commonly, a dc power supply fed by the mains consists in the cascade connection of a transformer ensuring voltage adaptation and the galvanic isolation, a rectifier and a filter. As a result, the main parts of the weight and the cost of the system

fall on these reactive components. By using an intermediary resonant inverter stage, it is possible to reduce drastically the size of the system, since the filtering and the galvanic isolation are now performed at medium frequency.

However, soft-switched converters generally require additional bulky filters built on reactive components and extra devices with accompanying control complexity, which increase the converter cost, decrease reliability, and add losses adversely affecting the converter size. Dynamical losses in power passives lead to decreasing both efficiency and power density resulting in new cooling and EMI problems. Also, this would slow down the dynamic response of a motor drive. In [49] an obvious necessity to improve parameters of such converters, primarily their size, weight, and efficiency, is shown.

As follows from a comprehensive overview [6], soft-switched converters generally could not receive acceptance for motor drives.

### **1.2.3 Power Quality Improvement**

Power quality depends on such particular parameters as ripple in dc quantities, harmonic distortion in ac quantities, and reactive power consumption. The following reasons constitute the power quality problems:

- motor drive equipment is very sensitive to power quality variations and power disturbances;
- increasing emphasis on the overall power system efficiency has resulted in a continued growth of adjustable speed drives with power factor correction equipment for the loss reduction that worsen the harmonic content of the power systems;
- many components are now interconnected in the grids, thus any failure of those may provoke important consequences.

Ideally, ac motor drive systems are designed to operate at a pure sinusoidal voltage of a given frequency and magnitude with symmetrical phases. Unfortunately, power converters distort significantly the waveforms being the source of additional losses and the motor torque ripples. Semiconductor converter operation results in waveforms that are made of discrete steps, rather than continuous sine waves or dc. The reason of this phenomenon lies in the modulation principle of the switch performance which originally comes to the synthesis of stepped waveforms. This strategy can be interpreted as a quantization process in which the referenced sinusoidal voltage is approximated by some discrete voltage levels [14]. Whether single phase or three phase, the ac line side of equipment typically incorporates circuits followed by some forms of a switching power system that distort the line current.

Diode and thyristor-based converters distort the ac line current and create the power quality problems in utility systems. Since these converters are very common and constantly growing, to restrict distortion influence various types of filters (active, passive, or hybrid) have been proposed. In IGBT converters, the

same problems are solved with the help of a front-end stage built on the controlled devices, primarily MOSFETs and IGBTs that shape the line current and bring the power factor to unity, leading, or lagging.

Many indices have been applied to restrict design specifications from multiple distortions [40]. Historically, these indices and associated limits have been established a long time ago in specific areas. With time, the numbers have expanded in terms of their application areas and migrated into standard limits. Typically, the following voltage and current indices are used:

- instantaneous waveform shapes;
- amplitude and rms values;
- harmonic spectrum;
- total harmonic distortion (THD);
- crest-factor.

Along with the development of new power equipment and power electronic technologies, these indices have lost some of their meaning and usefulness. Particularly, individual harmonic components have limited applicability for determining the impact of harmonic distortion on electrical equipment. Another important parameter, the peak voltage, which depends on an infinite combination of phase and amplitude values of the fundamental component and harmonics, influences partial discharges, intrinsic degradation, and space charge accumulation.

The diode rectifiers of motor drives draw current from the mains significantly distorted from the sinusoidal shape. One of the purposes of including either a dc link reactor or three-phase input line reactors in the drive power circuitry is to reduce the input current distortions in addition to limiting the peak dc link capacitor current and reducing the conducted interference. However, even when the ac line reactors are introduced with typical ratings of 3 % of the drive base impedance, the current distortions are still very substantial. In addition, the line voltage sag problem cannot easily be compensated in this circuit. Considering the present trend, it appears that in future phase-controlled converters and cycloconverters will be obsolete for operation on the drive systems.

On the other hand, the motor drive as a non-linear system is a prominent source of distortions. Even if the power supplied is a purely sinusoidal voltage of constant magnitude and frequency, the current drawn by the drive is not sinusoidal.

Harmonics have gained importance in the recent times due to their rapid increasing presence caused by growing percentage of non-linear loads, which draw currents that are not proportional to the applied voltage. They refer to all sinusoidal voltages and currents that are integral multiples of the fundamental power system frequency. The power distribution system characteristics



regarding harmonic distortion have been defined by several commercial standards. Among them, IEEE Standard 519 “IEEE Recommended Practices and Requirements for Harmonic Control in Electrical Power Systems”, as well as IEEE Standard 45 and MIL-STD-1399 Section 300 are the most popular [50]. Important standard specifications, IEC 60034-2-1 [51], of the harmonic currents which can be tolerated in motor drives are shown in Table 1.1.

*Table 1.1 Current distortion limits in the point of common coupling ( $I_{cc}$ ) in relation to the load current ( $I_L$ ), %*

$I_{cc}/I_L$	<11 kV	<17 kV	<23 kV	<35 kV
<20	4	2	1.5	0.6
<50	7	3.5	2.5	1
<100	10	4.5	4	1.5
>100	15	7	6	2.5

It is important that unnecessarily strict limits often increase ownership cost and equipment weight and reduce system effectiveness. Thus, presence of harmonics in the stator excitation results in the pulsating torque components effecting on the ripple of the rotor speed. On the other hand, inductances of motors reduce the harmonic currents of high ordinal number.

Today’s standards, however, limit contribution of individual customers who may connect loads on a shared distribution system [50]. In the case of an on-board system this concept does no longer apply since only one "customer" exists and the type and characteristics of loads are well known at the design stage. It may be more beneficial from the overall on-board system perspective to allow higher and more flexible limits in the future.

Another aspect is that the traditional harmonic limits were based primarily on thermal effects, whereas today the sensitivity of electronic equipment (e.g. controllers for power electronic converters) may actually be of more importance. Other considerations such as capacitor aging and short-term distortion need to be addressed as well. The time-dependence nature of the distortions and the type of equipment are to be taken into account in order to control damaging or disturbing effects of harmonic pollution. Particularly, in motor drive design under non-sinusoidal distortion conditions other indices such as crest factors and actual waveforms should be taken into account.

#### **1.2.4 Influence of Switching Frequency on the Drive Components**

Increase in the OPD basically comes from the volume reduction of a capacitance and an inductance as well as the size reduction of a heat sink, which are inversely proportional to the switching frequency. Therefore, the switching frequency is another important issue to realize the higher OPD. To reduce the negative impact of modulation and to enlarge the range of linear operation, the switching frequency of power converters is usually increased as high as the IGBT modules permit [22]. Continuing improvements in IGBT switching characteristics allow these devices to be used with switching frequencies that

range from 2 kHz in high power drives (1 MW and more) to more than 20 kHz in lower power ratings.

At the same time, while electronic power processing has steadily moved toward achieving the necessary output waveforms, high frequency operation does not reduce the total harmonic content but only shifts the harmonics having significant amplitude to higher frequencies. In power converters, the frequency of the first significant harmonic is proportional to the number of pulses per alternation, therefore the higher the number of pulses, the easier the filtering. At present it appears that in some high frequency power processing technologies, fundamental limits are being reached that will not be overcome without a radical change in the design and implementation of power systems. Over the last decades, performance of power electronics has been driven by improvements in fast switching semiconductor components. This leads to the substantial reductions of structural capacitances and inductances associated with device and system-level packaging. Among other advantages of high operating frequencies are the lack of audible noise and system dynamic improvement [52].

Nevertheless, increase of the switching frequency means the growth of power losses. Additional drawbacks are as follows:

- need in more expensive semiconductor devices;
- heightened electromagnetic interference;
- excess wear of moving parts of driven equipment;
- failure of the cable and motor winding insulation.

According to (1.6) - (1.12), high frequency commutations restrict converter performance by amplifying the peculiar inverter losses which grow along with the drive power and magnification of the load requirements. When the switching ripple is neglected, these losses are estimated based on the power and the number of switch commutations [25]. In the common-mode three-phase bridge inverters available at dc supply, the voltage across the switches may be considered to be constant. Therefore, all the converter losses depend on the magnitude of the current being switched. As the current is defined by the consumer requirements, the main efforts to improve an inverter performance are addressed for searching the best relation between the switching frequency, duration of transition intervals, and switched currents.

Simultaneously, the high rate of voltage rise due to the small switching times excites distributed elements of the drive components. This fact increases the influence of the distributed elements on the system - overvoltages on the motor terminal blocks and bearing currents. Besides, in a motor drive, high  $\frac{dU}{dt}$  deteriorates the machine insulation and causes machine terminal voltage boost with a long cable between the inverter and the motor.

According to [5], the resulting switching rates at the output terminals of IGBT inverters designed without snubbers can sometimes exceed 1000 A and 10 kV with undesired and, in some cases, harmful consequences. It has been confirmed that the high switching rates can interact with the inverter output cables and the machine windings to cause large transient voltages to appear across the outermost turns of the stator windings. Field experience has demonstrated that this situation sometimes leads to catastrophic failure of the stator winding insulation. Such conditions are most likely to occur in installations with unusually long cables between the drive inverter and machine. Some machine manufacturers have responded by strengthening the stator winding insulation, at least for the outermost turns.

It was also found that the high switching rates can induce unbalanced charge build-ups on the machine rotor by means of parasitic capacitances coupling the stator, rotor, inverter switches, and ground. This accumulated energy discharges through the bearings if no other galvanic current path is provided. Over time, it causes serious pitting of the bearing balls and races that eventually lead to bearing failures under some circumstances that have been experienced in many installations. Introduction of insulated bearings or grounded rotor shaft brushes is among the solutions adopted by machine manufacturers to prevent these breakups.

An important problem caused by the high switching rates relates to elevated levels of conducted interference in the drive input lines and ground that can easily exceed acceptable levels. Some of these problems have been solved by installing bulky low-pass filters at the motor terminals and by adding common-mode inductors in both the input and output lines, together with small capacitors between each dc link bus and earth ground to prevent these high-frequency currents from reaching the utility grid or machine. Alternately, much of the current research activity to decrease the switching losses is going on multilevel converters.

### **Resume of 1.2**

Power losses affect efficiency, weight, size, cost, power quality, power consumption, transient responses, and other motor drive characteristics. To evaluate converter effectiveness, an output power density was taken as an effective figure of merit, instead of efficiency. Increase in OPD relates to converter size and power consumption reducing, power quality improvement, along with the switching frequency growth. As the motor drives are the complex non-linear systems, all these methods are to be used together and their quality indices need in regular upgrade, common correction, and load-dependent application. Therefore, new modes of the power inverter operation in motor drive are required.

## 1.3 Regimentation of Control Systems for Inverter-Fed Induction Motor Drives

### 1.3.1 Overview of Control Methods

The control system of a motor drive shown in Fig. 1.1 generates the references using information from the input set-points, output sensors, and disturbance sensors [4] [15] [20].

As follows from the figures-of-merit given above for the IGBT-built power converters, most important value-added functionality of the motor drive is a power optimizing control that can be achieved both by static and dynamic minimization of energy needed for the application [3]. As energy becomes increasingly important in the world, this technology has the potential to rapidly accelerate the application of suitably controlled motor drives. Another reliability-oriented technology is an active thermal control as the highest priority control loop for converters required for the high ODP power conversion systems. Such control will necessarily deal with the power induced stresses and reliably prevent unwanted motor drive failures while maintaining highest possible power capability.

Advanced control and signal estimation techniques emerge for ac motor drives [6]. These include vector and field-oriented control, sliding-mode or variable-structure control, optimal controls, sensorless control, and modern intelligent controls based on artificial intelligence techniques, such as expert system, fuzzy logic, artificial neural network, and genetic algorithms. Improved digital signal processors and specified integrated circuit chips, along with the modern software tools, permit implementation of complex control and estimation of power electronic systems. Advent of powerful computers also plays an important role in control development.

Direct torque control gives fast response, and is somewhat simple to implement due to absence of the close loop current control, traditional modulation algorithms, and vector transformations. However, the inherent demerits of limit cycle operation, such as pulsating torque, pulsating flux, and additional harmonic loss accompany this control.

In a drive, where the machine parameter variation and load torque disturbance can be problems, various intelligent control techniques, such as self-tuning regulators, model-referencing adaptive control, and sliding-mode control have been proposed. Recently, powerful intelligent control techniques, based on artificial intelligence, have emerged. Intelligent control is often defined as learning control, self-organizing control, self-adaptive control, or adaptive control that provide system performance dependent on the plant parameter variation and load disturbance. The systems under consideration are usually nonlinear and parameter-varying ones.

### 1.3.2 Control Arrangement of Induction Motor Drives

The architecture for a typical induction motor drive of the 5 to 500 kW power range is illustrated in Fig. 1.5. The core of its power circuitry consists of the front end three-phase diode rectifier, preliminary charge circuit, dc link capacitor bank, and IGBT inverter stage. Other power components shown in this figure include the input line ac reactor, input filter, dc link reactor, dynamic brake, and output filter. They are all optional depending on the application requirements.

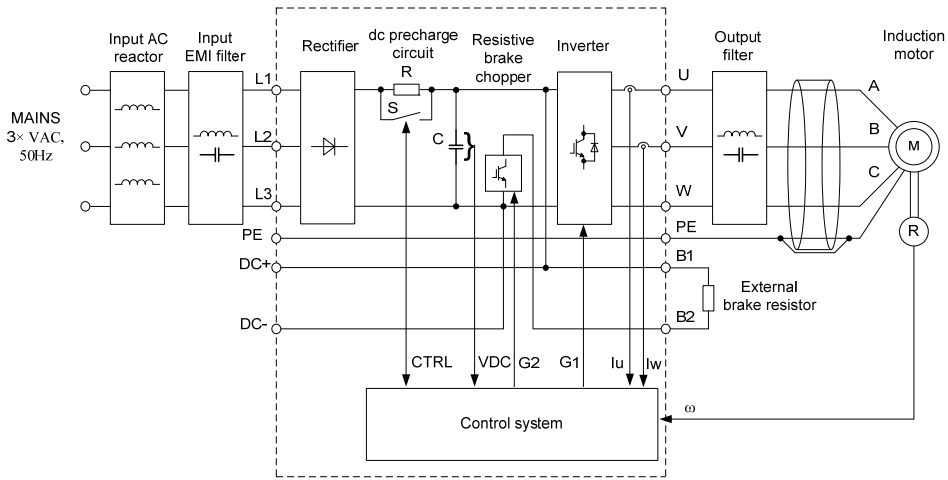


Fig. 1.5 Typical industrial asynchronous motor drive configuration

Usually, such converters have matured to a high state of electrical ruggedness that make it possible to design the inverter stages with a minimum of additional snubber circuitry to limit either the rate of current change  $\frac{dI}{dt}$  or the rate of voltage change  $\frac{dU}{dt}$  at the IGBT terminals. In fact, many new IGBT inverters are designed without any snubbers at all. This approach has the advantage of saving cost, space, and losses in the inverter.

The illustrated architecture having a diode rectifier stage is typical of the large majority of today's industrial drives (90 % according [5]) that do not permit braking power to be returned to the utility lines. Although the diode rectifier has the advantage of low cost, it also imposes several constraints and disadvantages on the drive system that are attracting more attention every year. An important constraint imposed by diode rectifiers is the need for preliminary charging of the dc link capacitors to avoid dangerous surge current when the drive is initially connected to the ac line. A variety of such circuits are used depending on the drive power rating, including the parallel combination of resistor  $R$  and bypass contactor  $S$  shown in Fig. 1.5.

For industrial drives with ratings greater than 30 kW, the diodes in the input rectifier stage are now partially or completely replaced by phase-controlled

thyristors and IGBT-diode switches. Although more expensive than the diodes, this front end serves multiple purposes by providing the preliminary charge function and serving as a fast electronic circuit breaker to remove power from the dc link in the case of ground-fault or inverter failures.

Many industrial drive applications that demand only limited and infrequent machine braking capability (e.g., conveyors) can be satisfied by means of a dynamic brake assembly that dissipates the excess electrical energy appearing on the dc link in external resistors. However, applications that involve frequent and extended periods of braking (e.g., cranes) can justify the introduction of a regenerative input converter bridge to provide the drive with bidirectional power conversion capabilities. Three-phase input line reactors are essential with the active input bridge configuration to provide the necessary input impedance characteristics. Electrolytic capacitors are the preferred choice for the dc link hoarder in almost all industrial drives.

### 1.3.3 Common Control and Protection Architecture

Control and protection technology is advancing rapidly. A basic partition of the control system for the general-purpose inverter-based drive application is shown in Fig. 1.6. It reflects the IEEE recommendations [26] which ease the technical and financial burden for the control system design and upgrade.

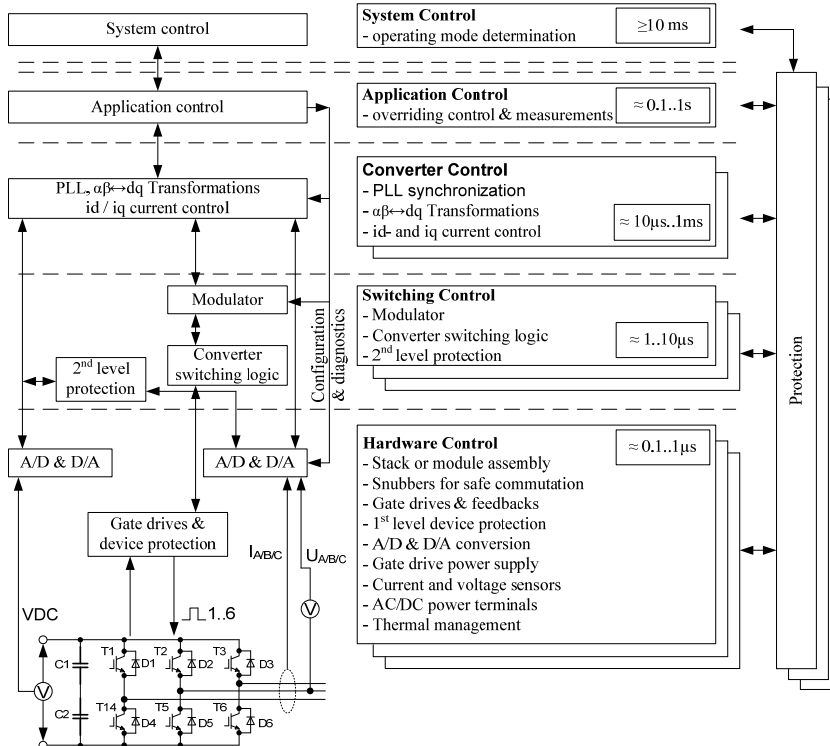


Fig. 1.6 Basic partition of the control system for the general-purpose inverter-based application

Hierarchical control and protection architecture is defined along with various functions that need to be handled within each control layer, the parameters that need to be communicated between the layers, and their required speed range. When the control functions of many different power electronics systems are investigated and evaluated, a significant degree of common functionality emerges, irrespective of the target application. Using the concept of system layers, it is possible to define hierarchical subordination for particular systems including the motor drive.

The system control layer involves all functions in the determination of the system mission and, thus, the duties of the power system or their mode of operation. This layer also includes all human-machine interfaces. From the viewpoint of the system controller, the lower control layers execute all motor drive system functions that are necessary to fulfill the system layer.

The application control layer dictates the operation of the power converter in order to meet the needs determined by the system control. From the viewpoint of the application controller, the lower control layers enable the system to be viewed as one of the two possible equivalent devices: controlled current source or controlled voltage source.

The primary characteristic of the converter control layer is the feedback control, while the other components support the input and output requirements of the closed-loop system. The converter control layer implements many of the functions common to all converters such as synchronous timing, current and voltage filtering, measurements, and feedback calculations.

The switching control layer and all lower layers enable the power electronics to behave as a switch-mode adjustable source. It is of primary importance from the viewpoint of the current research, namely modulation control and pulse generation. Here the switch-mode controlled source is defined as having its terminals directly at the power terminals of the system hardware. Control systems built on microcontrollers allow a reliable adjustment and monitoring of a sufficient number of variables stimulating implementation of both the traditional and the new types of control algorithms. Their main benefits are as follows:

- using the real-time tracking and sensor techniques, the load-dependent switching patterns can be generated;
- using preliminary calculated modulation schemes, the optimized switching patterns predetermined offline according to given optimization criteria can be introduced;
- using the ahead counted evolution of the current, the control signals can be searched and predicted in order to follow the power economical switching trajectories.

The hardware control layer manages everything specific to the power devices. It consists of multiple modules depending on the power requirements, such as gating, galvanic isolation, safe commutation, restriction of  $\frac{dI}{dt}$  and  $\frac{dU}{dt}$ , and the first level protections. Functions of this layer are common for virtually any application.

### **Resume of 1.3**

An overview of the contemporary control architecture exposes the new possibilities for effective load-dependent power control. Among them, the real-time load tracking, the preliminary calculated control schemes, and the ahead counted evolution of the current should be mentioned as the most prospective approaches. In the basic partition of the control system, switching control layer that enables power electronics to behave as an adaptive system was found of primary importance from the viewpoint of power economical performance.

## **1.4 Analysis of Switching Patterns for IGBT Inverters**

### **1.4.1 Six-Step Modulation**

Several techniques are known in the IGBT switching control practice: low commutation simple six-step modulation, high commutation pulse-width modulation (PWM) and progressive space vector modulation (SVM). The aim of this section is to compare their effectiveness from the viewpoint of drive applications.

Modulation techniques were originally restricted by the synthesis of stepped waveforms. In the three-phase systems, this strategy is interpreted as a quantization process in which the reference sinusoidal voltage is approximated by the six discrete voltage levels available at dc supply. Implementation of this type of control known as a six-step modulation is relatively simple and does not require high switching speed, which seems suitable for power converters of the general-purpose motor drives.

For the three-phase bridge inverter shown in Fig. 1.3, the states of the switches and the phase, neutral, line-to-neutral, and line-to-line voltages have the waveforms plotted in Fig. 1.7 [17]. Here, the on-states of the three half-bridges are phase-shifted by  $120^\circ$ . Each phase is under the current during half a modulating period and broken during another half a period. Therefore, a specific phase is switched from the positive pole to the negative one being alternately in series with the remaining two phases connected in parallel. When **VT1** is switched on, the load phase  $L1$  is connected to the positive terminal of dc supply  $U_d$ , resulting in the load phase voltage  $U_{L1} = \frac{U_d}{2}$  in relation to the load neutral. When **VT4** is switched on, the phase  $L1$  is connected to the



negative terminal of dc supply, resulting in  $U_{L1} = -\frac{U_d}{2}$ . Waveforms of  $L2$  and  $L3$  are the same as those of  $L1$ , except that they are shifted by  $120^\circ$ .

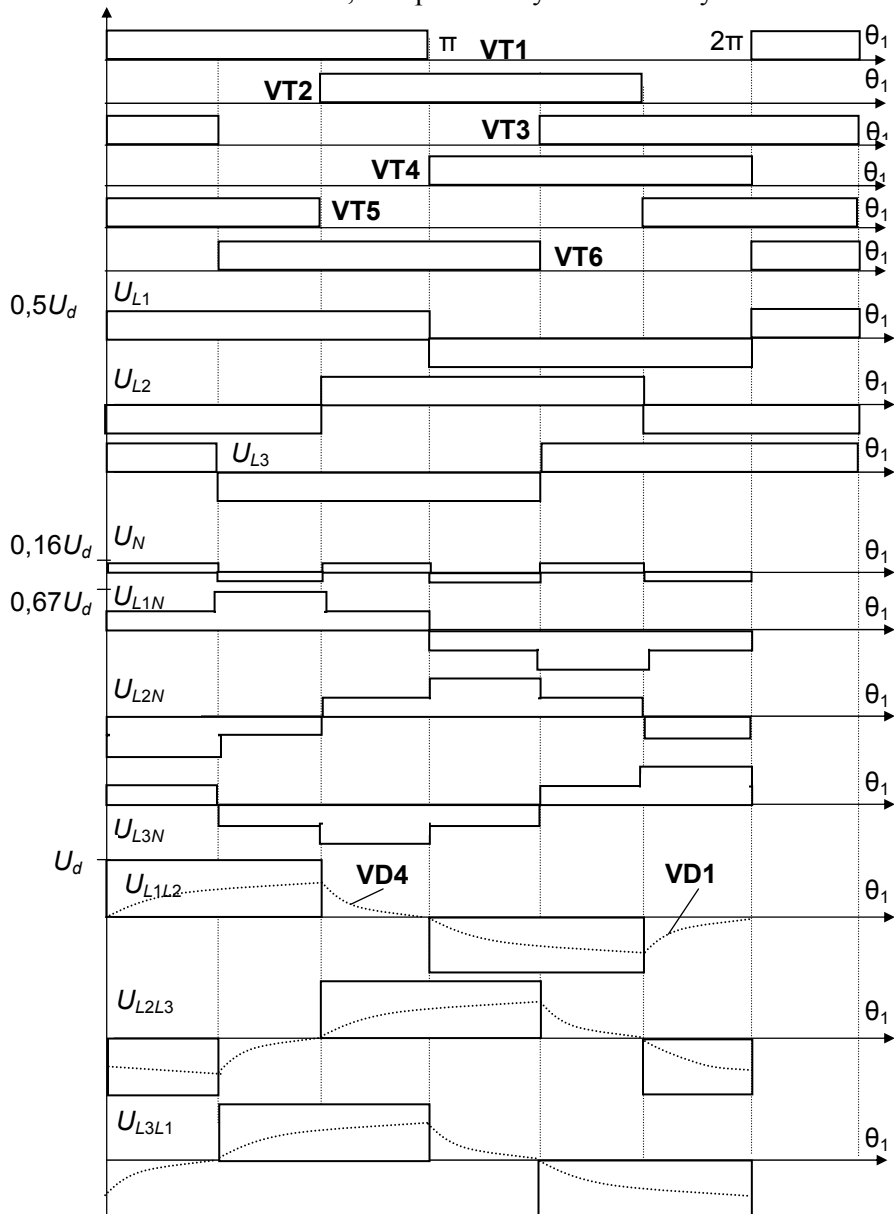


Fig. 1.7 Voltage and current traces for six-step modulation

The rms value of the inverter leg phase voltage in relation to the supply neutral depends only on dc link voltage  $U_d$  and can be expressed as

$$U_{LN} = \frac{\sqrt{2}U_d}{3} = 0,4714U_d. \quad (1.13)$$

The three-phase voltage system of the legs is unbalanced. The load neutral potential can be written as follows:

$$U_N = \frac{U_{L1} + U_{L2} + U_{L3}}{3}. \quad (1.14)$$

In each instant, this neutral potential of the triple frequency is either positive or negative as two upper or lower transistors are on in the inverter leg. From here, the inverter leg phase voltages may be obtained as follows:

$$U_{L1N} = U_{L1} - U_N, U_{L2N} = U_{L2} - U_N, U_{L3N} = U_{L3} - U_N. \quad (1.15)$$

Therefore, each inverter leg phase voltage in relation to the supply neutral is  $\pm \frac{U_d}{3}$  or  $\pm \frac{2U_d}{3}$  with the polarity of the voltage drop across the phase being determined by whether it is connected to the positive or negative pole. Such voltage waveforms have a characteristic six-stepped shape the presence of which explains why this type of modulation is called a six-step modulation.

The line-to-line voltages are related to the phase voltages as follows:

$$U_{L1L2} = U_{L1} - U_{L2}, U_{L2L3} = U_{L2} - U_{L3}, U_{L3L1} = U_{L3} - U_{L1}. \quad (1.16)$$

These voltages form the square waves with  $120^\circ$  pulse widths and rms value

$$U_{LL} = \sqrt{\frac{2}{3}}U_d = 0,8165U_d. \quad (1.17)$$

The line-to-line voltage contains a fundamental rms component  $\frac{\sqrt{6}U_d}{\pi}$ , therefore a standard 400 V motor needs in 512 VDC to be fed by the six-step inverter. Fourier analysis of the line-to-line waveform indicates a square-wave type of geometric progression for the harmonics, i.e., it contains a fifth part of the fifth harmonic, seventh part of the seventh harmonic, and so on. Harmonics of order three and multiples of three are excluded from both the line-to-line and line-to-neutral voltages and consequently from the currents.

The six-step algorithm provides the constant converter logical structure because the number of open and closed transistors is equal and does not change during the full modulating period. This is an advantage of the described modulation method inline with relatively simple implementation which does not require high switching speed. However, the six-step algorithm is the source of significant current harmonic distortion as its waveforms have low frequency [9] [30]. The output current depends on the load, but generally because of the high content of low-order harmonics in the output voltage, it strays substantially from a sine wave.

An important feature of this method is the impossibility of the voltage control. The need in a controlled rectifier to control the voltage of the inverter is an inherent weakness of the circuit. A line-commutated rectifier supplying the dc link is notorious here because it does not only produce the line currents with low orders of harmonics, but draws also substantial reactive currents of line frequency. Its large compensative capacitor slows the response time of the system. Therefore, the active front end seems the prospective decision.

Although the six-step inverters have found occasional use in motor drives, this technique is important for open-loop voltage-frequency control [18]. It is normally used in low-power applications where the voltage range is fixed and dynamic performance is not important, particularly in the frequency changers.

### 1.4.2 PWM Switching Pattern

Far more popular, especially for the converters with faster switching devices, are the PWM techniques. PWM is valuable for drive performance in respect to voltage and current harmonics, torque ripple, acoustic noise emitted from an induction motor and also electromagnetic interference [15] [19] [21]. An output of the PWM circuit represents the chain of constant magnitude pulses, the duration of which is modulated to obtain the necessary specific waveform on the constant modulating period  $T_c$ . Performance of a PWM converter significantly depends on the control algorithm. Different modulators are now available in a variety of designs and integrated circuits. A large number of PWM techniques are available, each having different performance notably in respect to the stability and audible noise of the load.

The objective of the most popular sinusoidal PWM is to synthesize voltages that produce currents as close to sinusoidal as possible. With the PWM control, the switching signals are generated by comprising a switching-frequency carrier triangular waveform  $u_c$  with the modulation signal  $u^*$ . One frequently used three-phase PWM algorithm is illustrated in Fig. 1.8 for the bridge circuit shown in Fig. 1.3. Here, the sinusoidal modulation signals  $u^*$  specify the required output waveforms. To obtain balanced three-phase output voltages in a three-phase PWM inverter, three reference sinusoidal modulated voltages that are  $120^\circ$  out of phase are needed, one per each phase. The high-frequency triangle carrier signal  $u_c$  is also applied. Its frequency is typically 2 to 200 kHz. The natural intersections of  $u^*$  and  $u_c$  determine both the offset and the duration of the gate control signals. When  $u^* > u_c$ , three transistors are turned on and another three are turned off.

Changing the pulse width of each half-cycle alters the output phase voltages  $U_{L1}$ ,  $U_{L2}$ ,  $U_{L3}$  of the inverter (with respect to mid dc link point). They are switched between positive and negative buses at the intersections of the carrier wave and the modulating waves. Here, unlike the six-step block modulation scheme, the conduction angle  $t_{on}$  of various transistors may be less than  $60^\circ$ .

The switching duty cycle  $q$  can be obtained from the waveforms as follows:

$$q = \frac{t_{on}}{T_c}. \quad (1.18)$$

The duty cycle can change between 0 and 1 depending on the magnitude and the polarity of  $u^*$ .

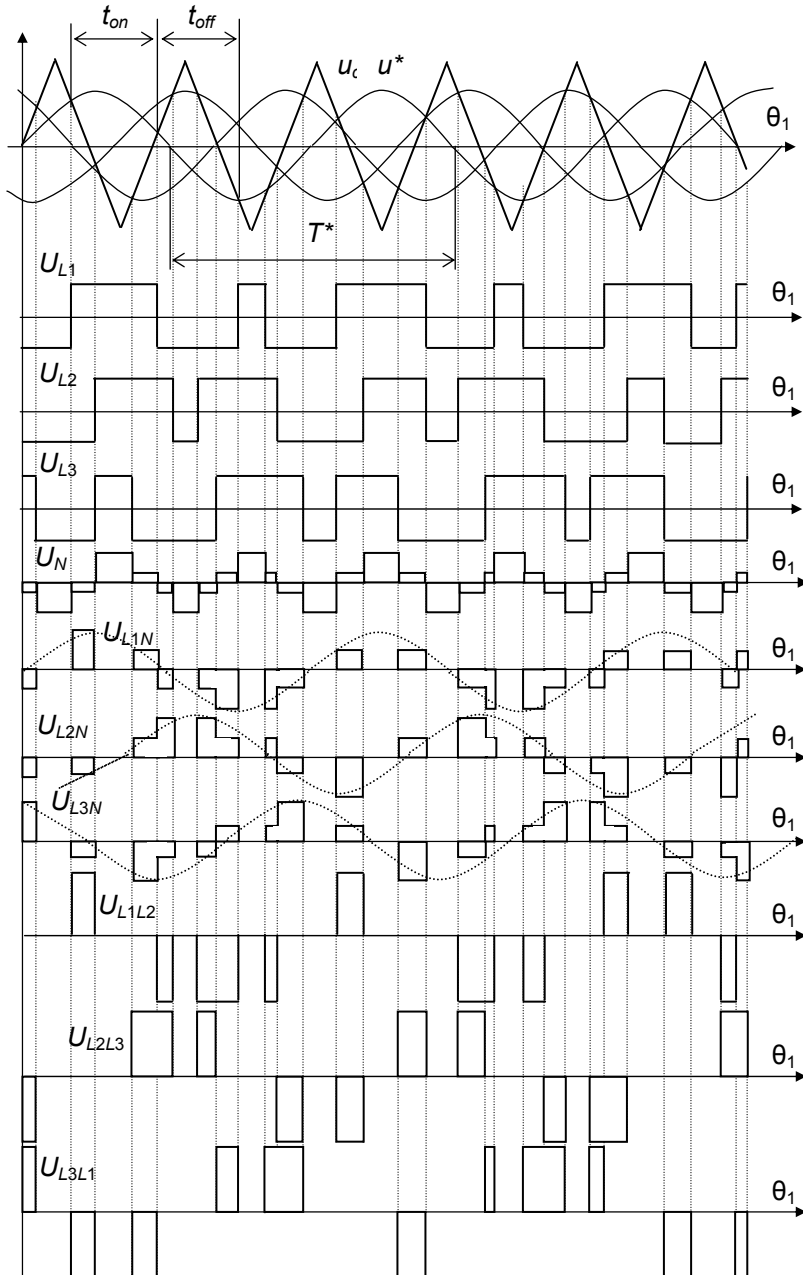


Fig. 1.8 Voltage and current traces for sinusoidal PWM

In the PWM, the carrier ratio (frequency ratio) determines the number of pulses in each cycle of the inverter output voltage:

$$k_f = \frac{f_c}{f^*}, \quad (1.19)$$

where  $f_c$  is the carrier frequency and  $f^*$  is the modulation frequency.

PWM results in a sinusoidal current with high-frequency ripple. The higher the carrier ratio, the more sinusoidal is the output current. Typically,  $k_f = 50$  to  $500$ .

The waveform of pulse pattern depends on the modulation index (modulation ratio) which is the ratio of the peak  $u^*$  to the peak  $u_c$  and determines the height of the pulses and hence the rms value of the inverter output voltage as follows:

$$k_{mod} = \frac{u_{\max}^*}{U_{c\max}}. \quad (1.20)$$

The modulation index can be varied between 0 and 1 to give a linear relation between the reference and output wave. In the case of sinusoidal PWM, the ideal maximum modulation index is equal to unity. At  $k_{mod} = 1$ , this line-to-line voltage contains a fundamental rms component  $\frac{\sqrt{3}U_d}{2\sqrt{2}}$ .

Different PWM schemes allow  $k_{mod} \leq 1$  that represents an important performance criterion, as the inverter maximum power depends on the maximum voltage at load terminals. In non-sinusoidal PWM schemes,  $k_{mod} > 1$  known as an overmodulation is also possible. For sufficiently large values of  $k_{mod}$  PWM degenerates into six-step modulation [20].

When **VT1** switches on, the load phase  $L1$  is connected to the positive terminal of dc supply making rms  $U_{L1} = \frac{k_{mod}U_d}{2}$ . When **VT4** switches on, the phase  $L1$  is

connected to the negative terminal of dc supply resulting in rms  $U_{L1} = \frac{-k_{mod}U_d}{2}$ .

Waveforms of  $L2$  and  $L3$  are the same as those of  $L1$ , except that they are shifted.

Again, similarly to the six-step modulation, for the balanced three-phase operation the voltage of the load neutral can be expressed by (1.14). The load neutral voltage has three times the referred frequency and thus contains the triple harmonics, which does not appear in the inverter phase voltages that may be obtained from (1.15). Therefore, each phase obtains the voltage equal to  $\pm \frac{k_{mod}U_d}{3}$ ,  $\pm \frac{2k_{mod}U_d}{3}$ , or zero. When  $k_{mod} = 1$ , the phase voltage is the same as

in the case of the six-step modulation. The corresponding line-to-line voltages are given by (1.16). Fourier analysis of the inverter voltage waveforms reveals that they have sinusoidal fundamental components but still noticeable losses as well as objectionable noise emitted by the converter and the load [15] [19]. As

Fig. 1.9 shows, increase of  $k_f$  and  $k_{mod}$  results in more symmetrical output waveforms, less losses, and better harmonic contents.

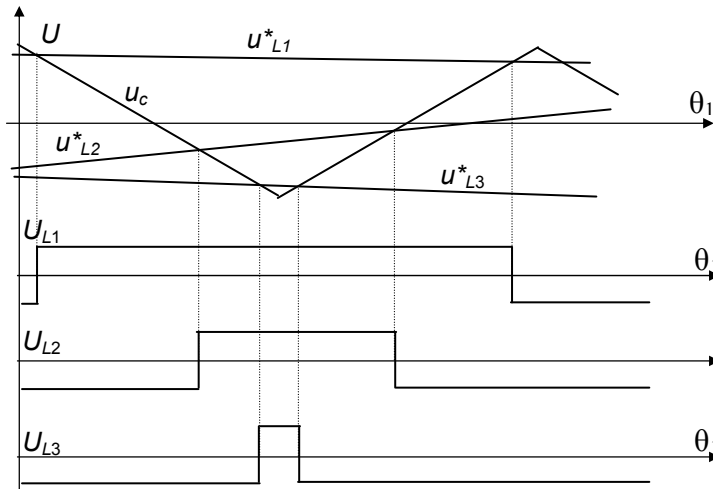


Fig. 1.9 Zoomed voltage traces for sinusoidal PWM

For a long time PWM served as a basic energy processing technique applied in power converter systems. When the sinusoidal PWM is used, the low-order voltage harmonics are greatly attenuated although other significant harmonics are represented close to the carrier frequency. Hence, this is a good solution where an electronic system is to be used across a wide voltage and frequency range. Since voltage and frequency are both controlled with the PWM, a quick response to changes in the demand voltage and frequency can be achieved.

Nevertheless, PWM inverters have several problems in terms of ac motors. Due to the highest switching frequency, they demand high-dynamic expensive IGBTs. As the modulating signals are generated by comparing a carrier signal separately with three sinusoidal reference signals, this is an obvious weakness of such technique which directly affects the efficiency of the overall system. Also, high frequency harmonics of output voltage increase the loss in the motor. PWM inverters generate high frequency voltage which increases the bearing currents of the motor and equipment connected by the shaft. They generate noises and destroy the bearings in severe cases. The spikes caused by high  $\frac{dU}{dt}$  have a serious effect on motor insulation. High speed of voltage change on the inverter output is reflected in the cable, which may cause the motor terminal voltage to increase up to double of the voltage step. This peak voltage depends on the power of the inverter output and the cable length. Therefore, different filters are attached to the inverter to reduce these spikes.

### 1.4.3 SVM Switching Patterns

Among many studies devoted to the optimization of the pulse patterns of IGBT switches, SVM is of primary importance. Today SVM is the most sophisticated method for generating a fundamental sine wave providing a higher voltage to the motor and lower switching losses as compared to PWM. Several SVM algorithms have been reported in [28] [31] [53] [54] [55] [56].

SVM provides all the possible switching states made up of the six-step system. Referring to the three-phase bridge inverter shown in Fig. 1.3, the real IGBT switches is approximated by a simplified switching model given in Fig. 1.10, *a*. Eight different switching combinations are designated by the binary variables 100, 110, 010, 011, 001, 101, 111, and 000, which indicate whether a switch is in the top (1) or bottom (0) position, thus defining all possible switching states shown in Fig. 1.10, *b*. During the modulating period, a phase voltage may be equal to  $\pm \frac{U_d}{3}$ ,  $\pm \frac{2U_d}{3}$ , or zero depending on which the transistors are in the on state. Clearly, to produce the output voltage, only one pair of the inverter switches needs to change its state: **VT2** with **VT5**, **VT1** with **VT4**, or **VT3** with **VT6** [25].

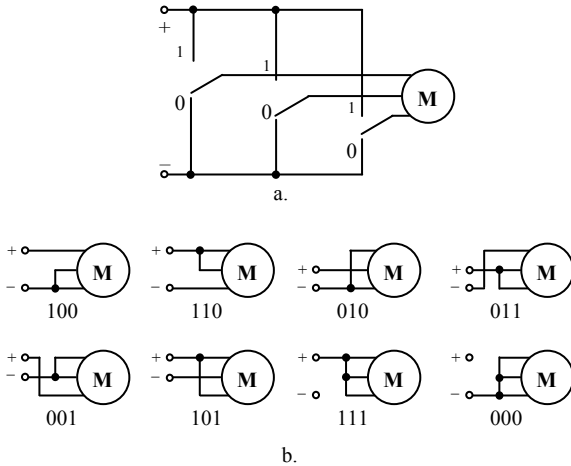


Fig. 1.10 Ideal inverter model

Important essence of SVM lies in the possibility to refuse the simultaneous commutation of all the inverter switches in favour of the commutation between some preliminarily selected states. To this end, each of the binary variables 100, 110, 010, 011, 001, 101, 111, and 000, is associated with a particular space vector  $U_0 \dots U_7$  the states of which correspond to the definite space position of the resultant motor voltage vector. Figure 1.11 illustrates the switching states and corresponding voltage vectors of the three-phase inverter. The vector set includes six active voltage space vectors  $U_1$  to  $U_6$  corresponding to the switching states 100, 110, 010, 011, 001, 101, and two zero voltage space vectors  $U_0$ ,  $U_7$  keeping with 111 and 000.

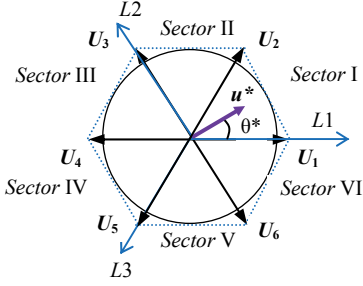


Fig. 1.11 Voltage space vectors of a three-phase inverter

The desired three-phase voltages across the output of the inverter could be represented by an equivalent space vector  $\mathbf{u}^*$  rotating in the counterclockwise direction at a constant angular frequency for steady state operating conditions. The magnitude of the space vector is related to the magnitude of the output voltage and the modulating time this vector takes to complete one revolution is the same as the fundamental time period  $T_m$  of the output voltage.

In SVM, the reference vector  $\mathbf{u}^*$  and its phase  $\theta^*$  are treated through adequate timing of adjacent non-zero and zero space vectors. It is composed by a switching sequence comprising the neighbor space vectors from  $\mathbf{U}_1 - \mathbf{U}_6$ , while filling up the rest of the time interval with zero vectors  $\mathbf{U}_0$  or  $\mathbf{U}_7$  during the voltage alternation. To travel between the neighbor vectors  $\mathbf{U}_i$  and  $\mathbf{U}_{i+1}$ , the switching sequence of pulses  $\mathbf{U}_i$ ,  $\mathbf{U}_{i+1}$  and  $\mathbf{U}_0$  or  $\mathbf{U}_7$  has to be generated in sampling intervals  $T_c$ , with the time durations  $t_i$ ,  $t_{i+1}$  and  $t_0$ , respectively. The solution for  $t_i$ ,  $t_{i+1}$  and  $t_0$  results in the following equations:

$$t_i = \frac{\sqrt{3}u^*}{2U_d} T_c \sin\left(\frac{\pi}{3} - \theta^*\right), \quad t_{i+1} = \frac{\sqrt{3}u^*}{2U_d} T_c \sin \theta^*,$$

$$t_0 = T_c - t_i - t_{i+1}, \quad \theta^* = T_c N, \quad (1.21)$$

where  $N$  is the number of the sampling periods counted from the sector starting point. While traveling between the adjacent sectors, the computations of (1.21) repeat. In fact, this technique produces an average of three voltage space vectors  $\mathbf{U}_i$ ,  $\mathbf{U}_{i+1}$ , and  $\mathbf{U}_0$  ( $\mathbf{U}_7$ ) in a sampling interval  $T_c$ .

In the linear operating region, the maximum line-to-line voltage amplitude can be achieved when  $\mathbf{u}^*$  is rotated along the largest inscribed circle of the space vector hexagon. The modulation index determines the value of the inverter output voltage as follows:

$$k_{mod} = \frac{u_{max}^*}{U_d}. \quad (1.22)$$

It is possible to obtain fundamental line-to-line voltage as high as  $U_d$  that is an important advantage of the SVM technique. Thereby, as compared to the



sinusoidal PWM, the fundamental output phase voltage amplitude of which is  $\frac{U_d}{2}$ , SVM allows  $\frac{U_d}{\sqrt{3}}$  or 15.5 % higher voltage and thus a higher output power of a converter with possible minimization of switching frequency. At  $k_{mod} = 1$ , the line-to-line voltage contains a fundamental rms component  $\frac{U_d}{\sqrt{2}}$ , therefore, a standard 400 V motor requires 566 VDC. Due to the high fundamental line-to-line voltage, the torque generated by the motor may reach high levels, resulting in better dynamic response of the motor as compared to the sinusoidal PWM method.

There are many SVM schemes for the three-phase converters that produce the same switching time for the active vectors [54] [55] [56]. The only difference between them is the choice of the zero vectors  $U_0$  and  $U_7$  and the sequence in which the vectors are applied within the sampling cycle  $T_c$ . Therefore, each scheme is suitable for different operating conditions. Usually, continuous and discontinuous SVM are distinguished.

In continuous space vector modes, both  $U_0$  and  $U_7$  are used in the same sampling cycle as shown in Fig. 1.11, *a*, for the first sector. In this strategy, the total zero voltage vector time  $t_0$  is allocated equally between  $U_0$  (111) and  $U_7$  (000), being symmetrically distributed at the start and end of the sampling period. Here, the switching sequence of the upper legs of the IGBT inverter looks like  $U_0 \rightarrow U_i \rightarrow U_{i+1} \rightarrow U_7 \rightarrow U_7 \rightarrow U_{i+1} \rightarrow U_i \rightarrow U_0$ . The scheme has three on states and three off states within a switching cycle  $T_c$ . Table 1.2 regulates the vector in other sectors. The waveforms for the continuous SVM are shown in Fig. 1.12 and their gate signals in the first modulating sector are given in Fig. 1.13, *a*.

Table 1.2 Switching sequences

	Sector					
	I	II	III	IV	V	VI
1	$t_0/2$	$t_0/2 + t_{i+1}$	$T_c - t_0/2$	$T_c - t_0/2$	$t_0/2 + t_i$	$t_0/2$
2	$t_0/2 + t_i$	$t_0/2$	$t_0/2$	$t_0/2 + t_{i+1}$	$T_c - t_0/2$	$T_c - t_0/2$
3	$T_c - t_0/2$	$T_c - t_0/2$	$t_0/2 + t_i$	$t_0/2$	$t_0/2$	$t_0/2 + t_{i+1}$

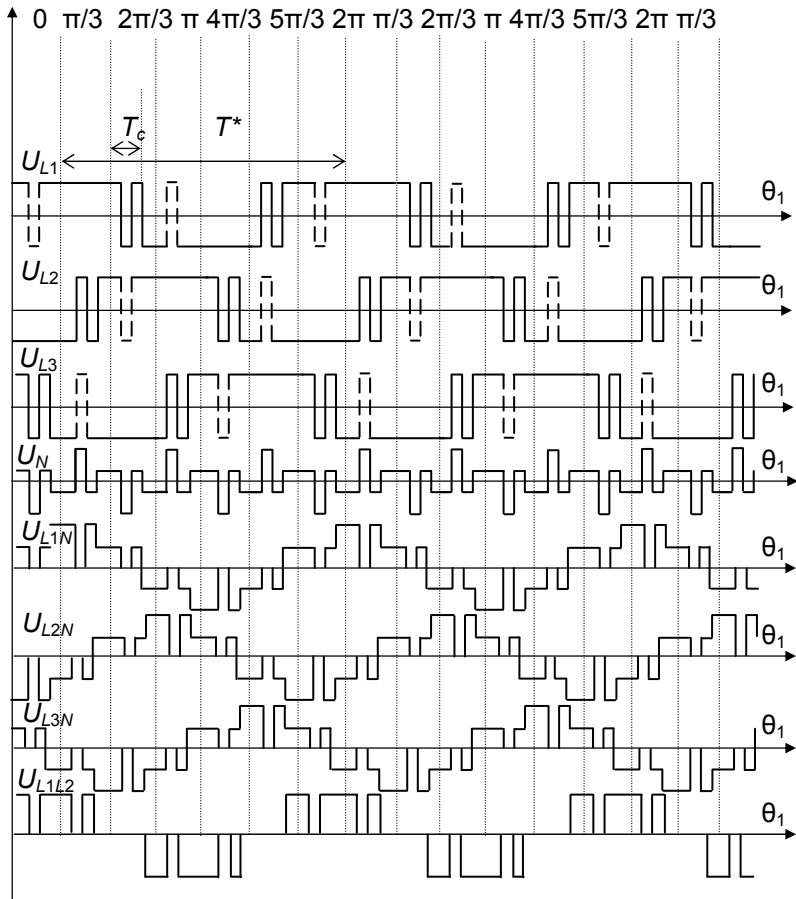


Fig. 1.12 Voltage traces for continuous SVM

An idea of the discontinuous modulation is based on the assumption that one phase is clamped by  $60^\circ$  to the lower or upper level of the dc voltage [57]. When the reference vector is in sector 1 of Fig. 1.11, the voltage in phase  $L1$  reaches the maximum as compared to the other phases. Switch **VT1** of the phase  $L1$  keeps in conduction all the time and phases  $L2$  and  $L3$  modulate, as shown in Fig. 1.13, *b*. This means that only one state vector can be used in this  $60^\circ$  period of time. Extending this conclusion to a complete sampling period, a distribution of zero vectors in the hexagon can be obtained where 111 and 000 vectors are used alternatively in the sectors (Fig. 1.13, *c*). As opposed to the continuous modulation, it gives only one zero state per sampling period, hence only one vector,  $U_0$  or  $U_7$ , is used in the switching cycle. Thus, one of the main advantages of the method is the reduction of the number of switching processes of **VT1** - **VT6** in a period  $T_c$  from 6 to 4, providing a 33% decrease in the switching losses. Referring to Fig. 1.13 it can be noted that the centre pulses in the SVM waveform are broader than the pulses where the fundamental voltage passes through zero.

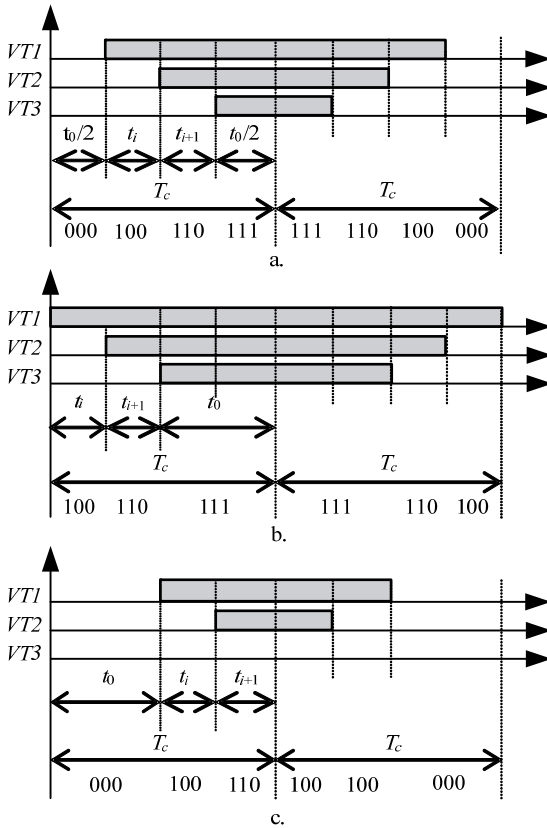


Fig. 1.13 SVM gate signals in sector 1

#### Resume of 1.4

The major techniques used in the IGBT switching control practice were studied carefully in this section - low commutation simple six-step modulation, high commutation PWM, and computer-based SVM. Total results of this study are summarized in Table. 1.3.

Six-step modulation is the simplest and the least expensive method resulted in the highest output and fundamental voltages. Its drawback is an impossibility of voltage control required by adjustable motor drives and the highest current harmonic distortion. It is recommended for the simplest open-loop motor drives with low static and dynamic requirements.

PWM provides the best smoothing of the output current being the most suitable technique for high precision quasi-linear operation of the motor drive. Unfortunately, its high frequency switching causes significant power losses and many other malfunctions.

SVM technique as a very robust signal processing method with quick and precise control response is well suited for the high-performance applications.

The essence of SVM lies in the possible denial of the simultaneous commutation of all the inverter switches in favour of the commutation between some preliminary selected states. Therefore, SVM was recognized as possibly the best among all the power converter control techniques in the field of variable drive applications and the most prospective method which, being implemented on microprocessors, produces highest performance because it requires direct online computation of the reference voltages.

*Table 1.3 Comparative data of modulation techniques*

Quantity	Six-step	PWM, $k_{\text{mod}} = 1$	SVM, $k_{\text{mod}} = 1$
Phase rms, $\frac{U_L}{U_d}$	$\frac{\sqrt{2}}{3} = 0.471$	$\frac{\sqrt{2}}{2\sqrt{\pi}} = 0.399$	$\sqrt{\frac{2}{3\pi}} = 0.459$
Phase amplitude, $\frac{U_{L\text{max}}}{U_d}$	$\frac{1}{2} = 0.500$	$\frac{1}{\sqrt{\pi}} = 0.564$	$\frac{1}{2} = 0.500$
Line rms, $\frac{U_{LL}}{U_d}$	$\sqrt{\frac{2}{3}} = 0.816$	$\sqrt{\frac{3}{2\pi}} = 0.691$	$\sqrt{\frac{2}{\pi}} = 0.798$
Line amplitude, $\frac{U_{LL\text{max}}}{U_d}$	1	$\sqrt{\frac{3}{\pi}} = 0.977$	1
Fundamental phase rms, $\frac{U_{(1)L}}{U_d}$	$\frac{\sqrt{2}}{\pi} = 0.450$	$\frac{1}{2\sqrt{2}} = 0.354$	$\frac{1}{\sqrt{2}\sqrt{3}} = 0.408$
Fundamental phase amplitude, $\frac{U_{(1)L\text{max}}}{U_d}$	$\frac{2}{\pi} = 0.637$	$\frac{1}{2} = 0.500$	$\frac{1}{\sqrt{3}} = 0.577$
Fundamental line rms, $\frac{U_{(1)LL}}{U_d}$	$\frac{\sqrt{2}\sqrt{3}}{\pi} = 0.780$	$\frac{\sqrt{3}}{2\sqrt{2}} = 0.612$	$\frac{1}{\sqrt{2}} = 0.707$
Fundamental line amplitude, $\frac{U_{(1)LL\text{max}}}{U_d}$	$\frac{2\sqrt{3}}{\pi} = 1.103$	$\frac{\sqrt{3}}{2} = 0.866$	1
Voltage THD, $\frac{\sqrt{U^2 - U_{(1)}^2}}{U_{(1)}}$ , %	31	52	51

## 1.5 Conclusions

1. Analysis of the contemporary motor drive technology issues exhibits a fast growth of motor drive applications. As a substantial part of the modern industry market is represented by induction drives, it confirms topicality of the research in this field. Especially, it concerns power converters of induction motor drives in the frame of their basic topology. As power economic requirements are

growing along with increasing consumption and diminishing resources of power energy, search for new ways in the development of economic power converters is considered a prospective scientific direction.

2. To evaluate an influence of power losses on efficiency, size, cost, power consumption, and other motor drive characteristics, an output power density (OPD) has been taken as an effective figure of merit, instead of efficiency. It was shown that the realization of the higher OPD relates to reducing a converter size and power consumption, improvement of power quality, along with an increase of the switching frequency. In this connection, focus was on the design of the motor drive performance modes with regular upgrade and correction of load-dependent quality indices.

3. As a result of regimentation of the control systems, new possibilities for effective load-dependent control of power converters were exposed. Among them, the real-time load tracking, the preliminary calculated modulation schemes, and the ahead-counted evolution of the current were selected as the most prospective approaches. In the basic partition of the control system, switching control layer that enables power electronics to behave as an adaptive system was found of primary importance from the viewpoint of power economical performance.

4. Careful analysis of switching patterns for IGBT inverters has revealed the progressive role of SVM as a very robust signal processing method where quick and precise response can be achieved in variable-speed drive applications. An important benefit of SVM lies in the possible denial of excess commutations of IGBT switches in favour of the commutation between some preliminary selected states. However, this is often achieved through abandoning the sinusoidal output that results in additional losses caused by higher harmonic components. Therefore, the problem of synthesis of the new switching patterns was formulated which should provide power economical performance for IGBT inverters of induction motor drives.

## **2. SIMULATION STUDY OF INDUCTION MOTOR DRIVES WITH IGBT INVERTERS**

In this chapter the new models and simulation techniques are proposed to explore the power converters feeding induction motors. For the first time, a comprehensive comparative analysis of different simulation toolkits is done from the viewpoint of their suitability for the simultaneous simulation of mechanical, electrical, and electronic processes. As voltage disturbance caused by modulation has an undesirable effect on the speed controlled drive, it is important to study the converter performance in disturbed voltage conditions. For this purpose different modulation methods were implemented in Matlab/Simulink environment and multiple model components have been developed. To validate simulated results, experimental tests and marketable tools were used.

### **2.1 Comparative Analysis of Power Converter and Motor Drive Simulators**

#### **2.1.1 Role of Simulation in Motor Drive Design and Study**

Simultaneously with increasing of the complexity of the motor drive circuits and systems, the role of simulation as an analyzing, verifying, and project tool has expanded significantly. As the list of power converter properties is extremely rich, their simulation meets many problems in the contemporary design and maintenance technologies. Advanced control and estimation normally require extensive computer simulation study, prior to breadboard or prototype development. In this way, simulation has become a cost-efficient way to begin the design process. Starting with original diode and thyristor phase-controlled converters, as novel devices emerged, many progressive simulation methods were born along with the new converter topologies. Therefore, both the large- and the small-signal simulators of motors, power converters, and control circuits are performed now to better predict and verify projects [7].

Computer models help specialists in solving their problems. A model is the main component of the development, study, and maintenance procedures, as well as the heart of software. It is of major importance that an effective model should involve some structural and information redundancy to be taken into account in the future progress of the simulating object [58] [59]. Simulation is an important step in understanding the nature and performance of a system. The act of simulating generally entails representing certain key characteristics or behaviors of a system, device, or studying process. An effective library of models serves as a suitable tool of the system design and exploring. The models help to examine and predict various situations occurring in an exploring system. Moreover, the models may be useful to plan the processes and to carry out different performance steps.

Effectiveness of a power converter depends on how well its characteristics fit into an application. Quality of the steady-state mode of the converter operation is evaluated by the static curves, such as the input curves, output curves, and control curves. To find the system dynamic index and to obtain the required speed of operation, the transfer functions, frequency responses, and timing diagrams are to be studied by the simulators. As a properly designed converter should have acceptable performance with regard to both the steady-state operation and the transient response, the simulation arrangement should support the system maintenance in both types of processes [13].

In view of the absence of the ready-to-use models that meet the thesis problems and tasks, the new models and simulation techniques are developed and described in this thesis to explore the power converters feeding the induction motors.

### **2.1.2 Overview of Toolboxes Used in Power Electronics and Motor Drives**

The state-of-the-art of information technologies opens up the broad possibilities in the development of power converter models. The most popular kinds of software are the toolboxes that operate in the uniform simulation environment [60] [61]. Among them such widespread tools as *Matlab/Simulink* from MathWorks, *PSIM* of PowerSys, *LabVIEW*, *Electronics Workbench* and *Multisim* of National Instruments, *Spice* from OrCad, and *Vissim* of Visual Solution are used. Other tools are *Saber*, *EMTP*, *ACSL*, *MatrixX*, *C++*, etc. Most of them suit for the design and research of automation systems or their components. The main advantages of the listed systems are their powerful mathematical backgrounds, high quality of sheets, graphics, and computing data presentations, as well as an interconnection with hardware and operation systems with comfortable adaptation to computers of different styles and productivity.

*Multisim* [62] is known as the powerful simulation tool for electronic design purposes. Its main modules anticipate the types of converters and only simulate these. Each of the components - an R-, L-, C-element, diode, transistor, thyristor, etc. - is inserted into the object and then the behaviors of the system are simulated and the overall system performance is presented. Modelling in *Multisim* enables a clear analysis of all electronic circuits, parameter variation within a broad range, and result evaluation with virtual measurements. The libraries of *Multisim* are well suited for electronic needs, providing the levels of passive components, amplifiers, and switches, from ideal to precision dynamic models. Its built-in tools enable data processing, frequency analysis, and interfacing with other simulation instruments, such as *Spice*, *Simulink*, and *LabView*. The toolkit has:

- a comprehensive database of more than 17500 devices and simulation models;

- integration with real measurement data for custom design verification;
- advanced management including project packing, version control, and the sheet view;
- supporting of *Ultiboard* layout for complete and streamlined prototyping.

Unlike *Multisim*, *PSIM* [63] is modern simulation software for power electronics, motor drive, and dynamic systems. This rapidly growing technology joins the automation and reasoning capabilities of computing. A complete *PSIM* system provides all the necessary tools for electromechanical system simulation including data collection, verification, analysis, resolution, and tracking. The *PSIM Basic* package consists of three programs: circuit schematics, *PSIM simulator*, and waveform display program *Simview*. *PSIM Basic* can be used for the analysis and design of power converter and control systems for a wide variety of applications, including:

- rectifiers, inverters and cycloconverters;
- active filters;
- battery charges;
- grid-link operations;
- power factor correctors and reactive power compensators;
- power components and adjustable speed drive systems;
- UPS systems and switch-mode power supplies.

Its comprehensive library contains numerous electrical engineering items to design power structures, system components and control loops within the scope of electrical engineering items:

- power circuits, such as RLC branches, switches and transformers;
- control circuits, including filters, function blocks, logical and commonly used elements;
- voltage, current, and time sources;
- others components, such as switch controllers, sensors, probes, and non-linear elements;
- PWM circuit components;
- zero-voltage-switching and zero-current-switching converters.

Simulation of motor drive systems is a non-trivial problem, from motor modelling to control. These tasks become much easier and simpler with *PSIM* because the motor drive module *MDM* is an add-on of *PSIM* software. It provides all the necessary elements for motor drive system studies. Different



machine and mechanical load models are available, and various control schemes can be implemented using the *PSIM* control library. *MDM* contains the following elements:

- 3-phase squirrel-cage and wound-rotor induction motors (linear and with saturation);
- dc machine;
- speed controlled brushless dc motor;
- permanent magnet brushless dc machine with trapezoidal electromotive force;
- permanent magnet and externally-excited synchronous machines;
- switched reluctance motor;
- general-type mechanical load with constant torque, constant power, or constant speed;
- gear boxes;
- torque and speed sensors.

The third toolbox is *Spice* [32] [33] [39] - the general-purpose open-source analog electronic circuit simulator. This powerful program is used in integral circuit and board-level design to check the integrity and to predict circuit behavior. *Spice* combines operating point solutions, transient analysis, and various small-signal analyses with the circuit elements and device models needed to simulate many systems. The software includes tools for the noise and transient analysis and parametric sweeps to analyze circuit performance with changing manufacturing tolerances or operating conditions. Loop gain and stability calculations, harmonic balance, and time-domain steady-state analyses improve the circuit design.

*Spice 2* includes many compact models of semiconductor device - three levels of the MOSFET model, a combined Ebers-Moll and Gummel-Poon bipolar model, and a model for a junction diode. In addition, it has many other elements, such as resistors, capacitors, inductors, independent voltage and current sources, ideal transmission lines, and voltage and current controlled sources. Into *Spice 3* sophisticated MOSFET models are accrued, which follow the advances in semiconductor technology. Commercial and industrial *Spice* simulators have added many other device models as technology enhanced and earlier models became inaccurate.

Today, *Matlab* is in high demand in the motor drive research [36]. It is a high-level 4<sup>th</sup> generation programming language and interactive environment that enables users to perform fast calculation-based tasks. The toolbox allows matrix manipulation, functions and data plotting, algorithm implementation, creation of the user interfaces, and interfacing with programs in other languages. *Matlab*

has been widely adopted for over 25 years in the academic community, industry and research centers. This software provides the users with a large collection of toolboxes and modules for a variety of applications in many fields of interest.

*Simulink* as an interactive graphical tool was added to *Matlab* to make the modeling and simulation of various systems as easy as connecting predefined and designed building blocks. *Simulink* contains many block sets that are used in almost all applications, such as the communication block set, signal-processing block, etc. [37] [38]. One advantage of *Simulink*-based simulation is that part of the modelling program can be translated to C++ language, and the corresponding object code can be used for the real-time controller implementation. It is remarkable that *Simulink/SimPowerSystems* [64] is gaining almost universal acceptance in power electronics.

Numerical simulators, including the *Silvaco* package, *Medici*, etc. are also available for circuit simulations. Among them, *Saber* is a comprehensive multi-technology circuit simulator which has strong program capability. Although giving accurate results, they are not suitable for normal users because they require device manufacturing parameters and are costly and time consuming. However, these numerical simulation packages are useful for device manufacturers since they offer a reduced design cost and period.

### 2.1.3 Comparison of Toolboxes in View of the Drive Application

Comprehensive comparative data of the toolboxes are presented in Table 2.1. For the comparison, the classification criteria suitable from the motor drive viewpoint were suggested. Based on these criteria, all the compared quantities were distributed between six layers. Currently, the term “virtual” is used here to designate the common-mode models the data of which are specified by the user. The “ready-to-service modules” are the virtual model blocks comprising the elementary electronic components, the data of which are specified by the user. The “manufacturer’s databases” are the models of the ready-to-service products applied for simulation without their change by the user.

As the table shows, the most suitable tools for the power converter development and study are *Matlab* and *PSIM*. To design the low-signal electronic circuits, *Multisim* (and *Spice* as well) has the best set of simulation quantities. On the other hand, they do not fit the requirements of studying the drive. They provide almost no possibilities to study electrical motors in different modes of driving operation and to design an electrical drive using the ready-to-service components from the industrial databases. Therefore, *PSIM* and *Simulink* serve as the main candidates to solve the creation and exploring problems of the power converters for the driving applications.

Table 2.1 Simulation quantities of toolboxes

Quantity	PSIM ver. 6	Matlab ver. 7	Multisim ver. 9
Simulation of IGBT power switches			
Overall number of parameters of virtual IGBT	4	8	0
Number of manufacturer's databases of IGBTs	0	0	1
Simulation of electronic components, besides IGBTs			
Overall number of types of virtual component simulators, including	83	90	>400
the number of virtual transistor simulators	4	2	20
the number of virtual diode simulators	3	1	5
the number of virtual passive circuit simulators	7	28	>70
the number of virtual analogue and digital circuit simulators	80	29	>100
the number of virtual source simulators	33	7	32
Number of manufacturer's databases of electronic components besides IGBTs	0	0	>100
Simulation of the ready-to-service modules of power converters			
Overall number of types of virtual converter simulators, including	8	2	5
the number of virtual ac/dc converter simulators	6	3	1
the number of virtual dc/ac converter simulators	2	3	0
the number of virtual ac/ac converter simulators	0	0	1
the number of virtual dc/dc converter simulators	2	0	3
Number of manufacturer's databases of power converters with the ready-to-service modules	0	0	0
Simulation of induction squirrel-cage motors			
Number of winding parameters	5	5	6
Number of other electrical parameters	3	3	0
Number of mechanical parameters	2	2	0
Number of manufacturer's databases of induction squirrel-cage motors	0	0	0
Simulation of electrical drives besides induction squirrel-cage motors			
Overall number of types of virtual motor simulators	5	4	5
Number of manufacturer's databases of motors, besides induction squirrel-cage motors	0	0	0
Overall number of types of virtual gearbox simulators	1	8	0
Number of manufacturer's databases of gearboxes	0	0	0
Overall number of types of virtual loop controllers	0	3	0
Overall number of types of virtual sensors	6	1	>20
Overall number of types of virtual filters	4	24	1
Exploring and analyses			
Overall number of types of virtual measuring devices	12	12	>30
Overall number of types of virtual signal generators	6	16	>10
Steady-state analysis	0	1	3
Transient analysis	4	4	>5
Frequency analysis	0	1	1
Spectral analysis	0	1	1

### **Resume of 2.1**

As the model is an inherent part of any design system, the simulation toolboxes were thoroughly studied in this section. With that end in view, the classification criteria suitable for the motor drive study were suggested. The comparison of the main toolkits resulted in the conclusion that the toolbox which should fully satisfy the motor drive design conditions is absent in the software market. Nevertheless, some toolkits are beneficial for the power converter design and exploring, such as *PSIM* and *Matlab/Simulink*. To resolve this contradiction, the search of the suitable interaction of different toolboxes and marketable software should be performed.

## **2.2 Physical Prototypes for Validation of Motor Drive Models**

### **2.2.1 Requirements to Physical Prototyping**

It is a well-known fact that even modern simulation programs cannot perfectly represent all parameters and aspects of real equipment. The accuracy of the simulation results depends on the accuracy of the component models and the proper identification and inclusion of auxiliary circuit elements such as parasitic inductance, capacitance and mutual coupling. Accuracy of component models in this context shall not mean that the model is actually faulty but rather that the limitations of the model are exceeded. In particular, the precise prediction of voltage and current traces during the fast switching transitions in power electronics circuits has been proven to be difficult. In addition, numerical convergence is often a problem, if the gate driver signals, with rise and fall times as steep as in real circuits, are applied.

As exact prediction of waveforms and parameters during switching transitions and steady-state operations is impossible, verification of the simulated characteristics generated by different models is an important stage of the comparative analysis.

To prepare a model, to test it, and to identify the results of a particular drive application, two types of physical prototypes are required.

First, an extraction sequence is needed to determine the values of all of the model parameters by measurements [35]. Therefore, as the first experimental setup, the marketable high-quality motor drive intended for identification should be applied. The identification procedure is divided into a sequence of steps where only a few unknown parameters are obtained at each step. This can be done by selecting electrical and mechanical characteristics that isolate a few unknown parameters at a time and fitting the measured data to the corresponding model. The parameters obtained at each step are then used as known values in subsequent steps. Parametric acquisition requires the ability to make precision calculations on waveforms obtained from computer-controlled instruments. The basic measurement system used to do this normally consists of

a computer that controls power supplies, a waveform digitizer, and a curve tracer. A typical extraction procedure sets parameters of the electronic instruments, initiates the measurement, and transfers the data to the computer where it is analyzed using model equations. Data acquisition software requires the features and options for parameter extraction in a wide range of device types and needs in a user interface with controls and displays for user interaction. Therefore, this setup must provide the capability to control instruments, retrieve data from the instruments, perform curve fitting and interpolation, calculate model equations, and support a user-friendly graphical interface.

The second experimental setup is to be designed to provide all the experiments needed for exploring the developed models and to verify the proposed control techniques.

### 2.2.2 ABB Setup for Motor Drive Identification

To compare simulation results obtained in different toolboxes with the prototype, a workplace was organized intended for identification procedures (Figs. 2.1 and 2.2) [65]. It includes two ABB ACS800 series motor drives, the testing drive and the loading one. Each drive has the same topology, consisting of an induction motor, power converter, remote console, as well as the cabinet, housing, measuring, and cabling equipment. The motor shafts of the drives have been mechanically coupled to provide their joint rotation. Both power converters are wall-mountable low-harmonic units supplying the motors. Each includes the line-side active rectifier and the motor-side inverter connected via the dc link.



*Fig. 2.1 View of the ABB ACS800 experimental setup*

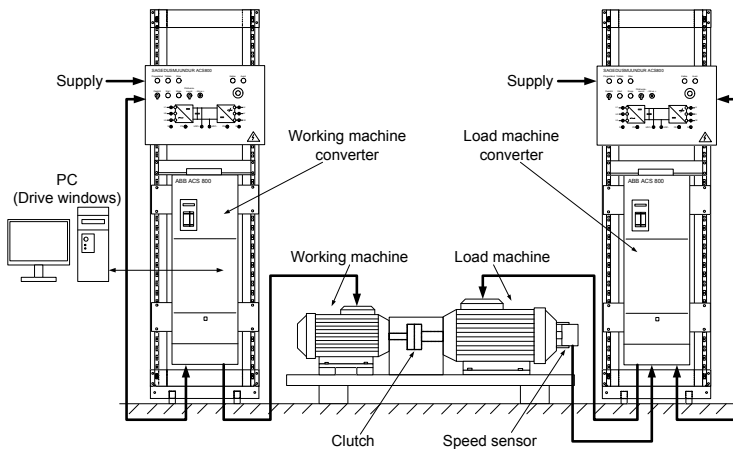


Fig. 2.2 Functional diagram of the ABB ACS800 setup

A typical drive cabinet contains:

- a power converter;
- a cooling fan under the top cover;
- a control drive panel mounted on the front cover;
- heat sink on the back side;
- a connection box under the bottom cover.

The main circuit diagram of a single motor drive is shown in Fig. 2.3. Each converter involves two modules coupled via a dc link. Both the line-side rectifier and the motor-side inverter have six IGBTs (SKM 145 GB 124 DN) with freewheeling diodes. In the motoring mode, the line-side rectifier passes the three-phase ac voltage into the intermediate dc link, which further supplies the motor-side inverter running the motor. Instead, in the braking mode, the motor-side inverter passes energy back from the motor to the supply lines through the dc link and the line-side rectifier. The line filter suppresses voltage and current harmonics. Electrolytic capacitors in the dc link serve for energy buffering. By default, the converter dc link voltage reaches the peak value of the line-to-line voltage and if necessary can be set also higher. The IGBT gating is based on the SVM modulation principle. To calculate the switch turn on/off instants and fault protection, the line currents and the dc link voltage are measured automatically by the converter sensors.

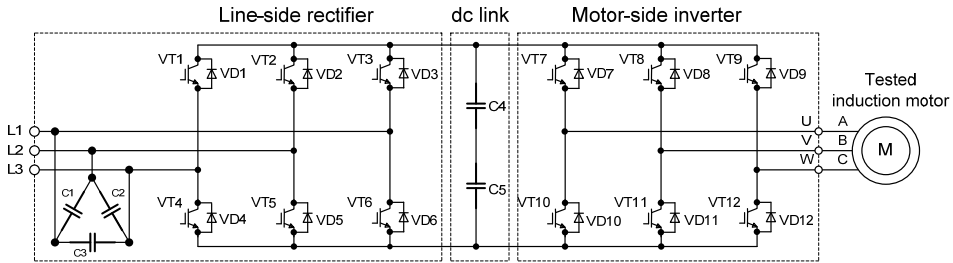


Fig. 2.3 Main circuit diagram of a single motor drive ABB ACS800

Power converters ACS800 enable two modes of operation - voltage / frequency control and direct torque control with direct and indirect measuring of the motor speed, torque, and current. Their technical data are as follows: input voltage 400 V, output voltage 0 to 415 V, output frequency from 8 to 300 Hz, and output power 15 kW with the speed and torque scalar and vector control, flux and mechanical braking, acceleration and deceleration ramps.

To control electric drives, the *DriveWindow* software has been installed. *DriveWindow* of ABB is integrated laboratory instrumentation software that includes libraries, analysis routines, and user-interface tools. It incorporates a large body of instrument drivers that simplify communication with electronics. A wide array of controls such as knobs, meters, gauges, dials, and graphs are provided. This facilitates the user control of the program operation, features selection, and visualization of the acquisition process.

The tested motor M3AA 132S has the following characteristics: rated power 5.5 kW, voltage 400 V, current 11 A, speed 1460 r/min, torque 36 Nm, moment of inertia 0.038 kgm<sup>2</sup>. The loading motor M3AA 160L has the following characteristics: rated power 15 kW, voltage 400 V, current 29 A, speed 1460 r/min, torque 98 Nm, moment of inertia 0.102 kgm<sup>2</sup>.

In experimentation the DC link voltage was kept at 564 V and sampling frequency 6 kHz. Table 2.2 summarizes the THD analysis obtained from this setup, which was carried out with Tektronix Digital Storage Oscilloscope TPS 2024.

Table 2.2 THD analysis of experimental study for ACS800

Frequency, Hz	Load, Nm	THD, %	
		Voltage	Current
50	0.1	54.3	2.7
	36	53.9	2.4
40	0.1	79.5	3.5
	36	81.4	2.3

Figure 2.4 shows the timing diagrams of the steady-state and starting modes of ACS800 operation.

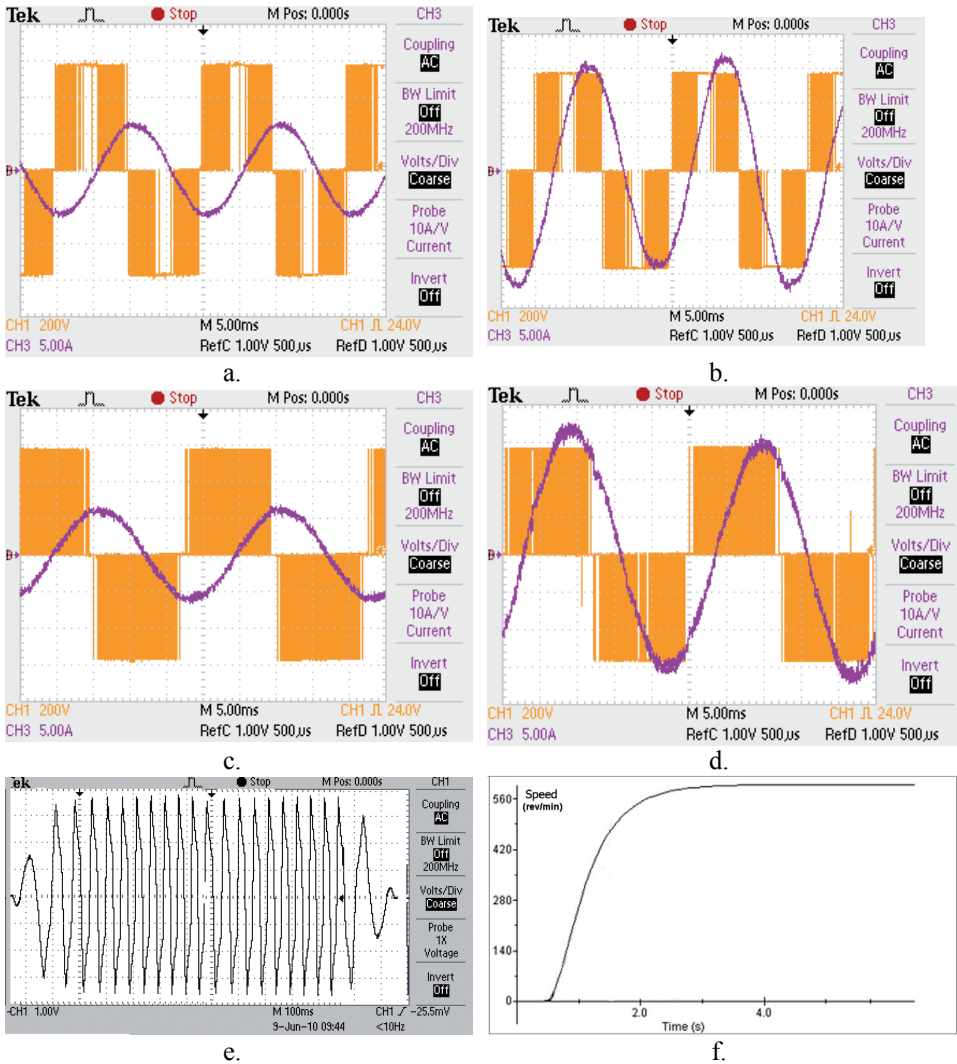


Fig. 2.4 Timing diagrams of ACS800 operation: (a) unload,  $f=50$  Hz, line-to-line voltage and phase current; (b) load,  $f=50$  Hz, line-to-line voltage and phase current; (c) unload,  $f=40$  Hz, line-to-line voltage and phase current; (d) load,  $f=40$  Hz, line-to-line voltage and phase current; (e) phase current at start-up; (f) motor speed at start-up obtained from ABB DriveWindow

### 2.2.3 TUT Experimental Setup

To validate the new modulation patterns and to test their effectiveness, a new experimental setup was manufactured at the Department of Electrical Drives and Power Electronics of TUT. It also consists of two motor drives, the testing drive and the loading one. The motor shafts of the drives are mechanically coupled. Data for the tested induction motor are given in Table 2.3.



Table 2.3 Datasheet of the tested induction motor from TUT experimental setup

Type designation	AE80A4
Output power, kW	0.55
Rated current, A	1.60
Starting current, A	5.30
Rated torque, Nm	3.80
Maximum torque, Nm	6.46
Stall torque, Nm	1.52
Phase voltage, V	220
Speed, r/min	1350
Moment of inertia, kg*cm <sup>2</sup>	29

The loading dc machine has the characteristics presented in Table 2.4.

Table 2.4 Datasheet of the loading machine from TUT experimental setup

Type designation	II-11M
Output power, kW	0.29
Rated current, In, A	2.04
Operating voltage, V	220
Speed, r/min	1500
Moment of inertia, kg*cm <sup>2</sup>	31

To supply it, the three-phase inverter was packed using six IGBTs IRG4PH40KD with ultrafast soft-recovery diodes, 1200 V, 15 A. To feed IGBTs and the loading motor, two programmable dc voltage sources 2TDK Lambda were applied. Gating was provided by 2SD106AI dual-scale driver core from Concept. The diagram of hardware configuration is shown in Fig. 2.5.

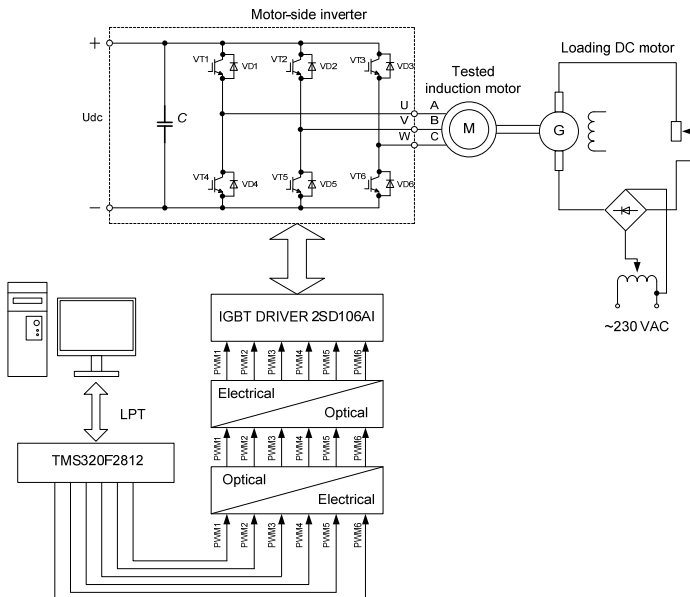


Fig. 2.5 Diagram of hardware configuration of TUT experimental setup

A converter drive board was produced on a TMS320F2812 controller from Texas Instruments at the working frequency 150 MHz, 64 KB on-board RAM and 128 KB on-chip flash memory, which has programmable switching dead time. It generates and converts three switching logic signals to six gating signals and supplies them to the converter bridge for IGBT adjustment. Figure 2.6 shows the photo of the experimental setup and the IGBT drive board.

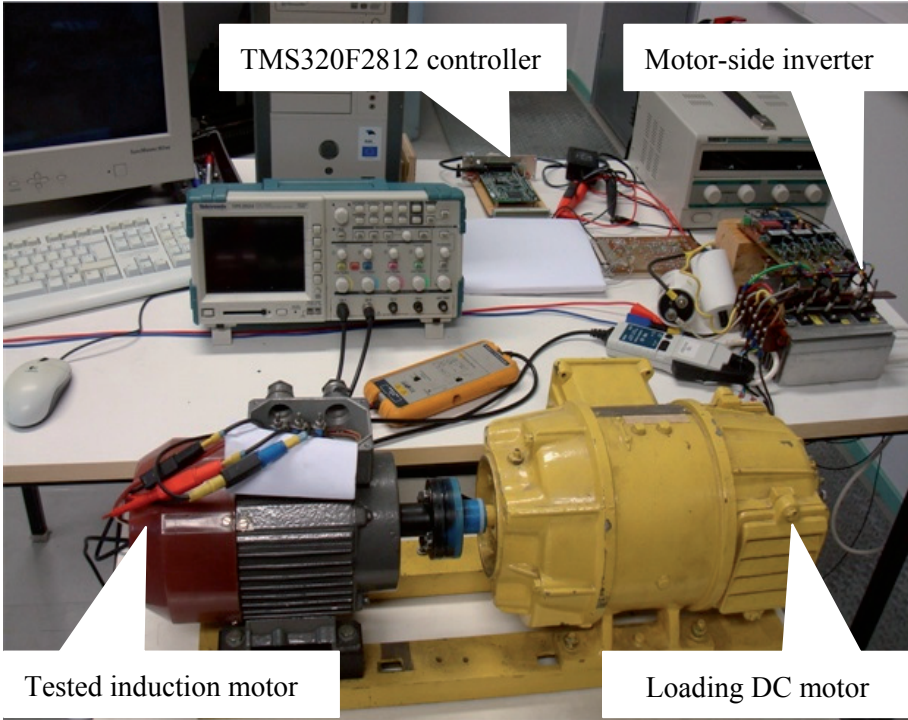


Fig. 2.6 Power and control modules of TUT experimental setup

Table 2.5 presents the THD and ripple analyses obtained from this setup, where a Tektronix Digital Storage Oscilloscope TPS 2024 was used.

Table 2.5 THD and ripple analyses for the experimental study of the six-step technique from the TUT setup

Frequency, Hz	Load, Nm	THD, %		Ripple, %	
		Voltage	Current	Speed	Torque
50	0.1	29.5	36.1	4.7	2.7
	2.1	29.6	34.2	2.2	1.5
40	0.1	29.3	36.9	6.6	4.9
	2.1	29.5	32.7	3.9	1.9

Figure 2.7 shows the control signals and timing diagrams of the steady-state mode six-step operation upon  $U_d = 500$  V and 400 V correspondingly.



Fig. 2.7 Timing diagrams of the six-step operation from the TUT experimental setup: (a) control signals; (b) unload,  $f=50$  Hz, line-to-line voltage and phase current; (c) load,  $f=50$  Hz, line-to-line voltage and phase current; (d) unload,  $f=40$  Hz, line-to-line voltage and phase current; (e) load,  $f=40$  Hz, line-to-line voltage and phase current

Figures 2.8, 2.9 show the control signals and timing diagrams of the steady-state and running modes of PWM operation upon  $U_d = 550$  V,  $k_{mod} = 0.866$  and  $0.693$  correspondingly.

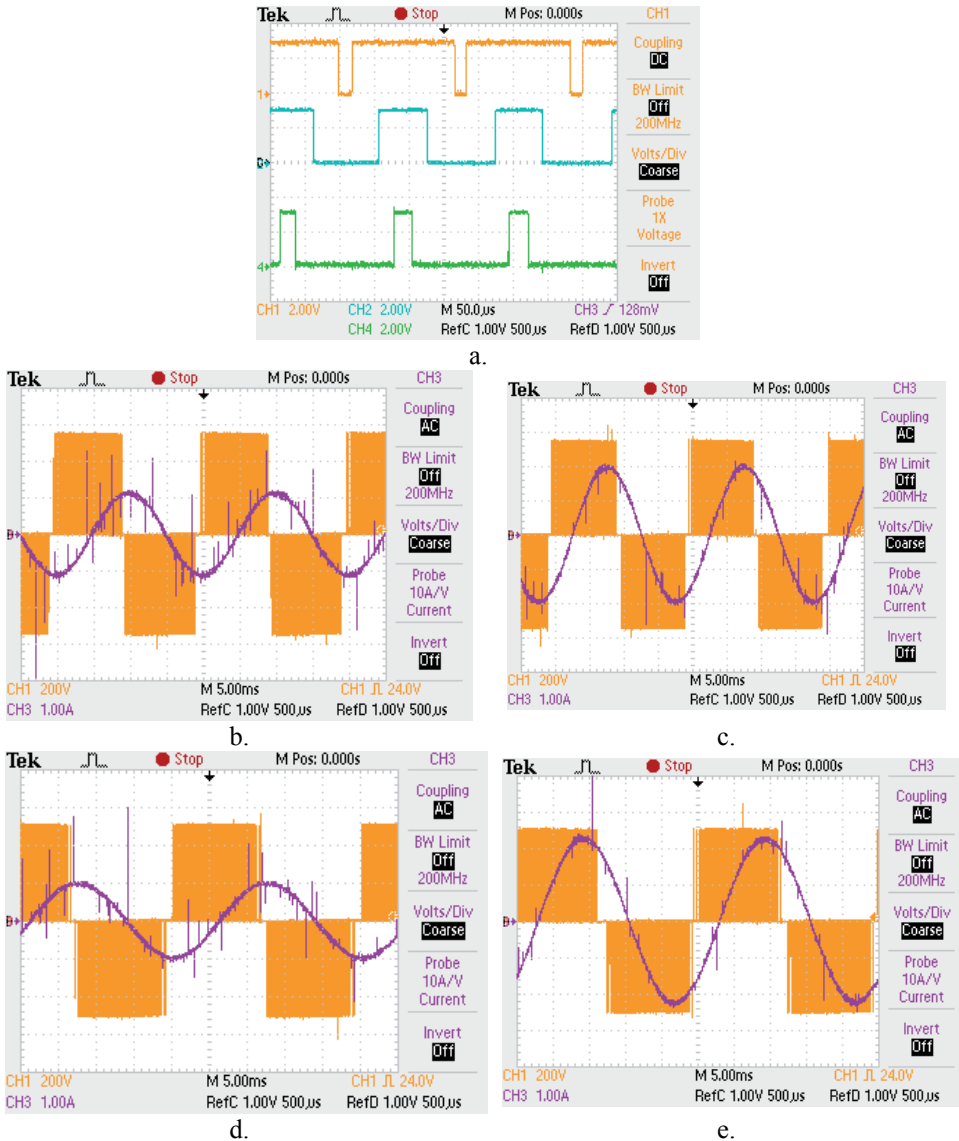


Fig. 2.8 Timing diagrams of PWM operation from the TUT experimental setup: (a) control signals; (b) unload,  $f=50$  Hz, line-to-line voltage and phase current; (c) load,  $f=50$  Hz, line-to-line voltage and phase current; (d) unload,  $f=40$  Hz, line-to-line voltage and phase current; (e) load,  $f=40$  Hz, line-to-line voltage and phase current

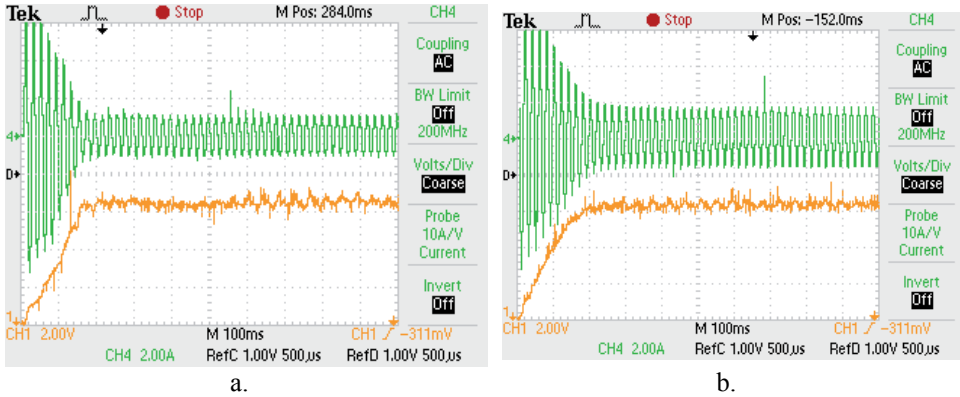


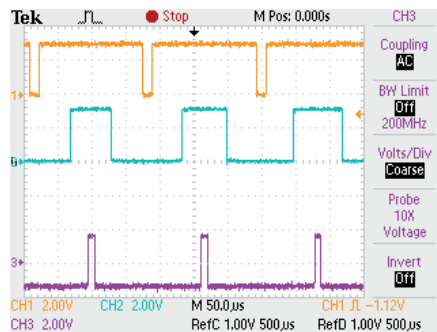
Fig. 2.9 Timing diagrams of PWM operation from the TUT experimental setup: (a) unload,  $f=50$  Hz, starting current and speed; (b) load,  $f=50$  Hz, starting current and speed

Table 2.6 gives the THD and ripple analyses obtained from the TUT experimental setup, the Tektronix Digital Storage Oscilloscope TPS 2024 was used.

Table 2.6 THD and ripple analyses for the experimental study of the PWM technique from the TUT setup

Frequency, Hz	Load, Nm	THD, %		Ripple, %	
		Voltage	Current	Speed	Torque
50	0.1	50.9	4.5	1.4	2.4
	2.1	48.0	3.0	1.2	0.7
40	0.1	65.0	3.6	1.4	3.2
	2.1	62.9	2.9	1.4	0.9

Figures 2.10, 2.11 show the control signals and timing diagrams of the steady-state and starting modes of continuous SVM operation upon  $U_d = 512$  V,  $k_{mod} = 0.866$  and  $0.693$  correspondingly.



a.

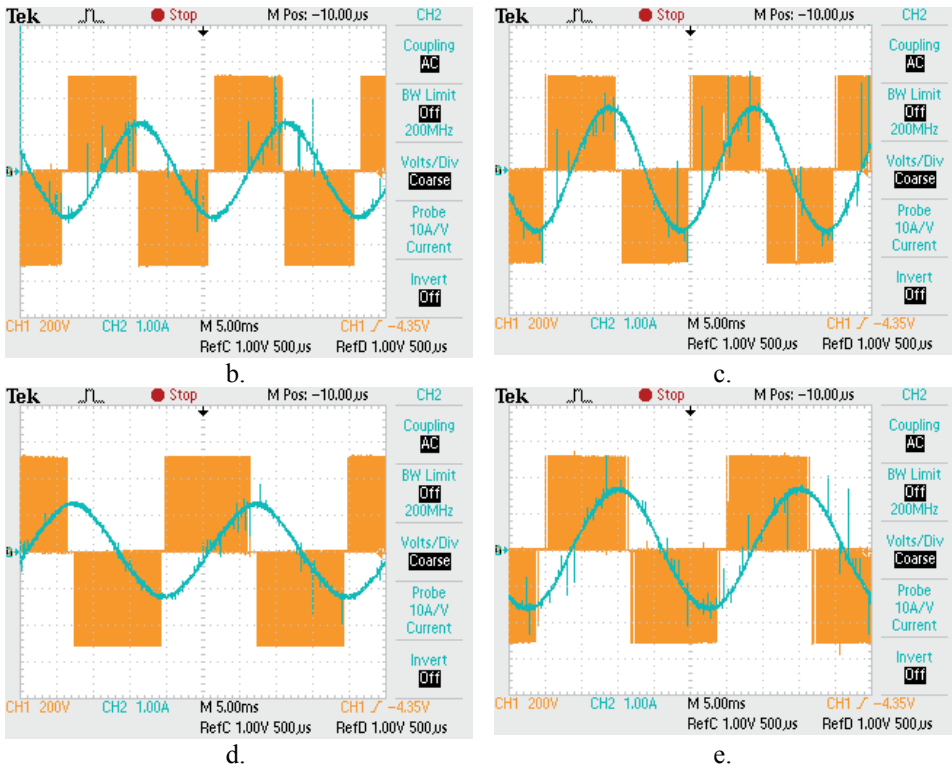


Fig. 2.10 Timing diagrams of continuous SVM operation from the TUT experimental setup: (a) control signals; (b) unload,  $f=50$  Hz, line-to-line voltage and phase current; (c) load,  $f=50$  Hz, line-to-line voltage and phase current; (d) unload,  $f=40$  Hz, line-to-line voltage and phase current; (e) load,  $f=40$  Hz, line-to-line voltage and phase current

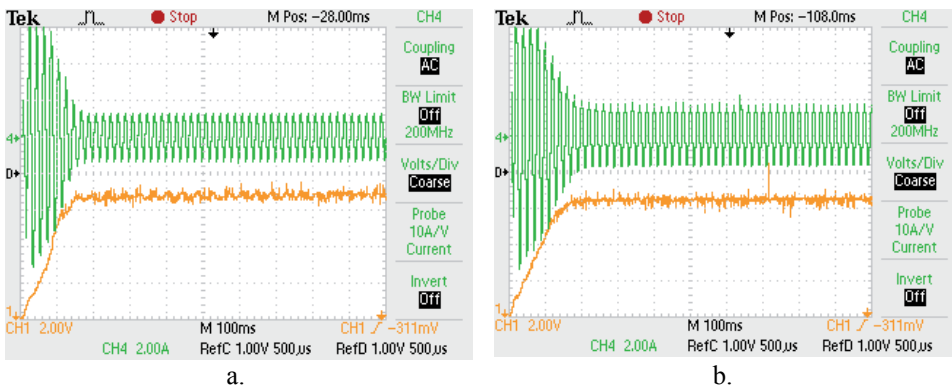


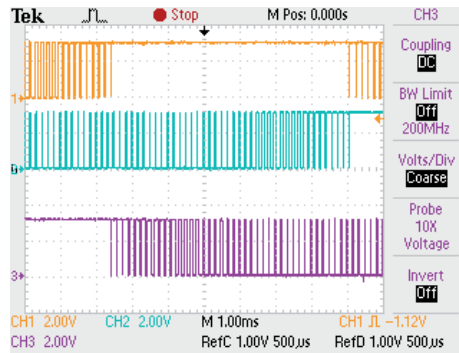
Fig. 2.11 Timing diagrams of continuous SVM operation from the TUT experimental setup: (a) unload,  $f=50$  Hz, starting current and speed; (b) load,  $f=50$  Hz, starting current and speed

In Table 2.7 the THD and ripple analyses are proposed obtained from TUT experimental setup.

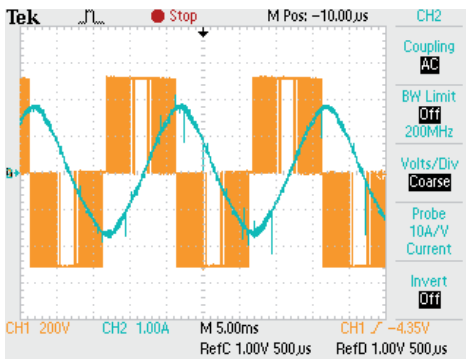
Table 2.7 THD and ripple analyses for the experimental study of the continuous SVM technique on the TUT setup

Frequency, Hz	Load, Nm	THD, %		Ripple, %	
		Voltage	Current	Speed	Torque
50	0.1	38.4	3.9	3.1	2.9
	2.1	38.2	2.4	1.4	0.6
40	0.1	42.8	2.9	3.3	3.5
	2.1	46.1	2.3	1.5	0.8

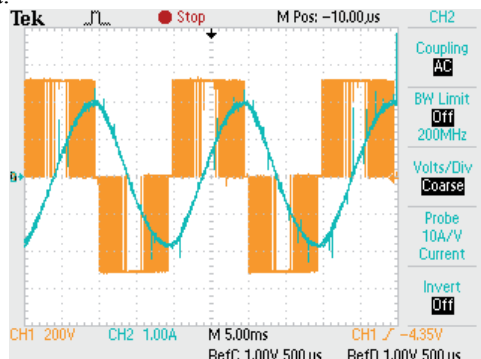
Figures 2.12, 2.13 show the control signals and timing diagrams of the steady-state and starting modes of discontinuous SVM operation upon  $U_d = 512$  V,  $k_{mod} = 1$  and  $0.693$  correspondingly.



a.



b.



c.

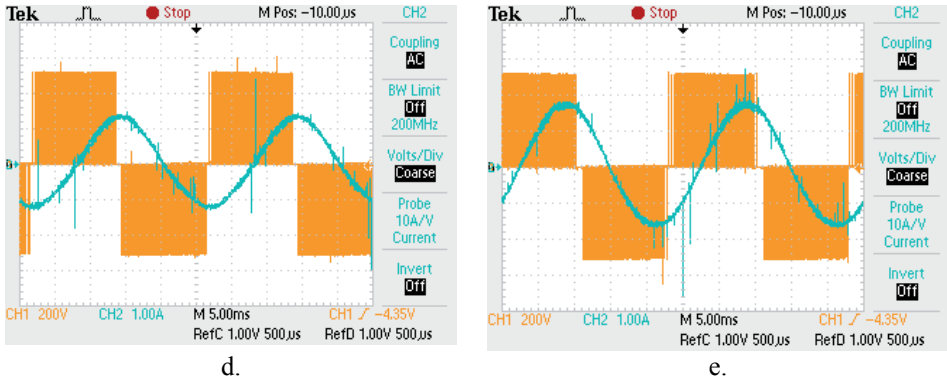


Fig. 2.12 Timing diagrams of discontinuous SVM operation from the TUT experimental setup: (a) control signals; (b) unload,  $f=50$  Hz, line-to-line voltage and phase current; (c) load,  $f=50$  Hz, line-to-line voltage and phase current; (d) unload,  $f=40$  Hz, line-to-line voltage and phase current; (e) load,  $f=40$  Hz, line-to-line voltage and phase current

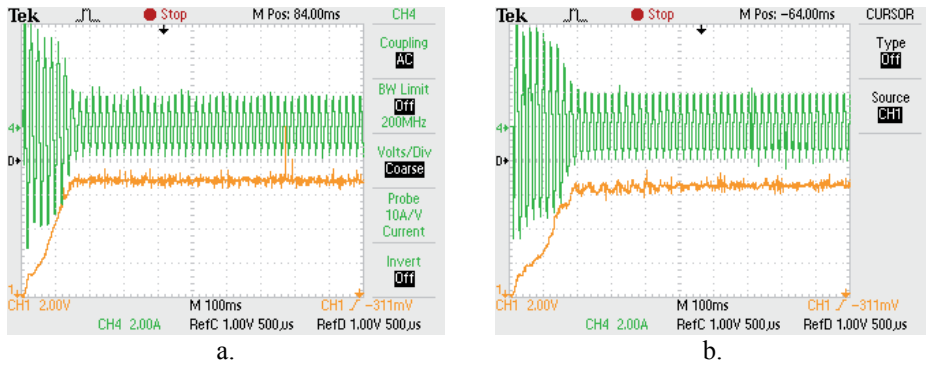


Fig. 2.13 Timing diagrams of discontinuous SVM operation from the TUT experimental setup: (a) unload,  $f=50$  Hz, starting current and speed; (b) load,  $f=50$  Hz, starting current and speed

Table 2.8 presents the THD and ripple analyses obtained from the TUT experimental setup, the Tektronix Digital Storage Oscilloscope TPS 2024 was used.

Table 2.8 THD and ripple analyses for the experimental study of the discontinuous SVM technique from TUT setup

Frequency, Hz	Load, Nm	THD, %		Ripple, %	
		Voltage	Current	Speed	Torque
50	0.1	36.2	5.0	3.0	2.7
	2.1	36.5	4.1	1.1	0.6
40	0.1	55.1	4.6	3.1	5.3
	2.1	56.0	6.8	1.6	0.9



## Resume of 2.2

Even modern simulation programs cannot perfectly present all parameters and aspects of real equipment. This is the reason why verification of the simulated characteristics generated by different models is an important stage of the comparative analysis. In this section, two experimental setups developed in TUT are described. To build the former one, ABB motor drives were used with ACS800 converters equipped with *DriveWindow* toolkit suitable for identification targets. The latter setup built on IR IGBT modules uses the programmable controller suitable for validation of the new control algorithms proposed in the next sections. Experimentation on the steady-state and dynamical operation modes show that different switching patterns can be studied and compared using these physical prototypes.

## 2.3 Modelling of Inverter-Fed Induction Motor Drives in Matlab/Simulink

### 2.3.1 Basic Circuit Topology and Specification

To perform computer simulation, a library of models was developed to investigate the adjustable induction motor drives in *Matlab/Simulink*. The models designed in the simulation environment were equipped with an induction motor, loading device, and independent bridge-connected IGBT simulators (Fig. 2.14). The controller circuit in the study is enveloped in Fig. 1.1 above. Simulation was performed for the voltage/frequency control mode of an induction motor drive using the six-step, PWM and continuous and discontinuous SVM techniques.

The goal of modelling and simulation was to find an adequate description of the processes in power converters and in electromechanical equipment of a motor drive. In turn, the aim of the verification stage was to study the differences of the transient and steady-state characteristics between the tested drive and the simulated ones. The steady-state operation and two motor running modes were compared - direct start-up from the industrial mains and inverter-fed motor running. Both the idle running and the nominal loading operations were examined.

The power converter model was equipped with an independent bridge-connected IGBT simulator where the three-phase bridge inverter shown in Fig. 1.3 consists of three legs with IGBTs and freewheeling diodes. The switches were examined in eight different combinations designated by the binary variables 100, 110, 010, 011, 001, 101, 111, and 000, which indicate whether the switch is under the positive (1) or negative (0) supply, thus defining all possible switching states. With the modulating frequency  $f_m$ , a phase voltage sequentially changed its values depending on which the switches were on-state.

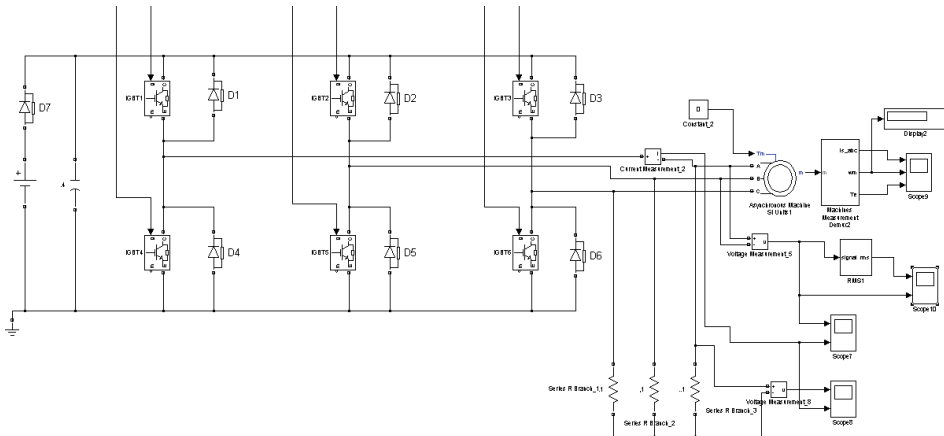


Fig. 2.14 Simulink model of the power section of the induction motor drive

To obtain sufficient resolution, the modulating period is presented by six sectors each divided into 20 sampling periods  $T_c$ . Therefore, the sampling frequency was  $120 f_m$  (max 20 kHz). All the schemes assume digital implementation, therefore calculations were performed at the beginning of each sampling period, based on the value of the reference voltage and speed at that instant. In this way, the reference was updated at every sampling interval  $T_c$ .

To simulate a dc link, *Simulink DC Voltage Source* was used. For voltage and current measuring and tracing, *Simulink Voltage and Current Measurement Blocks* and *Scopes* were linked. *Simulink Series RLC Branches* were used to reach the dc link and load neutral points.

### 2.3.2 Simulation Study of Inverter-Fed Drive with Six-Step Modulation

To generate the six-step control signals, six *Simulink Pulse Generators* were connected directly to the IGBT gate simulators (Fig. 2.15).

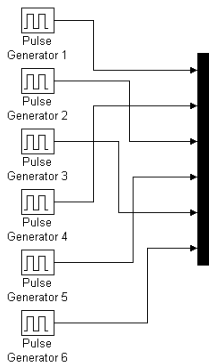


Fig. 2.15 Simulink model of the six-step modulator

Here, switching of the three inverter legs supplied by the dc voltage is phase-shifted by  $120^\circ$  and each of the phases,  $L1$ ,  $L2$ , and  $L3$ , is kept under the current during half a modulating period and open in another half-period. In this way, a

specific phase is alternately switched from the positive pole to the negative one being sequentially in series with the remaining two parallel-connected phases. The neutral, load phase (line-to-neutral) and line-to-line voltages were obtained in accordance with (3.3)-(3.6). For the reversing switches, six switching combinations were designated by the binary variables 100, 110, 010, 011, 001, 101. During the modulating period, a phase voltage sequentially becomes equal to  $\pm \frac{U_d}{3}$ ,  $\pm \frac{2U_d}{3}$ , depending on which the transistors are in the on- and off-states.

The traces of the gate signals, line-to-line voltages, and the phase current for the six-step-driven ACS800 are shown in Fig. 2.16 for the idle and loaded drive running at rated and reduced speeds. In simulation the dc link voltage was kept at 500 V and 400 V correspondingly.

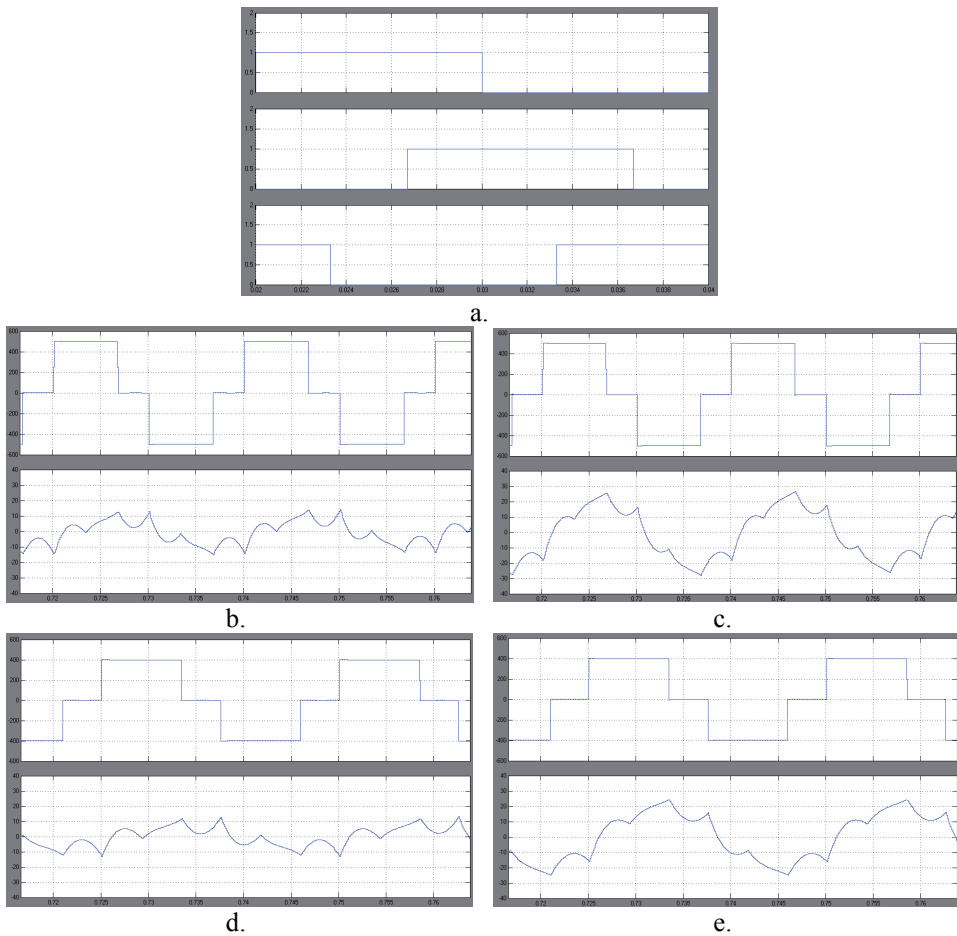


Fig. 2.16 Timing diagrams for six-step-driven ACS800 obtained from Simulink: (a) control signals; (b) unload,  $f=50$  Hz, line-to-line voltage and phase current; (c) load,  $f=50$  Hz, line-to-line voltage and phase current; (d) unload,  $f=40$  Hz, line-to-line voltage and phase current; (e) load,  $f=40$  Hz, line-to-line voltage and phase current

The THD analysis of the timing diagrams is represented in Table 2.9.

Table 2.9 THD analysis of the six-step simulation for ACS800 in Simulink

Frequency, Hz	Load, Nm	THD, %	
		Voltage	Current
50	0.1	30.6	51.6
	36	30.5	21.1
40	0.1	31.0	64.8
	36	31.3	23.3

Another group of results was obtained by the simulation of the TUT experimental setup in the six-step mode of operation. They are given in Fig. 2.17 and Table 2.10.

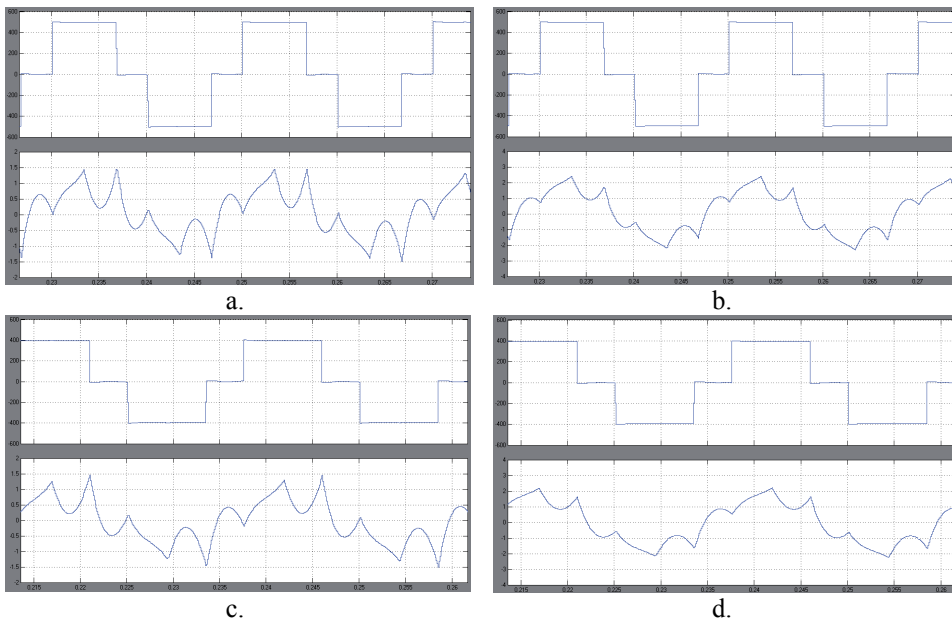


Fig. 2.17 Timing diagrams for the six-step-driven TUT experimental setup obtained from Simulink: (a) unload,  $f=50$  Hz, line-to-line voltage and phase current; (b) load,  $f=50$  Hz, line-to-line voltage and phase current; (c) unload,  $f=40$  Hz, line-to-line voltage and phase current; (d) load,  $f=40$  Hz, line-to-line voltage and phase current

Table 2.10 THD analysis of the six-step simulation for the TUT experimental setup in Simulink

Frequency, Hz	Load, Nm	THD, %	
		Voltage	Current
50	0.1	30.2	28.4
	2.1	30.6	26.1
40	0.1	30.2	29.2
	2.1	30.2	26.5

A simple form of the modulation pattern results in a minimum switching duty of the semiconductor switches. This low switching frequency scheme guarantees fast response along with the significant steady-state tracking error.

### 2.3.3 Simulation Study of PWM Patterns

A model developed to simulate the PWM controller in *Simulink* is presented in Fig. 2.18. It includes three sine-wave generators accompanied by speed-amplitude and modulating index reference blocks, a carrier generator, three comparators. In this way, the symmetrical triangle double-sided wave of the carrier frequency is currently compared with the modulating wave thereby generating the control pulses. The control output represents the chain of constant magnitude pulses the duration of which is modulated to obtain the sinusoidal waveform.

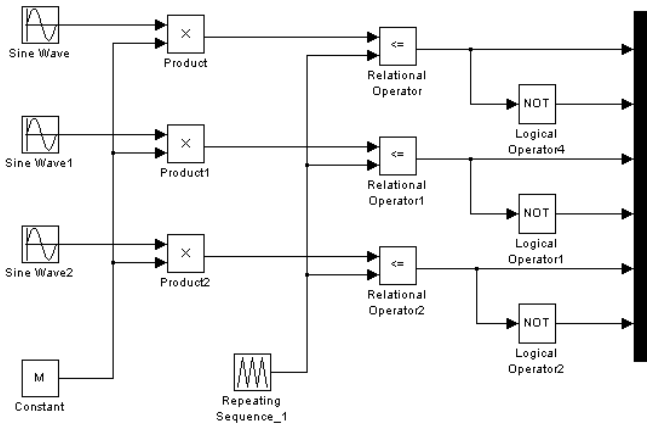


Fig. 2.18 Simulink model of a PWM modulator

The traces of the gate signals, line-to-line voltages, and the phase current for the PWM-driven ACS800 are shown in Fig. 2.19 for the idle and loaded drive running at rated and reduced speeds with a commutation frequency of 6 kHz. In the simulation dc link voltage kept at 630 V.

THD analysis of the simulated timing diagrams is represented in Table 2.11.

Table 2.11 THD analysis of the PWM simulation of ACS800 in Simulink

Frequency, Hz	Load, Nm	THD, %	
		Voltage	Current
50	0.1	30.1	3.7
	36	29.9	1.3
40	0.1	44.3	5.3
	36	44.5	1.1

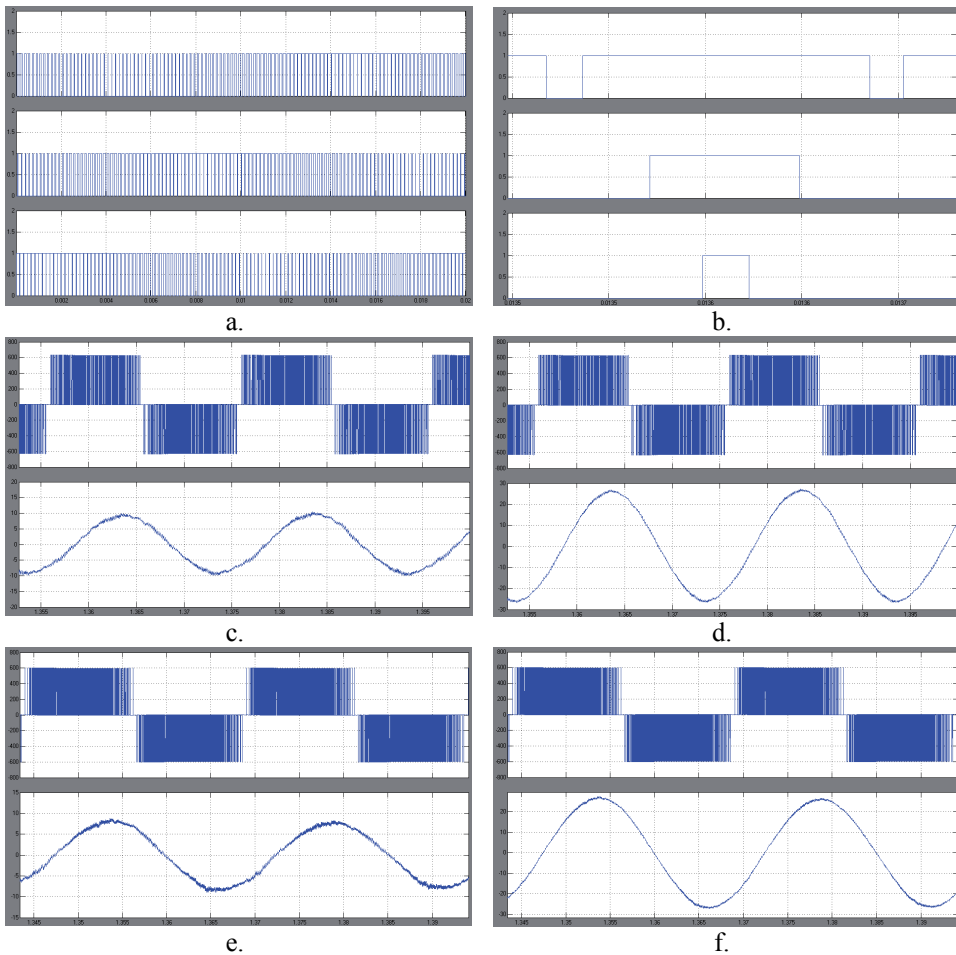


Fig. 2.19 Timing diagrams for the PWM-driven ACS800 obtained from Simulink: (a) control signals; (b) control signals in sector 1; (c) unload,  $f=50$  Hz, line-to-line voltage and phase current; (d) load,  $f=50$  Hz, line-to-line voltage and phase current; (e) unload,  $f=40$  Hz, line-to-line voltage and phase current; (f) load,  $f=40$  Hz, line-to-line voltage and phase current.

The traces of the line-to-line voltages and phase currents for the PWM-driven TUT experimental setup obtained from *Simulink* are shown in Fig. 2.20 for the idle and full-loaded drive running at the rated and reduced speeds upon the commutation frequency 6 kHz.

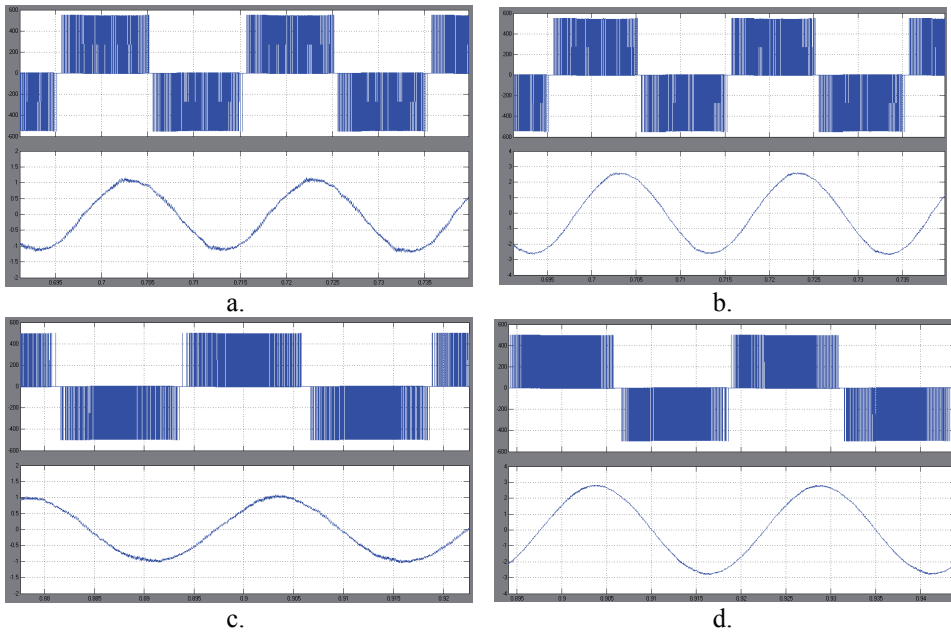


Fig. 2.20 Timing diagrams for the PWM-driven TUT experimental setup obtained from Simulink: (a) unload,  $f=50$  Hz, line-to-line voltage and phase current; (b) load,  $f=50$  Hz, line-to-line voltage and phase current; (c) unload,  $f=40$  Hz, line-to-line voltage and phase current; (d) load,  $f=40$  Hz, line-to-line voltage and phase current.

THD analysis of the PWM simulation for the TUT experimental setup is presented in Table 2.12.

Table 2.12 THD analysis of the PWM simulation of the TUT experimental setup in Simulink

Frequency, Hz	Load, Nm	THD, %	
		Voltage	Current
50	0.1	29.6	2.5
	2.1	30.1	1.7
40	0.1	44.1	2.4
	2.1	44.6	1.5

Simulation opens several problems of PWM inverters in terms of motor drives. They cannot produce as high voltage magnitudes as the six-step inverters can, therefore the supply dc voltage cannot be utilized to the maximum. As the sine PWM inverter prevents the full fundamental voltage from reaching its maximum value, operation at a reduced voltage becomes costly, implying higher currents for a given horsepower requirement. This increased current duty impacts on the choice of switching devices used in the inverters.

### 2.3.4 Simulation Study of SVM Patterns

An SVM controller simulator was designed on the basis of *Simulink* embedded *Matlab* function block where both continuous and discontinuous SVM algorithms were composed and studied (Fig. 2.21). Here, the switching sequence of pulses was searched in each sampling interval, the time durations of which were computed in real time based on the value of the reference voltage and speed at the beginning of each sampling period. Three inputs of the function block carry the reference amplitude, speed and clock signals.

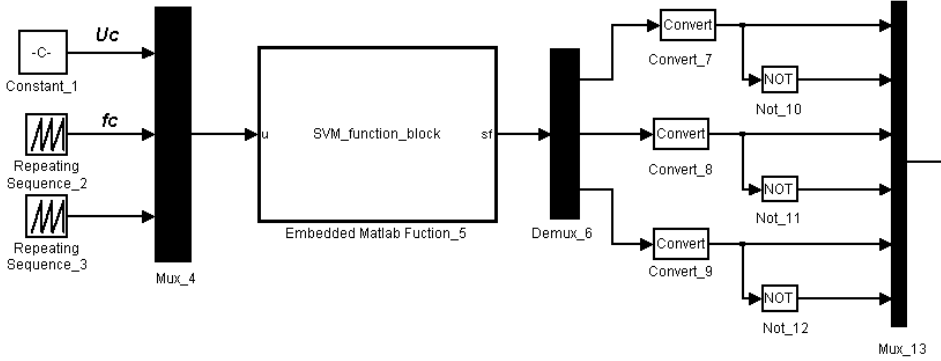


Fig. 2.21 Simulink model of the SVM modulator

The traces of the gate signals, line-to-line voltages, and phase currents obtained from *Simulink* for the continuous SVM-driven ACS800 are shown in Fig. 2.22 for the idle and full-loaded drive running at nominal and reduced speeds with the commutation frequency 6 kHz. In the simulation, the dc link voltage was kept at 564 V and modulation indexes reached 0.866 and 0.693 correspondingly.

THD analysis of the continuous SVM simulation for ACS800 obtained from *Simulink* is presented in Table 2.13.

Table 2.13 THD analysis of continuous SVM simulation of ACS800 in *Simulink*

Frequency, Hz	Load, Nm	THD, %	
		Voltage	Current
50	0.1	67.0	8.3
	36	67.8	2.9
40	0.1	91.0	4.7
	36	90.7	1.5



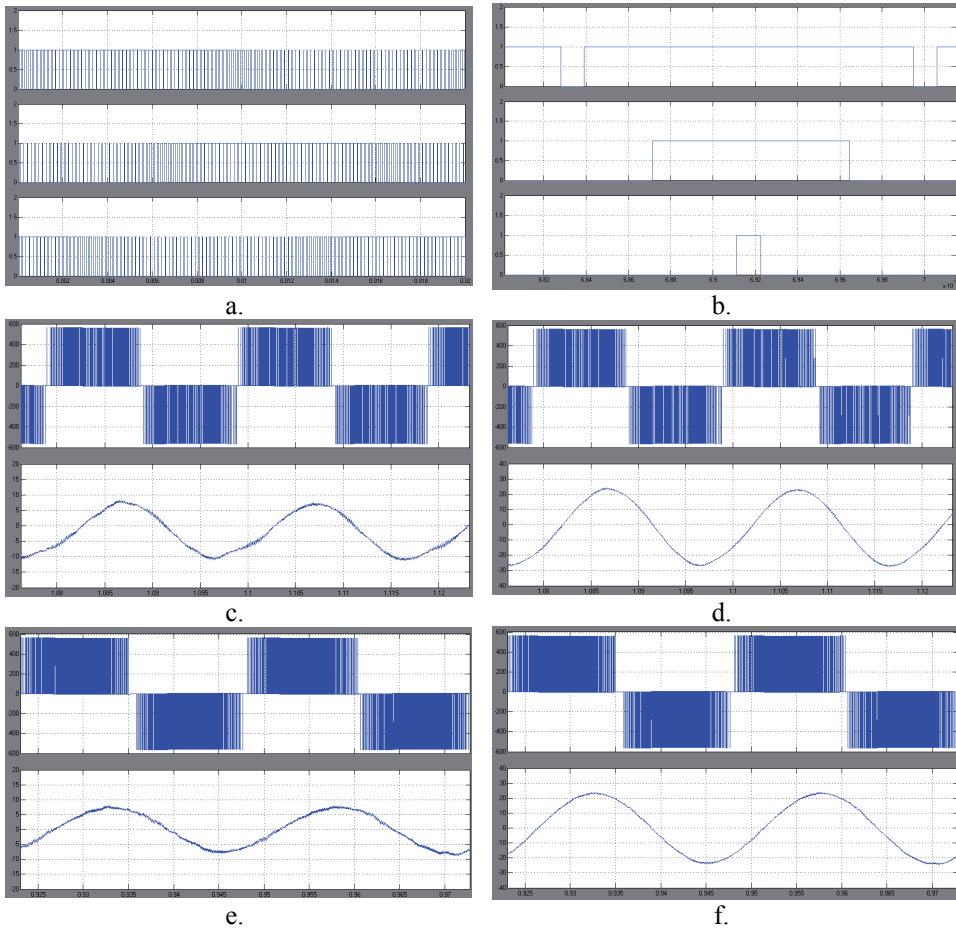


Fig. 2.22 Timing diagrams for the continuous SVM-driven ACS800 obtained from Simulink: (a) control signals; (b) control signals in sector 1; (c) unload,  $f=50$  Hz, line-to-line voltage and phase current; (d) load,  $f=50$  Hz, line-to-line voltage and phase current; (e) unload,  $f=40$  Hz, line-to-line voltage and phase current; (f) load,  $f=40$  Hz, line-to-line voltage and phase current.

The traces of the line-to-line voltages and the phase currents for the continuous SVM-driven TUT experimental setup obtained from *Simulink* are shown in Fig. 2.23 for the idle and full-loaded drive running on the rated and reduced speeds upon the commutation frequency 6 kHz. In the simulation, the dc link voltage was kept at 512 V and modulation indexes reached 0.866 and 0.693 correspondingly.

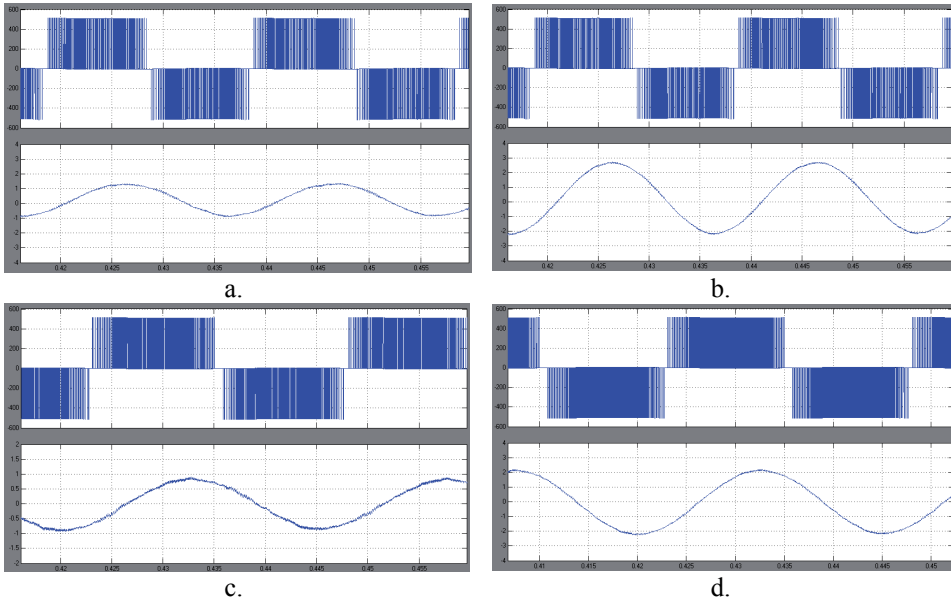


Fig. 2.23 Timing diagrams for the continuous SVM-driven TUT experimental setup obtained from Simulink: (a) unload,  $f=50$  Hz, line-to-line voltage and phase current; (b) load,  $f=50$  Hz, line-to-line voltage and phase current; (c) unload,  $f=40$  Hz, line-to-line voltage and phase current; (d) load,  $f=40$  Hz, line-to-line voltage and phase current.

THD analysis of the continuous SVM simulation of the TUT experimental setup is presented in Table 2.14.

Table 2.14 THD analysis of the continuous SVM simulation of the TUT experimental setup obtained from Simulink

Frequency, Hz	Load, Nm	THD, %	
		Voltage	Current
50	0.1	68.5	3.4
	2.1	67.4	2.6
40	0.1	89.9	2.5
	2.1	91.2	2.1

For the discontinuous SVM-driven ACS800, the traces of the gate signals, line-to-line voltages, and phase currents are shown in Fig. 2.24 for the idle and loaded drive running at the rated and reduced speeds upon the commutation frequency 6 kHz. In the simulation, the dc link voltage was kept at 564 V and modulation indexes reached 1 and 0.693 correspondingly.

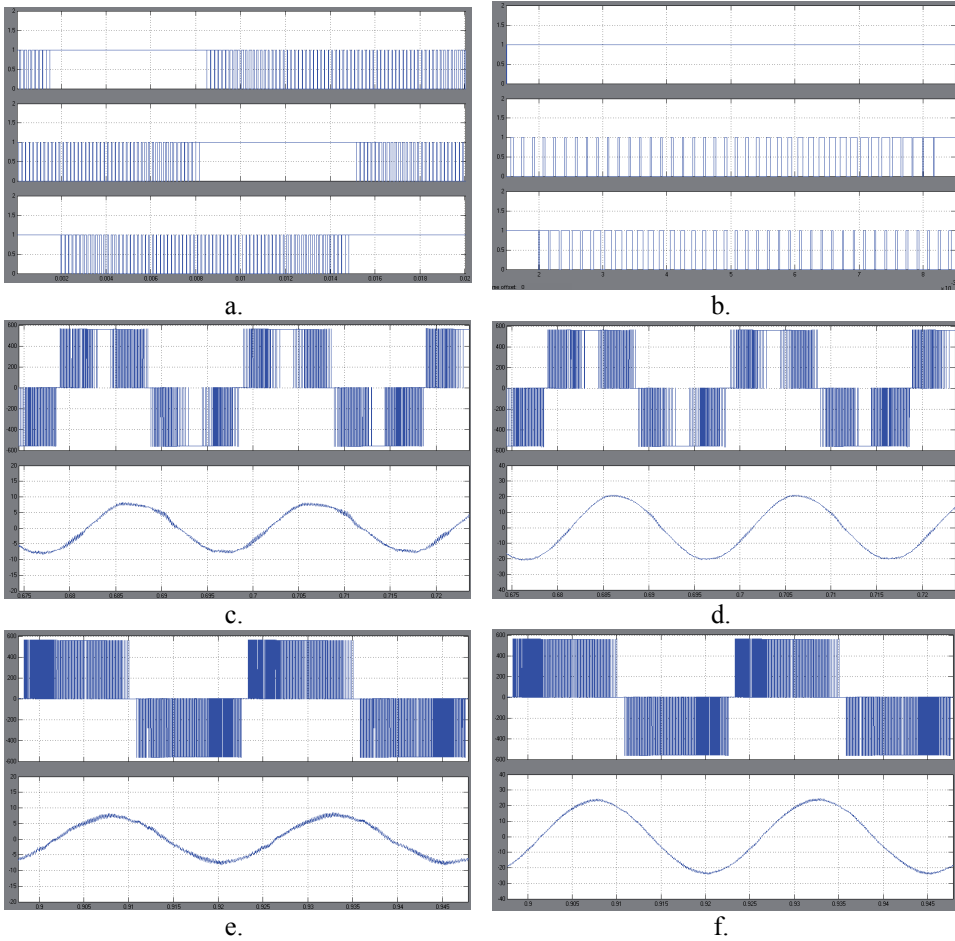


Fig. 2.24 Timing diagrams for the discontinuous SVM-driven ACS800 obtained from Simulink: (a) control signals; (b) control signals in sector 1; (c) unload,  $f=50$  Hz, line-to-line voltage and phase current; (d) load,  $f=50$  Hz, line-to-line voltage and phase current; (e) unload,  $f=40$  Hz, line-to-line voltage and phase current; (f) load,  $f=40$  Hz, line-to-line voltage and phase current.

THD analysis of the discontinuous SVM simulation of ACS800 in Simulink is presented in Table 2.15.

Table 2.15 THD analysis of the discontinuous SVM simulation of ACS800 in Simulink

Frequency, Hz	Load, Nm	THD, %	
		Voltage	Current
50	0.1	52.0	5.6
	36	51.8	2.5
40	0.1	91.2	5.8
	36	91.5	2.4

For the discontinuous SVM driven TUT experimental setup, the traces of the line-to-line voltages and the phase currents are shown in Fig. 2.25 for the idle

and loaded drive running at the rated and reduced speeds with the switching frequency 6 kHz.

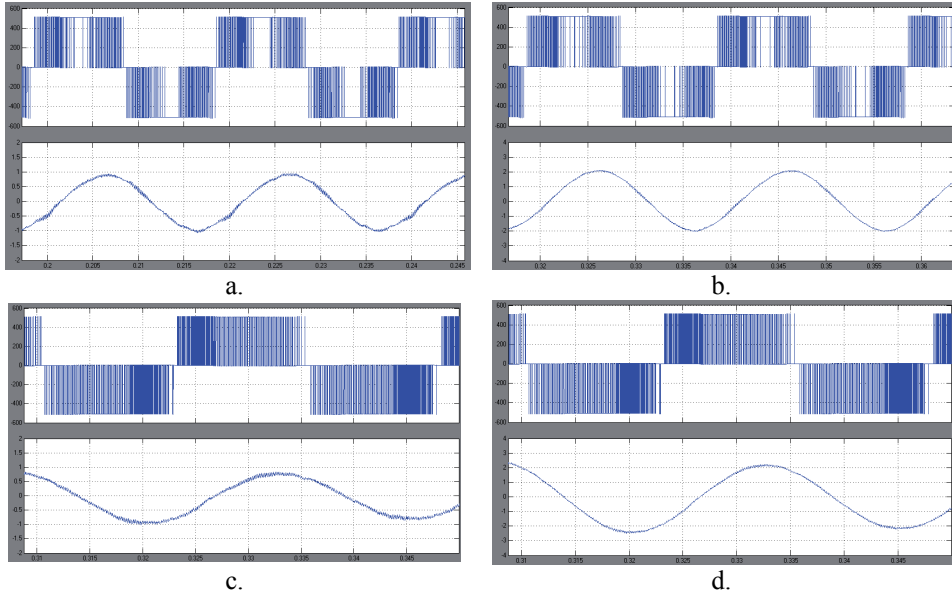


Fig. 2.25 Timing diagrams for the discontinuous SVM-driven TUT experimental setup obtained from *Simulink*: (a) unload,  $f=50$  Hz, line-to-line voltage and phase current; (b) load,  $f=50$  Hz, line-to-line voltage and phase current; (c) unload,  $f=40$  Hz, line-to-line voltage and phase current; (d) load,  $f=40$  Hz, line-to-line voltage and phase current.

THD analysis of the discontinuous SVM simulation of the TUT experimental setup obtained from *Simulink* is provided in Table 2.16.

Table 2.16 THD analysis of the discontinuous SVM simulation of the TUT experimental setup obtained from *Simulink*

Frequency, Hz	Load, Nm	THD, %	
		Voltage	Current
50	0.1	52.3	5.5
	2.1	52.1	4.5
40	0.1	90.7	6.7
	2.1	91.2	4.8

### Resume of 2.3

The library of the motor drive models was developed in the *Matlab/Simulink* environment - low-frequency simple six-step modulation, high-frequency PWM, and progressive space vector modulation. The control systems were studied using the proposed models. Good agreement between simulation and experimental results was obtained. An impact of the modulation method on the voltage and current harmonics was demonstrated. Benefits and drawbacks of different control methods were illustrated in the steady-state and dynamic modes of the converter performance in ac drive applications. Simulation revealed that the accuracy of the reproduction depends on the accuracy of the built-in electronic and electromechanical models. Therefore, torque ripple,

acoustic noise emitted from the motor, and electromagnetic interference could not be studied by this software. The same concerns the auxiliary circuit elements such as parasitic inductance, capacitance and mutual coupling.

## **2.4 Vendor's Software to Explore IGBT with Power Loss and Heating**

### **2.4.1 Problems of IGBT Modelling**

To evaluate and select power equipment, the leading electronic companies have developed specific toolkits. Among them, the guides and software of International Rectifier (IR), Siemens, Semikron, Eupec, ABB, Mitsubishi Electric, etc. are presented. Using the marketable tools, a designer has an opportunity to choose a converter type, to impose restrictions, to estimate results, and to repeat an inquiry on other conditions. Later, one can restructure a list of power modules and circuits and conduct a search in appropriate databases to compose the optimum power system. Then, the control system is developed and the final tuning is executed [18] [66].

Equipment designers have to insure that the power stage operates reliably within the thermal constraints of the application. The fact that they have a handful of IGBT candidates is a step in the right direction, but much work remains to be done to calculate power losses and heat sink size. A number of design tools are commonly available to perform various design functions, including thermal simulation. Some are capable of simulating almost any circuit. Some are very narrow in scope, targeted to a specific topology and operated with a specific control strategy.

IGBT simulation is a major function of the toolboxes, therefore it attracts special attention. IGBT models are required by circuit designers and device manufacturers to predict circuit behavior, to understand device internal mechanisms and to improve structures. Typically, the IGBT model is used in a circuit simulator by selecting a pre-characterized component from the software vendor's library or by extracting the necessary model parameters from terminal electrical measurements. Since the invention of the IGBT in 1982, more than fifty papers have been published on IGBT models [29]. In IGBT modelling, the authors apply different methods and aim diverse objectives, aspects, and performance. Today, various circuit simulators including the *Saber*, *Spice* family discussed above, and some others are commercially available to support the modelling process. Many of such models are used in several simulators.

Table 2.17, built on the basis of research reported in [47] includes the main possibilities and comparative characteristics of the most popular marketable design tools.

Table 2.17. Characteristics of the toolboxes for IGBT module calculation with loss analysis

Toolbox	<i>Semisel</i> (Semikron)	<i>Iposim</i> (Eupec)	<i>Melcosim</i> (Mitsubishi)
Circuit types	3-phase inverter, bridge rectifiers, choppers, ac/ac converters	3-phase inverter	3-phase inverter
Pick temperatures counting	Yes	Yes	No
Overload counting	Yes	No	No
Counting of motor running and frequency control	Yes	Yes	No
Dynamic analysis of overloading	Yes	No	No
Counting of the customer duty cycle	Yes	Yes	No
Possibilities to correct power losses by designer	Yes	No	No
Selection of the cooling method and mode	Yes	No	No
Possibility to describe the cooling parameters	Yes	No	No
Accounting of the number of modules on the heat sink	Yes	No	No
Accounting of additional heat sources	Yes	No	No
Driver calculation	Yes	No	No

The group of mathematical models refers to an analytical description based on semiconductor physics. They solve physics equations with definite simplifications. These expressions can be implemented into different simulators to emulate IGBT behavior for multiple applications. The second IGBT modeling category is the so-called semi-mathematical group. Such models are partly based on physics while combining existing models (in *Spice* family, *Saber*, etc.) for other components. The third model category, known as behavioral or empirical, simulates an IGBT without considering its physical mechanism. The measured IGBT characteristics are fitted by different methods and the resultant expressions, databases, or components are then used in a simulator to describe the IGBT behavior. The last IGBT model category is referred to as a numerical one. In these models, unlike the models discussed in previous paragraphs, the finite element methods are used to describe the devices. Because of the complexity and difficulty in IGBT modelling, multiple numerical methods are often employed which increase simulation accuracy. In some of them, diffusion equations are solved numerically in the discrete base.

Although the models in this category have been implemented into *Saber*, they are often inconvenient for implementation into normal circuit simulators.

One important problem of IGBT simulation concerns the power loss and heat calculation. To perform these analyses, knowledge of the dependences between saturation voltages and currents is required. Appropriate diagrams are usually presented in the manufacturer datasheets along with the transistor resistances. IGBT conduction intervals, transients, and voltage drops are defined there by the circuit topology and temperature. Due to these obstacles, the power loss and heat usually cannot be calculated without the vendors' databases and their specialized software.

#### **2.4.2 IGBT Simulators of International Rectifier**

IR company has deployed several tools. Of particular interest to IGBT users is a tool that calculates the operating condition of a power module in an induction motor drive, known as *The IGBT IPM Evaluation Tool*. It compares performance and efficiency of three different modules and provides a wealth of information, in graphic form and in tabular form, including transient temperature rise during overloads of short duration. One limitation of this tool is that it assumes the backside of the module at a constant temperature. The next generation of tools overcomes this limitation by suggesting a heat sink suitable for the application and calculates the current capability of the inverter as a function of the heat sink size. It provided valuable information at a time when the equipment designer had a limited number of choices and available IGBTs shared similar technologies.

Recently, IR has introduced the software called *The IGBT Selector Tool*. The purpose of the tool is to trim the list of candidates to a handful, sorted out by price or power dissipation. Some key data need to be entered, like voltage, current and frequency, as well as the package type and short circuit rating. The toolkit uses these data to calculate power losses in the specified application conditions and only those devices that would operate at a junction temperature at least 25 °C below maximum rating are returned as potential candidates. Enough heat sinking is assumed to keep the case temperature at 100 °C.

In this toolbox, conduction and switching losses are calculated with the help of statistical IGBT models obtained with a large number of measurements at different currents and temperatures. These models can be profitably used to cross a competitive part to an IGBT from IR. *The IGBT Cross-Reference Tool*, available in the IR website, matches key datasheet parameters from a large number of commonly available IGBTs to one or more part numbers. In the end, despite the availability of tools, the switching waveform in the form of an oscilloscope trace remains as the only device characteristic. This result of the interaction between device features, board layout, and stray parameters has significant implications for one of the most difficult design challenges - electromagnetic conformance to regulations.

### 2.4.3 IGBT Loss Simulator Melcosim from Mitsubishi Electric

This loss simulation program provides a comprehensive means of evaluating many Powerex IGBTs in inverter and chopper type applications [67]. For a given set of operating conditions the loss simulator calculates power module losses and module junction temperatures that aid the design engineer to select the products properly. Three modes of operation are available here, two modulation schemes based on a three-leg inverter topology and one based on a chopper topology. *Loss Simulation Program* is compatible with Microsoft newer *Windows* versions.

The main functions of the program are selected from the main menu bar, the tool bar, and the analysis window organized into four sections:

- *Target Device* - user-defined power module selected for simulation.
- *Application Conditions* - the section to setup the terms that will be used during the simulation under the user-defined operating conditions.
- *Device Data Profile* - the section to display pertinent thermal data for the target device.
- *Calculation Results* - the section that displays different power losses, temperature rises and junction temperatures calculated by the simulation as a function of the application conditions.

A device for the analysis may be chosen in two ways - by selecting the module within the series or by selecting the module from an inclusive list of all the modules in the simulator. In either case, the selected module part number will appear in the main window along with device data profile information being shown and initial application conditions. Having selected the module, the application conditions should be reviewed and changed to meet the application conditions that consist of several parameters that designers may change to fit the simulator to their application:

- modulation scheme used in the analysis (a three-phase sine wave or a single-phase inverter or a chopper circuit typically used in dc/dc converters);
- circuit output peak or rms current;
- circuit dc bus voltage;
- switching frequency;
- gate resistance value;
- output power factor;
- modulation ratio as the ratio of the modulation signal to the carrier signal;
- duty ratio of on time to cycle time in the chopper mode;
- heat sink temperature under the IGBT module.



A separate section displays the results of the simulation (Fig. 2.26).

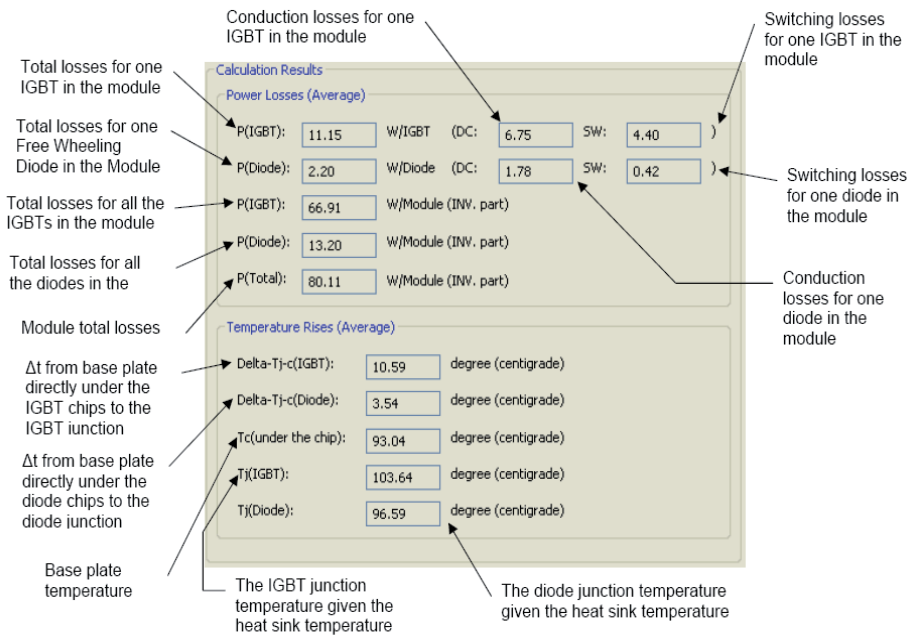


Fig. 2.26 Melcosim section of simulated data

Results are saved in text format that can be pasted into the text editors or word processors for viewing and printing. The same text output can be printed directly.

Ripple is not included in the inverter simulation. The program assumes a sine wave current shape. For the chopper, the program assumes a constant current output (i.e. perfect filtering). As the calculations may be performed beyond the intended ranges of various operating conditions, some calculated results are impossible to achieve in the real world. IGBT calculations are based on 125°C for both conduction and switching. Diode calculations are based on 125°C for switching and 25°C for conduction resulting in losses and temperatures slightly higher than the real world results.

#### 2.4.4 Semiconductor Selector SemiSel from Semikron

The *SemiSel* program (*Semikron's Online Simulation Tool*) [68] is focused on technicians and developers to provide support during the planning of power electronics projects. It calculates the losses and temperatures of semiconductors in typical circuits and helps users to select the correct Semikron products for different applications and operating conditions. The tool has been in use since 2001 and has proven to be very successful. Its database is continually updated as new silicon generations in existing housings are introduced.

*SemiSel* always calculates losses and temperatures as an average value of periodical functions. The results are average losses and, consequently, average

device temperatures. For inverters with high output frequencies ( $f_{out} \geq 50\text{Hz}$ ) this is acceptable. If the frequencies are low in relation to the device time constants, a substantial temperature ripple around the average value has to be taken into account. This ripple increases as the inverter output frequency decreases.

There are four design ways available in *SemiSel*:

- *Step by Step Design* - straightforward calculation.
- *StackSel* - a program part where temperatures and losses of ready assembled power electronic circuits (stacks) from the Semikron Solution Centres can be calculated with various operating conditions.
- *Device Proposal* - a toolkit to provide a selection of suitable devices for given nominal operating conditions and heat sink temperature.
- *DriverSel* - a tool for selection a suitable IGBT driver circuits considering switching frequency, gate charge, peak and average current as well as operating voltage of the IGBT.

For the first three design versions the users should first select the corresponding type of circuit of their application. These are sorted into four basic types of circuits, rectifier (ac/dc), inverter (dc/ac), dc controller (dc/dc), and ac controller (ac/ac). Circuit diagrams support this selection.

A rectifier circuit is used for a single or three-phase rectification. A designer can select one from six rectifier circuits in a bridge configuration:

- B2U - uncontrolled single-phase rectifier with 4 diodes;
- B2H - half-controlled single-phase rectifier with 2 thyristors and 2 diodes;
- B2C - controlled single-phase rectifier with 4 thyristors;
- B6U - uncontrolled three-phase rectifier with 6 diodes;
- B6H - half-controlled three-phase rectifier with 3 thyristors and 3 diodes;
- B6C - controlled three-phase rectifier with 6 thyristors.

An ac/ac converter circuit is used to control the ac voltage with thyristors at a single or three-phase line. It is called W1C or W3C:

- W1C - single-phase ac controller with 2 anti-parallel connected thyristors;
- W3C - three-phase ac controller with 3 x 2 anti-parallel connected thyristors.

An inverter circuit is used to change dc voltage into ac one. A designer can calculate losses and temperatures for a single-phase or a three-phase output:

- single-phase PWM-fed inverter with 4 transistors and 4 freewheeling diodes with sinusoidal output current;
- three-phase PWM-fed inverter with 6 transistors and 6 freewheeling diodes with sinusoidal output current;
- direct single-phase inverter with 4 transistors and 4 freewheeling diodes with alternating output current.

The dc/dc circuit is used to change the dc voltage level. The toolkit manages two common circuit topologies, buck and boost converters. The buck converter can be also used for dc current operation of single and three-phase inverters:

- buck converter (chopper) sets the voltage down to a lower level using a transistor and a freewheeling diode;
- boost converter pushes the voltage up to a higher level using a transistor and a freewheeling diode;
- asymmetrical H-bridge supplies a switch reluctance motor.

With the *StackSel* of *SemiSel* it is possible to check the performance of ready assembled stacks, which are designed, manufactured and tested from the Semikron Solution Centres worldwide. A stack consists at least of one power semiconductor device, cooling system, and some interconnections or terminals. It can be the complete power part of an inverter including driver and protection functions. The selection is divided into four basic types of power electronic circuit topologies, ac/dc, ac/ac, dc/ac, and dc/dc. Available circuit configurations are displayed in the corresponding menu and in the circuit diagrams. Furthermore, the blocking voltage of the semiconductor and the nominal current of the stack can be used for more detailed pre-selection.

For the selected stack, the power dissipation and the junction and heat sink temperatures at the nominal current are calculated. It is possible to change the circuit parameter of the selected stack to investigate the system behavior under overload conditions or with load cycles.

The section *Device Proposal* calculates a first selection of suitable devices for one of the available circuits at a specified operating condition. It starts with the selection of one of the four basic types of circuit topologies. One set of parameters can be given for the steady-state operation without an overload condition. The thermal conditions are specified with a fixed heat sink temperature and the junction temperature, which is regarded as the design limit. The number of displayed devices per product family can be changed. It is recommended to have at least 3 devices, because often it is impossible to give a 100% clear recommendation.

There is a run through the database, calculating power dissipation for each particular device at the given operating point. All the user inputs are verified for feasibility. All the catalogue types of the Semikron product portfolio are included in the built-in database. Filters and preset values support the user in

making the correct selection of a suitable component. Calculations are carried out both for static and, if applicable, also for dynamic load conditions. The user gets the results in the form of a report with the input parameters used for the calculation, details on static losses and temperatures as well as a graphic display of the calculation for dynamic processes. *SemiSel* improves the degree of certainty that the right power semiconductor is selected. Comparisons between various components and operating points can be done quickly. The parameter input can be saved. *SemiSel* makes the expertise of Semikron engineers available on-line.

#### **Resume of 2.4**

As neither *Matlab/Simulink* nor *PSIM* can be used effectively for the heating and power loss analysis of IGBT switches, additional toolkits of IGBT vendors must be involved. Their accuracy is higher because of the more accurate component and auxiliary circuit models that take into consideration parasitic inductance, capacitance, mutual coupling, and many other manufacturers' parameters. At the same time, this software cannot predict such motor drive characteristics as torque and speed ripple, acoustic noise emitted from the motor, electromagnetic interference, etc.

## **2.5 Conclusions**

1. Using the developed classification criteria focused on the motor drive design, the main toolkits used in the worldwide power electronic practice have been compared. As a result of the analysis, a conclusion was drawn that a toolbox which should fully satisfy the motor drive design conditions is absent in the software market. Nevertheless, some toolkits have been found that are beneficial for the power converter design and exploring, such as *PSIM* and *Matlab/Simulink*. Their restrictions are to be taken into account in modelling.
2. Two original experimental setups have been developed in the frame of the thesis to provide identification and verification of the developed models. Experimentation on the steady-state and dynamical operation modes show that different switching patterns can be studied and compared using these physical prototypes.
3. A powerful library of the motor drive models has been developed in the *Matlab/Simulink* environment - low-frequency simple six-step modulation, high-frequency PWM, and progressive SVM. The control systems of power converters have been studied using the proposed models. Good agreement between the simulation and experimental results were obtained. An impact of the modulation method on the voltage and current harmonics was demonstrated. Benefits and drawbacks of different control methods were illustrated in the steady-state and dynamic modes of the converter performance in asynchronous drive applications. Simulation revealed that the accuracy of the results depends on the accuracy of the built-in electronic and electromechanical models.

4. As neither *Matlab/Simulink* nor *PSIM* can be used effectively for the heating and power loss analysis of IGBT switches, a technology of combined use of both the traditional simulation packages and marketable toolkits in motor drive design has been proposed. Nevertheless, it was shown that torque ripple, acoustic noise emitted from the motor, and electromagnetic interference could not be studied by this software. The same concerns the auxiliary circuit elements such as parasitic inductance, capacitance and mutual coupling.

### **3. IMPLEMENTATION AND PERFORMANCE EVALUATION OF LOAD-DEPENDENT SWITCHING PATTERNS**

Power losses of the motor drive depend to a large extent on the switching frequency, currents, and supply voltage of the power converter. As these three parameters affect the motor torque and speed, they must be considered in the synthesis of the inverter adjustment algorithms. A successful control system improves the motor drive economic indicators being a core of effective drive design. In this chapter, first an analytical solution of the problem is proposed. Next, some new methods of the load-dependent control of motor drive inverters are discussed and examined by simulation and experimentation.

#### **3.1 Load-Dependent Control of Motor Drive Inverters**

##### **3.1.1 A Problem of Current, Voltage, and Frequency Restrictions**

As follows from the foregoing analyses, power losses affect efficiency, weight, size, cost, power quality, power consumption, transient responses, and other motor drive characteristics. As the motor drive is a complex non-linear system, consideration of the motor parameters along with the power converter development or choice inevitably leads to the power economic design and reduction of loss. In this section, focus is on the inverter characteristics related to the properties of the induction motor.

Due to the influence of electromagnetic processes occurring in the inverter-motor system, the character of the load voltage transients has no direct equivalence with the reference signals. The degree of such discrepancy depends on both the motor parameters and the mode of inverter operation. Often, it results in additional voltage distortion and reduced use of supply power. Therefore, the load parameters should be considered in the synthesis of the switching patterns, mainly by setting the commutation law and duration of the switching intervals.

To take into account the motor current and voltage, two ways may be selected:

- using voltage and current predefined values in the switching pattern generation procedure;
- correction of the switching patterns using the current/voltage feedback signals of the motor drive.

Both methods lead to an enhancement of the motor drive performance [69]. The former is less expensive through less accurate. The latter requires additional equipment but can result in a higher effect.

In the majority of contemporary inverters, the switching frequency is selected as high as the IGBT rating permits. In this way, the chosen IGBT switches define

the commutation frequency. Such approach leads to high losses of the motor drive therefore the problem of the maximum switching frequency restriction must be solved. There are two factors that define the frequency top and bottom bounds in the motor drive.

On the one hand, there is no point in making the switching period less than a decile of an electromagnetic time constant of the motor. While the frequency is very high, the conduction delays of IGBT inverters are too short to change the motor current, speed, or torque. It results in unnecessary inverter losses.

At the same time, the switching frequency must be sufficiently high to keep the required motor torque and speed ripples. As shown in 1.2, for the voltage-frequency adjustable motor drives both the ripple and the current THD values should fall into 3 to 5 % intervals. As there is no direct relation between the mentioned motor and converter parameters, their correlation is examined in the following section.

### 3.1.2 Relationship Between the Inverter and Electromagnetic Motor Models

An important parameter that defines the load action is an electromagnetic time constant of the motor drive

$$T_e = \frac{L}{R}. \quad (3.1)$$

To calculate it on the basis of the motor data, the methodology [13] oriented on the induction motor drive having the stabilized rotor flux linkage is used. In the motors inductances are defined by the magnetic conductivity and the number of turns. Introduction of electromagnetic link factors and a leakage factor

$$k_1 = \frac{L_{12}}{L_1}, \quad k_2 = \frac{L_{12}}{L_2}, \quad \sigma = 1 - \frac{L_{12}^2}{L_1 L_2} = 1 - k_1 k_2. \quad (3.2)$$

yields the following formulae for motor resistance and inductances calculations:

$$R = R_1 + k_2^2 R_2, \quad L = \sigma L_1, \quad L_{12} = \frac{3}{2} \cdot \frac{X_{12}}{2 \cdot \pi \cdot f}, \quad L_1 = \frac{X_1}{2 \cdot \pi \cdot f} + L_{12}, \quad L_2 = \frac{X_2}{2 \cdot \pi \cdot f} + L_{12}. \quad (3.3)$$

Here index 1 designates the stator parameters, index 2 indicates the rotor parameters, and index 12 marks the mutual inductance.  $R_1$  and  $R_2$  are phase winding resistances,  $L_1$  and  $L_2$  are the stator and rotor inductances, and  $L_{12}$  is their mutual inductance.  $X_1$ ,  $X_2$ , and  $X_{12}$  are the rated reactances obtained from the motor data sheet or online identification procedures.

Many factors determine the impact of electromagnetic parameters on the combined inverter-motor performance. Using the above described models, the averaged dependence between the current THD, modulation index, and

electromagnetic time constant obtained was found on the switching frequency 6 kHz. Fig. 3.1 presents the diagram of this relation.

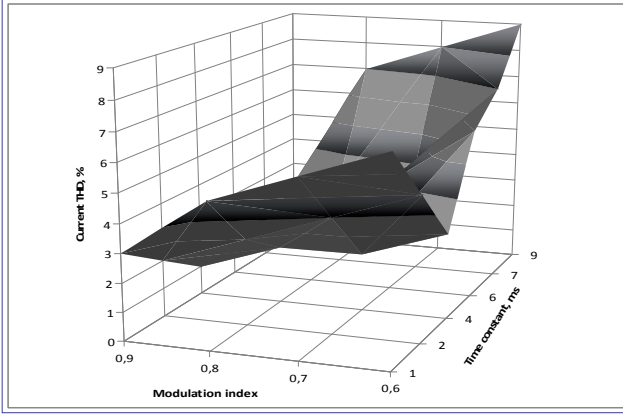


Fig. 3.1 Current THD vs the modulation index and the electromagnetic time constant

This diagram indicates that a small  $T_e$  has low influence on the inverter-motor system behavior. Also, at high  $T_e$ , THD increases because of stepping change of the control signals. The best effect is displayed in the middle range of  $T_e$  (3-6 ms) upon the high modulation indexes ( $k_{mod} > 0.7$ ) where the minimal values of THD are expected.

### 3.1.3 Correlation Between the Inverter and Electromechanical Motor Models

A motoring torque of the drive is derived using the torques equilibrium equation [10]:

$$M = M_s + M_d = M_s + J \frac{d\omega}{dt}. \quad (3.4)$$

Here,  $M_s$  is a static load torque (counter-torque),  $M_d$  is the dynamic torque of the load,  $J$  is the moment of inertia,  $\omega$  is an angular frequency of the motor shaft,  $t$  is the time.

Solution of this differential equation relative to the speed depends on the nature of the torque. The mechanical torque on the motor shaft is defined by the electromagnetic torque  $M_e$  and the friction losses  $\Delta M$  as follows:

$$M = M_e - \Delta M. \quad (3.5)$$

An electromagnetic torque of the induction motor may be found on the basis of the vector equation

$$M_e = \psi I, \quad (3.6)$$

where  $\psi$  determines the flux linkage, and  $I$  is a vector of stator and rotor currents.



As the inverter serves as a source of current and voltage, its outputs directly affect the motor performance. In this way, the stator and rotor currents  $I_1, I_2$ , flux linkages  $\psi_1, \psi_2$ , and inductances  $L_{12}, L_1, L_2$  are the important factors that define the inverter-motor operation.

To calculate the converter and motor currents and to link them with the inverter outputs, a nonlinear time-variant detailed motor model [10] is applied in orthogonal reference frame  $x,y$  which interprets a three-phase multi-pole system as an equivalent two-phase bipolar machine [8]. An electrical equilibrium of the stator and rotor windings rotated with angular frequency  $\omega_k$  in  $x,y$  coordinates is depicted by Kirchoff's equations:

$$\begin{aligned}
 U_{1x} &= R_1 I_{1x} + s \psi_{1x} - \omega_k \psi_{1y}, \\
 U_{1y} &= R_1 I_{1y} + s \psi_{1y} + \omega_k \psi_{1x}, \\
 U_{2x} &= R_2 I_{2x} + s \psi_{2x} - (\omega_k - \omega_1 + \omega_2) \cdot \psi_{2y}, \\
 U_{2y} &= R_2 I_{2y} + s \psi_{2y} + (\omega_k - \omega_1 + \omega_2) \cdot \psi_{2x}.
 \end{aligned} \tag{3.7}$$

In the orthogonal coordinate frame,

$$\begin{aligned}
 U_1 &= \sqrt{U_{1x}^2 + U_{1y}^2}, \\
 U_2 &= \sqrt{U_{2x}^2 + U_{2y}^2}, \\
 I_1 &= \sqrt{I_{1x}^2 + I_{1y}^2}, \\
 I_2 &= \sqrt{I_{2x}^2 + I_{2y}^2},
 \end{aligned} \tag{3.8}$$

where  $U_1, I_1$  are the stator voltage and current,  $U_2, I_2$  - rotor voltage and current, and  $s = \frac{d}{dt}$ . Possible torque expressions via current and flux linkage amplitudes are as follows:

$$\begin{aligned}
 M_e &= \frac{3}{2} p L_{12} (I_{1y} I_{2x} - I_{1x} I_{2y}), \\
 M_e &= \frac{3}{2} p \frac{k_1}{\sigma L_2} (\psi_{1y} \psi_{2x} - \psi_{1x} \psi_{2y}), \\
 M_e &= \frac{3}{2} p (\psi_{1x} I_{1y} - \psi_{1y} I_{1x}), \\
 M_e &= \frac{3}{2} p (\psi_{2y} I_{2x} - \psi_{2x} I_{2y}),
 \end{aligned} \tag{3.9}$$

where  $p$  is the pole pair number. Considering the phase winding resistances to be symmetrically shared along the rotor circle, the following equations unify the motor flux linkages, inductances, and currents:

$$\begin{aligned}
\psi_{1x} &= L_1 I_{1x} + L_{12} I_{2x}, \\
\psi_{1y} &= L_1 I_{1y} + L_{12} I_{2y}, \\
\psi_{2x} &= L_2 I_{2x} + L_{12} I_{1x}, \\
\psi_{2y} &= L_2 I_{2y} + L_{12} I_{1y}.
\end{aligned}
\tag{3.10}$$

Thanks to the orthogonal orientation of the axes, the flux linkages are available from their projections:

$$\begin{aligned}
\psi_1 &= \sqrt{\psi_{1x}^2 + \psi_{1y}^2}, \\
\psi_2 &= \sqrt{\psi_{2x}^2 + \psi_{2y}^2}.
\end{aligned}
\tag{3.11}$$

Now, the relation between the motor speed, torque, and electromagnetic time constant on the one hand and the inverter current and voltage on the other hand is found. In this way, all the factors that influence the inverter-motor system performance are known.

### 3.1.4 Loss Analysis

Next, we proceed to the converter loss analysis taking into account that the loss depends on the current and switching frequency values. The character of such dependence is defined by the particular IGBT parameters. Using the Semikron online package *Semisel*, ver. 3.1.1.3 [70], the group of 18 IGBT modules was explored and compared, such as Skiip, MiniSkiip, Semitrans, Skim, Semitop, and Semix. Figure 3.2 presents an averaged relationship between IGBT junction temperature, switching frequency, and phase currents in regard to the operational conditions of the discovered products.

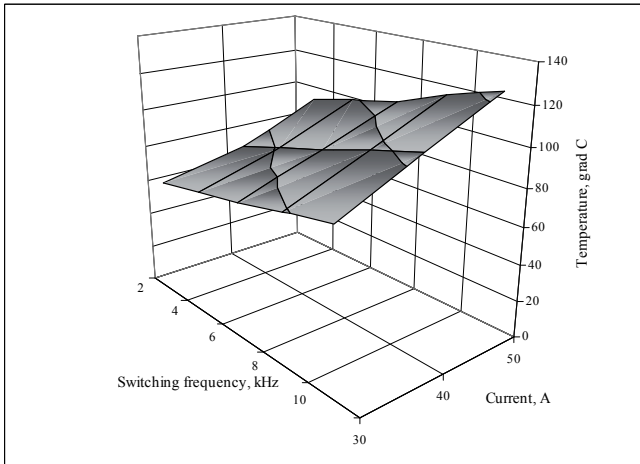
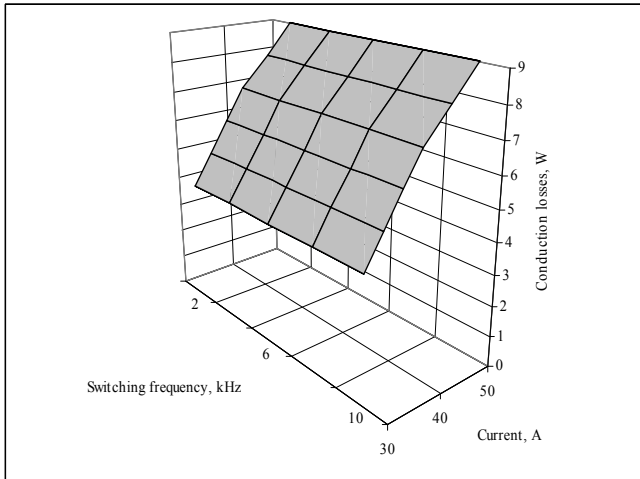
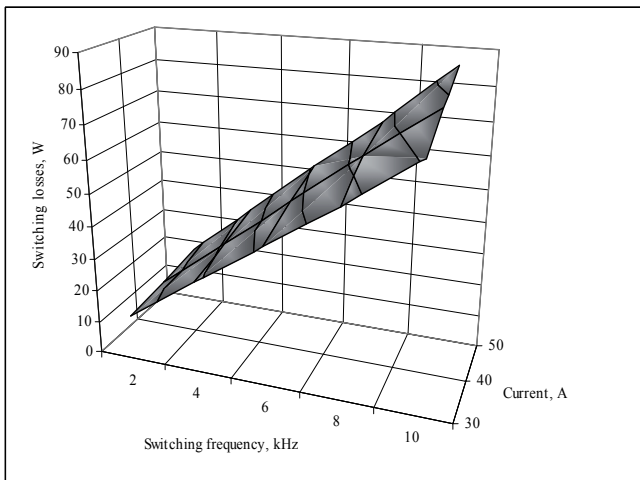


Fig. 3.2 Temperature-frequency-current correlation of Semikron modules

A similar study was conducted by applying the *Power Module Loss Simulator Melcosim*, ver. 4.04 of Mitsubishi Electric [71]. In this package, a group of CM900DU-24NF modules was explored (Fig. 3.3, 3.4).



*Fig. 3.3 Conduction losses of Mitsubishi Electric modules*



*Fig. 3.4 Switching losses of Mitsubishi Electric modules*

Figures 3.2 - 3.4 show that temperature and switching losses increase proportionally to both the current and the switching frequency, reaching a maximum at 50 A and 10 kHz. Conduction losses depend on the current only, reaching their maximum at 50 A.

### **Resume of 3.1**

The switching patterns of IGBT inverters are often the source of additional voltage and current distortion and reduced use of supply power. To overcome this drawback, the concept of load-dependent control for the supply inverter is proposed. In compliance with such proposition, the motor parameters, such as

inductances, resistances, and flux linkages, are to be taken into account while an inverter is designed and tuned. A suitable induction motor model was developed to implement this approach. To ground the new concept, simulators *Semisel* from Semikron and *Melcosim* from Mitsubishi were used.

## 3.2 Current-Dependent Clamping of Inverter Legs

### 3.2.1 Principle of Current-Dependent Clamping of Inverter Legs

As it follows from the analyses presented in 1.2.1 and 3.1.4, the power losses of the inverter-fed motor drive are proportional to the magnitude of the switching current. Therefore it would be advantageous to avoid switching of inverter legs carrying the highest currents. This is possible in most cases because all adjacent vectors given in 1.4.3 differ in the state of switches in only one leg. Using this idea, effective current-dependent discontinuous SVM methods were proposed in [11] [30].

In SVM, the optimized switching patterns predetermined offline according to the optimization criteria are stored in a memory and used in real time in the procedures of a microprocessor controller. Particularly, thanks to preliminary current calculation, the switching patterns may be determined by counting ahead of the real current. The effect of the prediction of the current evolution can be estimated before it occurs therefore the required control signal is selected in order to follow the referenced trajectory.

Figure 3.6 presents the output six-step modulated phase voltages on the modulation period  $T_m$ . Each state of the output SVM voltage system presents a particular switching vector in the complex plane drawn in 1.4.3. Thus, six active switching vectors  $U_1$  to  $U_6$  and two vectors corresponding to the zero states are obtained. Active vectors having the magnitude of  $\frac{2}{3}U_d$  are at  $\frac{2\pi}{3}$  out of phase each other.

To find the current state vectors [24] [28], the phase current by the time integral of the phase voltage is derived:

$$I_L = \frac{1}{L} \int U_L dt. \quad (3.12)$$

The variation slope of the phase current is doubled when the phase voltage is doubled. The maximum value of the phase current is herein denoted with  $I_{\max}$ . Within the time interval  $[t_3, t_4]$ , the output voltage vector is  $U_3$ . Choosing the time origin in  $t_3$ , the load currents and voltages are expressed from Fig. 3.5 as follows:

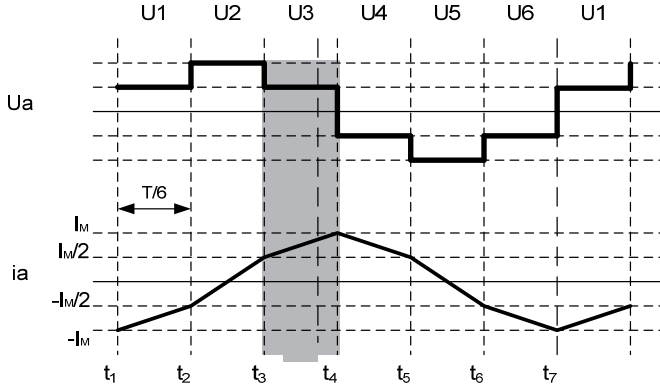


Fig. 3.5 Output phase voltage and current waveforms

$$U_{L1} = \frac{U_d}{3}, U_{L2} = \frac{U_d}{3}, U_{L3} = -\frac{2U_d}{3}. \quad (3.13)$$

$$I_{L1}(t) = \frac{I_{\max}}{2} + \frac{U_d}{3L}t, I_{L2}(t) = -I_{\max} + \frac{U_d}{3L}t, I_{L3}(t) = \frac{I_{\max}}{2} - \frac{2U_d}{3L}t. \quad (3.14)$$

The space vectors associated with the current and voltage waveforms are given by:

$$U(t) = \frac{2}{3} [U_{L1}(t) + aU_{L2}(t) + a^2U_{L3}(t)] \quad (3.15)$$

$$I(t) = \frac{2}{3} [I_{L1}(t) + aI_{L2}(t) + a^2I_{L3}(t)] \quad (3.16)$$

where

$$a = -\frac{1}{2} + j\frac{\sqrt{3}}{2}, a^2 = -\frac{1}{2} - j\frac{\sqrt{3}}{2}. \quad (3.17)$$

This results in

$$U(t) = \frac{2}{3}U_d + j0, I(t) = \left[ \frac{I_{\max}}{2} + \frac{U_d}{3L}t \right] + j \left[ \frac{\sqrt{3}}{2}I_{\max} + \frac{\sqrt{3}U_d}{2L}t \right]. \quad (3.18)$$

The maximum value of the current yields from the current vector equation within the time interval  $[t_3, t_4]$ , considering the linear variation of the phase current of the inductive load:

$$I_{\max} = \frac{2}{3L} \cdot \frac{T_m}{6} U_d. \quad (3.19)$$

Voltage space vector  $U(t)$  coincides with the switching vector that has generated it. With regards to the current space vector  $I(t)$ , its resulting trajectory is a

hexagon oriented along the voltage-switching vectors, as presented in Figs. 1.11 and 3.6.

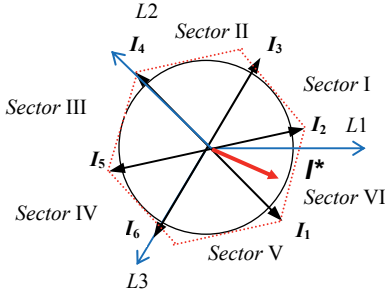


Fig. 3.6 Current space vector diagram

In the general case of a three-phase inductive load, the current space vector can be defined by analyzing the effect of each voltage switching vector. While the voltage space vector is time-constant, the load is characterized by the following function of time:

$$U = I \cdot R + L \frac{dI}{dt}. \quad (3.20)$$

The solution of the differential equation yields:

$$I(t) = \frac{1}{R} U \cdot C e^{-\frac{t}{T_e}}, \quad (3.21)$$

where  $C$  is the complex constant and  $T_e$  denotes the electromagnetic time constant of the load. Decomposing the current space vector expression on  $\mathbf{Re}$  and  $\mathbf{Im}$  axes demonstrates that the current vector trajectory is a continuous function during each time interval for which the voltage is constant. In the six-step modulation mode, since the voltage space vector changes its discrete positions at each 60 degrees, the current space vector trajectory results close to hexagonal for large inductances, as presented in Fig. 3.6. In PWM and SVM modulation modes the current space vector moves smoothly.

Now, the current vector position may be identified off-line and stored in a lookup table before modulation. At the beginning of each modulation sector, the control system calculates and selects from the lookup table the voltage phase, which is expected to pass the highest current, and clamps an IGBT switch of this phase by 60° alternately to the lower and upper levels of the dc voltage, thus preventing the high current commutation. An example of the prohibited switches counted in respect to Fig. 3.6 is presented in Table 3.2.

Table 3.2 IGBT switches with the highest current destined for clamping

	I sector	II sector	III sector	IV sector	V sector	VI sector
Clamped switches	VT1	VT3	VT2	VT1	VT3	VT2

In favourable conditions, when the modulation is clamped in phase conducting maximum current, switching losses should decrease up to 50 % [30].

Using an alternate way, an online current calculation can be executed in every sector to implement the same algorithm. This approach may be effectively implemented by sensing the maximum phase currents before each sector processing rather than its calculation and storing in a lookup table. To this end, the current sensors of the power switches should be used. By comparison three phase current values, the control circuit selects the highest one for exclusion from the commutation process.

### 3.2.2 Simulation

The voltage and current waveforms obtained by the simulation of the proposed current-dependent SVM method are presented in Fig. 3.7. Here, the states of the top switches **VT1**, **VT2** and **VT3** of the inverter shown in Fig. 1.3 as well as the line-to-line voltages and currents of an unloaded and loaded motor drive are given. Switch **VT1** is clamped at sectors I and IV, when the corresponding current obtains its maximum. Similarly, **VT2** is clamped at sectors III and VI, and **VT3** is clamped at sectors II and V, when the corresponding currents reach their maximum. Simulation was executed for the maximum shaft rotation frequency 50 Hz, modulation index 0.866, dc link voltage 512 V, and electromagnetic time constant 4 ms.

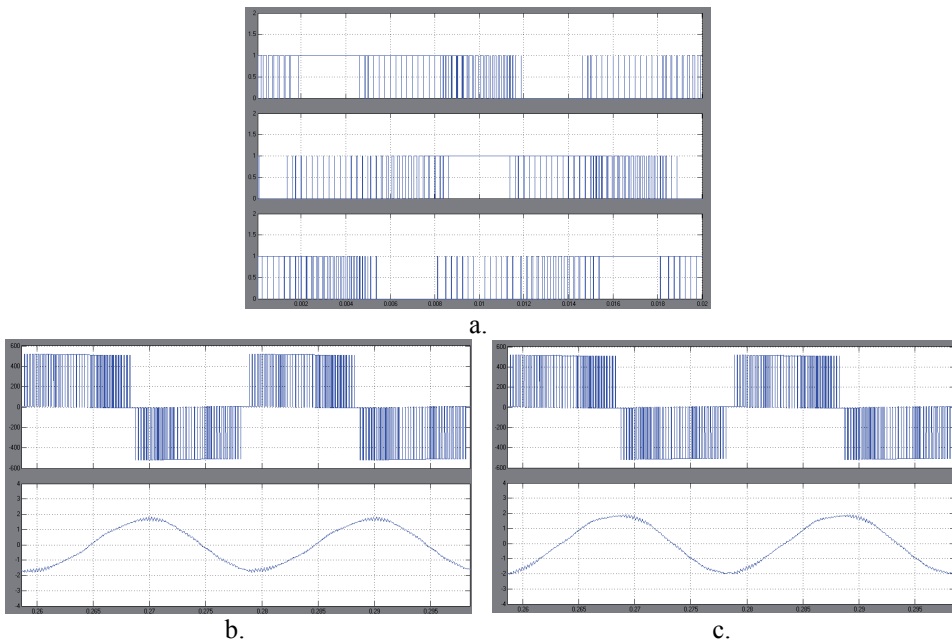


*Fig. 3.7 Waveforms of the SVM-driven TUT experimental setup with current-dependent clamping obtained from Simulink: (a) control signals; (b) unload, line-to-line voltage and phase current; (c) load, line-to-line voltage and phase current*

THD analysis of the timing diagrams is presented in Table 3.3.

Table 3.3 THD analysis of the simulation of the SVM-driven TUT experimental setup with current-dependent clamping obtained from Simulink

Frequency, Hz	Load, Nm	THD, %	
		Voltage	Current
50	0.1	67.7	4.4
	2.1	68.6	2.5
40	0.1	91.4	5.1
	2.1	92.4	2.9

### 3.2.3 Experimentation

Figures 3.8, 3.9 show the timing diagrams of the steady-state and starting modes of current-dependent clamping operation at the rated speed. Here, the states of the top switches of the inverter as well as the line-to-line voltages, currents, and motor shaft speed are presented by Tektronix Digital Storage Oscilloscope TPS 2024.

Table 3.4 summarizes the THD and ripple analyses of current-dependent clamping obtained from a Tektronix Digital Storage Oscilloscope TPS 2024 for the TUT experimental setup.

Table 3.4 THD and ripple analyses of current-dependent clamping obtained from the TUT experimental setup

Frequency, Hz	Load, Nm	THD, %		Ripple, %	
		Voltage	Current	Speed	Torque
50	0.1	42.2	4.5	3.6	3.9
	2.1	43.0	3.6	1.8	0.7
40	0.1	58.0	5.1	3.1	7.1
	2.1	57.5	2.4	6.5	0.8

Further loss analysis of the converter IGBT switches was conducted in Semikron online package *Semisel*. In the course of the simulation it was found that the proposed current-dependent modulation method decreases the switch temperature on an average by 12 % thanks to the commutation frequency mitigation and additionally by 10 % due to the current reduction.

A similar study was performed by applying *Power Module Loss Simulator Melcosim*. Unlike the Semikron products, in a group of CM900DU-24NF modules the temperature was changed only by 5 % though the conduction and switching power losses were diminished significantly, thus increasing application efficiency.





Fig. 3.8 Timing diagrams of current-dependent clamping from the TUT experimental setup: (a) control signals; (b) unload, line-to-line voltage and phase current; (c) unload, phase voltage and current; (d) load, line-to-line voltage and phase current; (e) load, phase voltage and current

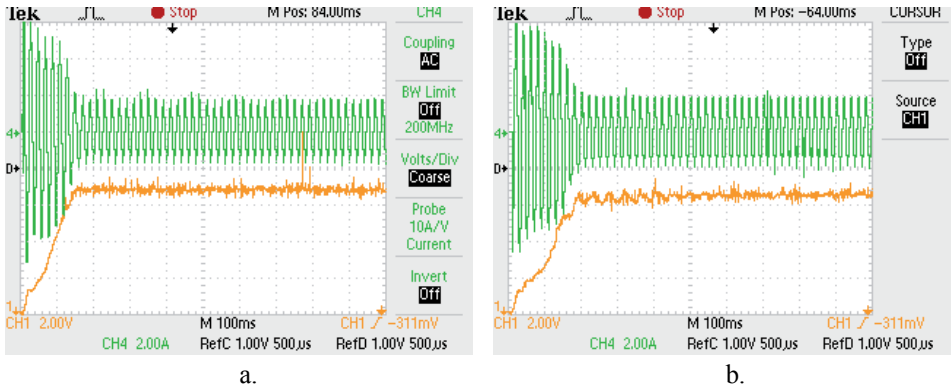


Fig. 3.9 Timing diagrams of current-dependent clamping from the TUT experimental setup: (a) unload, starting current and speed; (b) load, starting current and speed

### Resume of 3.2

A space vector based approach, current-dependent clamping of inverter legs, has been grounded in this section to decrease the losses and temperature of IGBT inverters. This technique is destined for industrial applications with open ended and close-loop induction motor drives. Advantages of the method are illustrated by the performance simulation and experimental study of a three-phase IGBT inverter-fed induction motor drive. Transition to the current-dependent clamping reduces the number of commutations without any noticeable current and motor torque distortion. At the same time, additional elimination of high current commutations is obtained. Temperature diminishing along with the reduction of power losses demonstrates the effectiveness of the proposed technology.

## 3.3 Elimination of Short Pulses from Switching Patterns

### 3.3.1 Principle of Elimination of Short Pulses

When the conduction delays of IGBT inverters become very short  $I_L$ , there is insufficient time to reverse bias the off-going IGBT or to change the motor current which defines the speed and torque of the drive. This is the reason why the protective intervals and the inherent delays of the switching devices should be taken into account. At the same time, it concerns the differences between the turn-on and turn-off times, which can cause a considerable distortion of the converter characteristics at low output voltage and frequency. Hence, if the voltage across this device increases in a positive sense too soon, the device will again conduct and high losses will occur without change in the motor torque and speed. Therefore, if the modulation scheme calls for a delay width below the minimum time, then this delay should be omitted.

Taking this consideration into account, both the continuous and discontinuous SVM algorithms can be accomplished in two different ways. In both cases, the control system is entrusted to an online or offline comparison of each calculated

time interval  $t_i$ ,  $t_{i+1}$  and  $t_0$  with the decile of an electromagnetic time constant  $T_e$  of the motor.

Using the first way (Fig. 3.10), while an interval is less than  $0.1T_e$ , its value is omitted from the gate driver sequence and memorized in the controller before the next sampling. Within the next sampling, this value is added to the calculated time interval and the sum is compared with  $T_e$  again. When the total time overcomes  $0.1T_e$ , it is used in the commutation process.

In the second case (Fig. 3.11), while an interval is less than  $0.1T_e$ , the sampling period  $T_c$  is increased and  $t_i$ ,  $t_{i+1}$  and  $t_0$  calculations repeat. Since all the time intervals overcome  $0.1T_e$ , they are ready to be used in the commutation process.

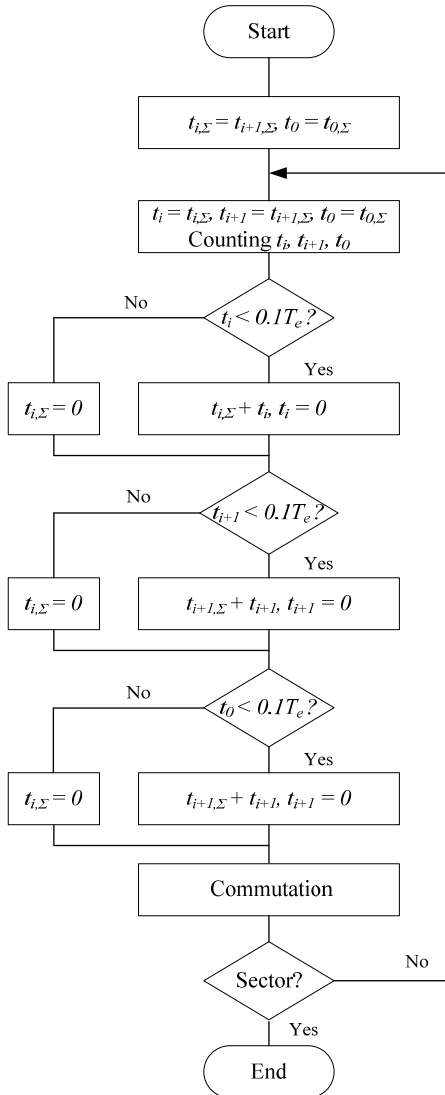


Fig. 3.10 First way to eliminate the short pulses

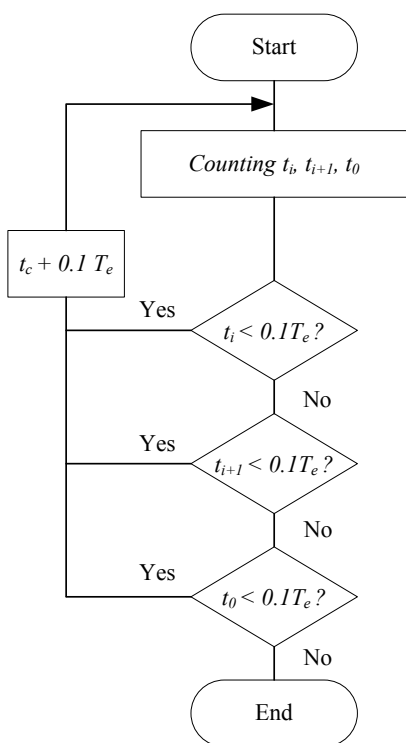


Fig. 3.11 Second way to eliminate the short pulses

### 3.3.2 Simulation

To verify the proposed algorithm, numerical simulations were performed. As a prototype, an experimental IGBT-fed induction motor drive setup was used. To obtain sufficient resolution, each of the six sectors of the modulating period  $T_m$  was divided into sampling periods  $T_c$  with a starting sampling frequency of 6 kHz. The number of samples per a motor shaft turn was defined by the reference motor speed. All the discovered schemes were calculated at the beginning of the sampling periods based on the value of the reference voltage vector and the electromagnetic time constant. Therefore,  $\mathbf{u}^*$  and  $T_c$  were updated at every sampling interval until the reduced sampling frequency became 3 kHz. The inverter maximum dc link voltage and modulation index were changed according to the simulation requirements.

The waveforms for the continuous SVM and discontinuous SVM with the elimination of narrow pulses are given in Fig. 3.12. Here, the states of the top switches of a converter shown in Fig. 1.3, **VT1**, **VT2** and **VT3**, as well as the line-to-line voltages and currents are presented. Zoomed sector 1 is shown to demonstrate the control peculiarity. Simulation was executed for the idle and loaded running upon the maximum shaft rotation frequencies 50 and 40 Hz, dc link voltage 512 V, and electromagnetic time constant 4 ms.

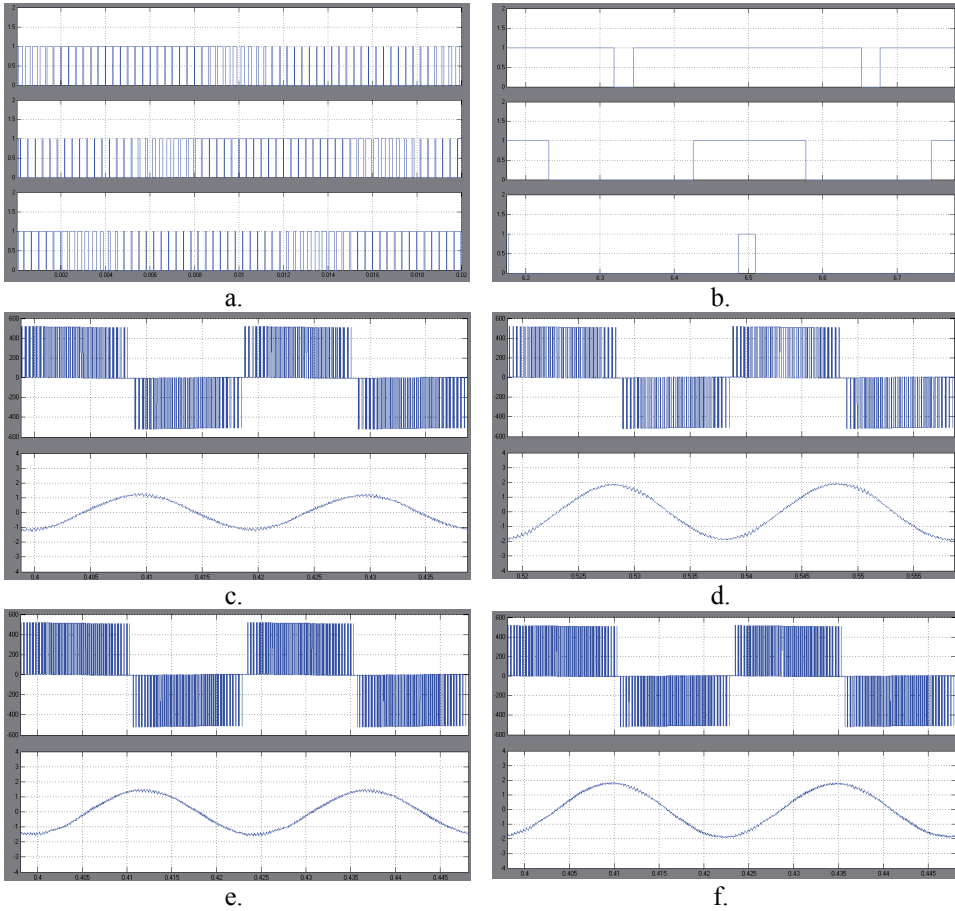


Fig. 3.12 Waveforms of SVM-driven TUT experimental setup with the elimination of short pulses obtained from Simulink: (a) control signals; (b) zoomed control signals in sector 1; (c) unload, 50 Hz, line-to-line voltage and phase current; (d) load, 50 Hz, line-to-line voltage and phase current; (e) unload, 40 Hz, line-to-line voltage and phase current; (f) load, 50 Hz, line-to-line voltage and phase current

THD analysis of the timing diagrams is represented in Table 3.5.

Table 3.5 THD analysis of the simulation of the SVM-driven TUT experimental setup with the elimination of narrow pulses obtained from Simulink

Frequency, Hz	Load, Nm	THD, %	
		Voltage	Current
50	0.1	69.0	4.7
	2.1	70.1	3.6
40	0.1	92.8	4.3
	2.1	93.3	3.4

As it follows from the analysis presented in Fig. 3.1, three important areas of the effectiveness of this method may be underlined. While the time constant  $T_e$  is low (1 to 2 ms), the method seems ineffective. In the middle range of  $T_e$  (3 to

6 ms) the minimal values of THD are obtained. At high  $T_e$ , THD increases again because of the stepping change of the control signals.

### 3.3.3 Experimentation

Figures 3.13, 3.14 show the timing diagrams of the steady-state mode for the continuous SVM with the elimination of narrow pulses obtained from the TUT experimental setup at different speeds and loads.

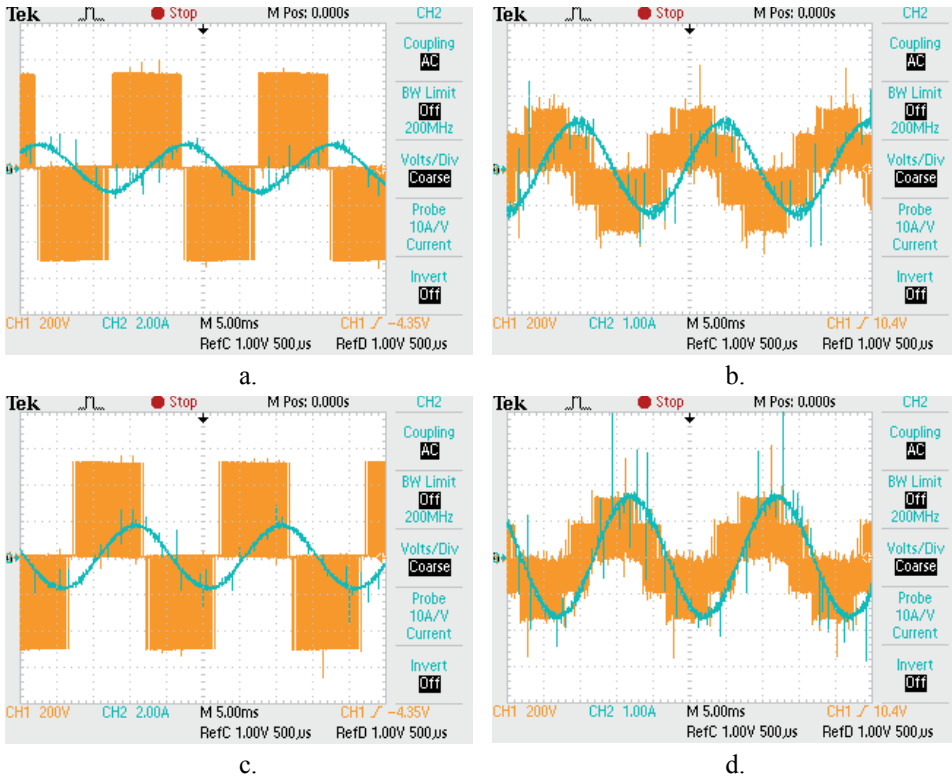


Fig. 3.13 Timing diagrams of the continuous SVM with the elimination of short pulses acquired from the TUT experimental setup: (a) unload, 50 Hz, line-to-line voltage and phase current; (b) unload, 50 Hz, phase voltage and current; (c) load, 50 Hz, line-to-line voltage and phase current; (d) load, 50 Hz, phase voltage and current

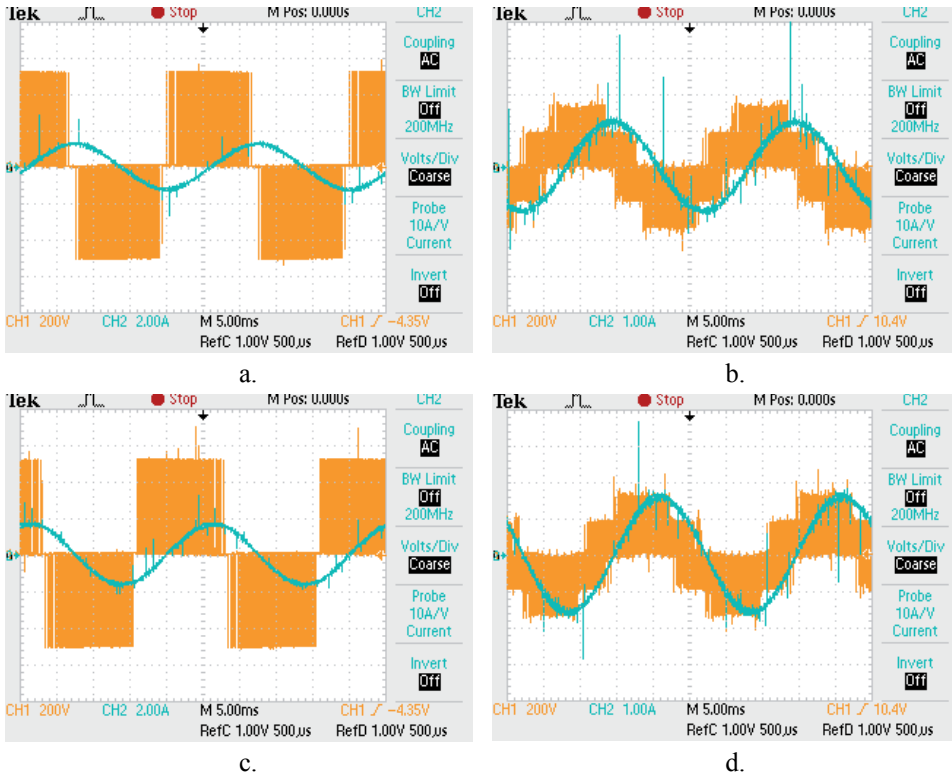


Fig. 3.14 Timing diagrams of the continuous SVM with the elimination of short pulses acquired from the TUT experimental setup: (a) unload, 40 Hz, line-to-line voltage and phase current; (b) unload, 40 Hz, phase voltage and current; (c) load, 40 Hz, line-to-line voltage and phase current; (d) load, 40 Hz, phase voltage and current

Figures 3.15, 3.16 show the diagrams of the starting mode for the continuous SVM with the elimination of short pulses obtained from the TUT experimental setup at different speeds and loads.

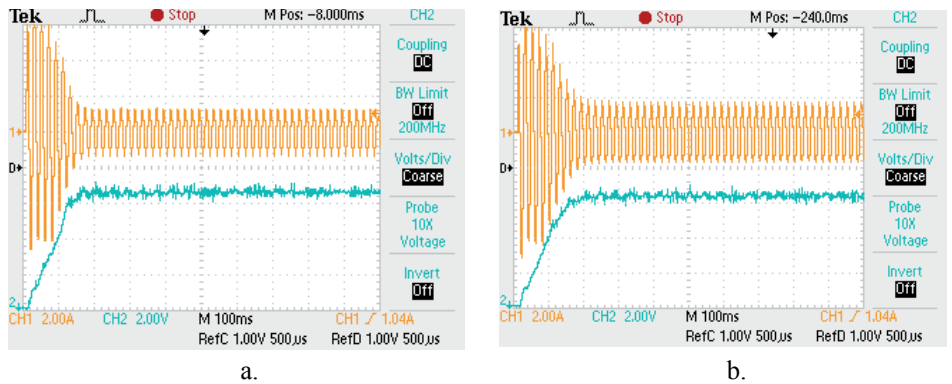


Fig. 3.15 Starting diagrams of the continuous SVM with the elimination of short pulses acquired from the TUT experimental setup: (a) unload, 50 Hz, speed and current; (b) load, 50 Hz, speed and current

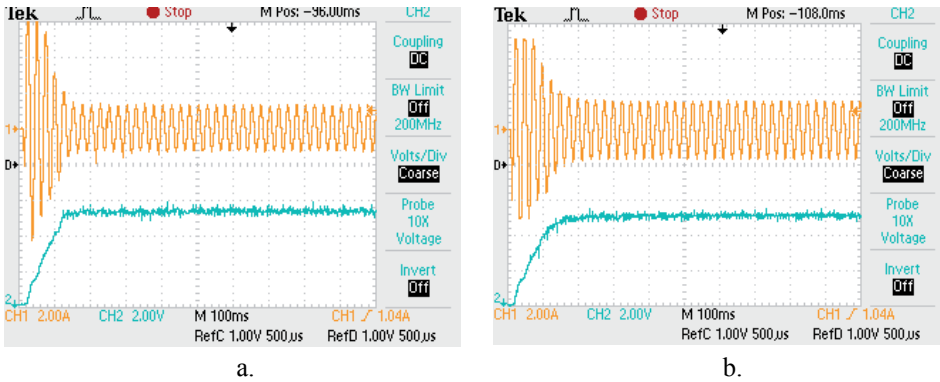


Fig. 3.16 Starting diagrams of the continuous SVM with the elimination of short pulses acquired from the TUT experimental setup: (a) unload, 40 Hz, speed and current; (b) load, 40 Hz, speed and current

Table 3.6 summarizes the THD and ripple analyses of the continuous SVM with the elimination of short pulses obtained from a Tektronix Digital Storage Oscilloscope TPS 2024 for the TUT experimental setup.

Table 3.6 THD and ripple analyses of the continuous SVM with the elimination of short pulses obtained from the TUT experimental setup

Frequency, Hz	Load, Nm	THD, %		Ripple, %	
		Voltage	Current	Speed	Torque
50	0.1	47.4	6.3	3.0	3.9
	2.1	47.0	3.2	1.8	1.3
40	0.1	60.3	4.7	4.6	6.7
	2.1	58.9	4.1	5.5	0.9

### Resume of 3.3

A space vector based approach that decreases switching losses was explored in this section. The principle of elimination of short pulses from the switching pattern reduces the number of commutations within the modulating interval. This method demonstrates how to choose the optimal switching frequency in respect to the particular application performance. Advantages of this method are illustrated by the simulation and experimentation in the scope of an inverter-fed motor drive.

## 3.4 Concluding Remarks on Load-Dependent Control

### 3.4.1 Comparison of THD

As shown in the previous chapters, the most important performance index for a power converter refers to the harmonic content in the output current. Therefore, the current THD was studied thoroughly using the TUT experimental setup. THD measurements were taken by a digital oscilloscope TPS2000 upon the rated speed motor running on the load 2.1 Nm. Table 3.7 summarizes the measurement results obtained from the TUT experimental setup.



Table 3.7 THD data of different modulation methods obtained from the TUT experimental setup

Modulation	THD, %	
	Voltage	Current
Six-step	29.6	34.2
PWM	48.0	3.0
Continuous SVM	38.2	2.4
Continuous SVM with elimination of narrow pulses	47.0	3.2
Discontinuous SVM	36.5	4.1
Discontinuous SVM with current-dependent clamping	43.0	3.6

Comparative data of experimental study are presented in Fig. 3.17.

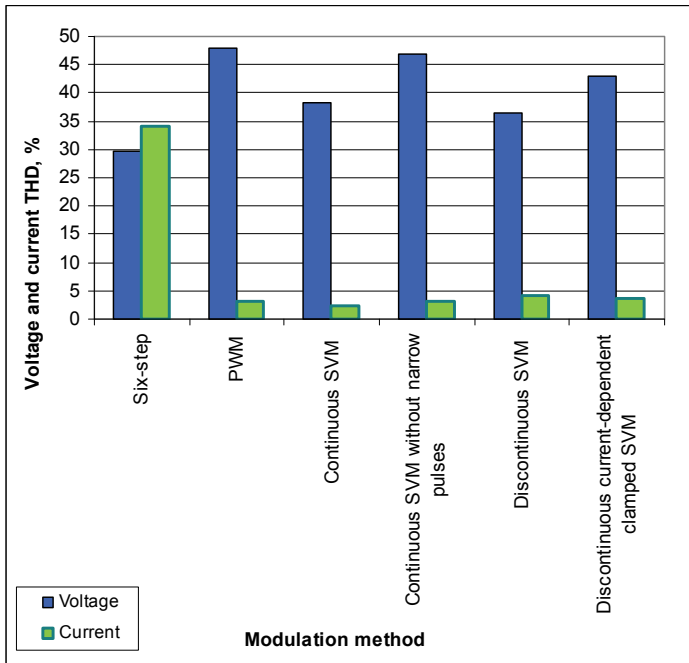


Fig. 3.17 Comparative THD data of modulation techniques examined on the TUT experimental setup

The best harmonic content is achieved for the conventional continuous SVM with a high modulation index ( $k_{mod} = 0.866$ ). The continuous SVM with the elimination of short pulses (3 kHz sampling frequency) results in almost the same THD as high-frequency PWM (6 kHz sampling frequency), thus it may be effectively used instead of PWM. The discontinuous SVM with a current-dependent clamping gives a better current THD value than the conventional discontinuous SVM. In view of the reduced commutation current, this method is recommended instead of the conventional one.

### 3.4.2 Comparison of Heat

To evaluate and compare different methods directed to the improvement of the power economical motor drive performance, an experimental analysis concerning heat was performed. The portable infrared thermometer from Raytek with 13 mm spot was used for IGBT and motor temperature measurements. The TUT experimental setup was studied upon the rated speed motor running on the load 2.1 Nm. The temperature measurements were taken in 0.5 hours after the motor running. Table 3.8 summarizes the measurement results obtained as the differences  $\Delta t$  between the room and on-chip temperatures as well as the room and motor cover temperatures.

Table 3.8 Temperature data of different modulation methods

Modulation	IGBT $\Delta t$ °C	Motor $\Delta t$ °C
Six-step	10.4	24.2
PWM	7.6	16.2
Continuous SVM	6.8	14.8
Continuous SVM with elimination of short pulses	5.6	15.4
Discontinuous SVM	5.6	17.2
Discontinuous SVM with current-dependent clamping	5.2	14.8

The temperature traces in Fig. 3.18 display the graphical representation of Table 3.8.

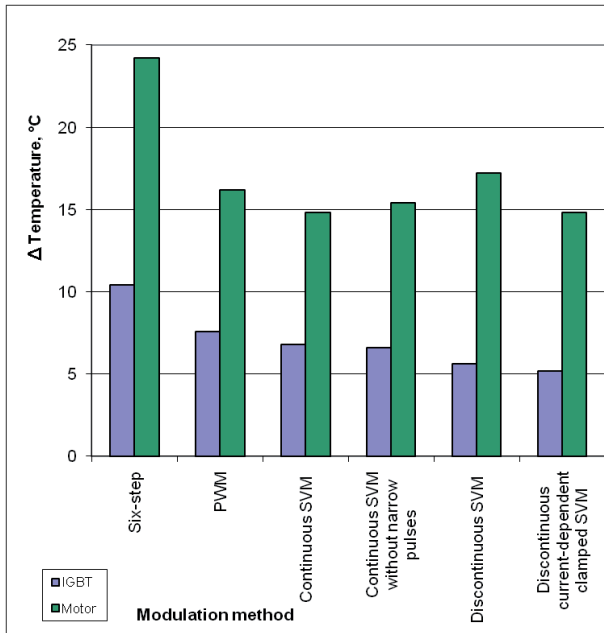


Fig. 3.18 IGBT and motor temperatures of different modulation methods

As it follows from these data, the six-step method causes the highest heating because of the significant current THD level and torque ripple. The IGBT losses of the continuous SVM without short pulses are less than those of the PWM and continuous SVM. At the same time, the discontinuous SVM causes higher motor heating than those of the PWM and continuous SVM, resulting in higher losses. The discontinuous current-dependent clamping SVM provides minimal losses.

### 3.4.3 Comparison of Motor Speed and Torque Ripples

To evaluate and compare new methods of power economical motor control, motor speed and torque ripples were analyzed experimentally. As a criterion, the ripple factor has been chosen i.e. the ratio of the peak-to-peak value of superimposed ac value to the ideal dc value. The ripple factors  $\Delta A$  were calculated using an oscilloscope TDS 2000 as follows:

$$\Delta A = \frac{A_{pp}}{A_d} \cdot 100\%, \quad (3.22)$$

where  $A_{pp}$  is an ac peak-to-peak speed or torque value and  $A_d$  is a dc portion of the same signals. Speed information was acquired from a tacho mounted on the motor shaft. Beforehand, the tacho's own ripples were measured under the motor supply from the net. In the calculation, this noise was excluded from the speed wave. To derive the torque, the current of the loading motor was measured using the current probe Model PR30 from LEM. Again, its own noise was taken into account. The torque was counted as the product of the measured current and the dc motor constant.

The summary of the speed and torque ripples is collected in Table 3.9.

*Table 3.9 Speed and torque ripples of different modulation methods*

Modulation	Speed, %	Torque, %
Six-step	2.2	1.5
PWM	1.2	0.7
Continuous SVM	1.4	0.6
Continuous SVM with elimination of short pulses	1.8	1.3
Discontinuous SVM	1.1	0.6
Discontinuous SVM with current-dependent clamping	1.8	0.7

The ripple diagram in Fig. 3.19 displays the graphical representation of Table 3.9.

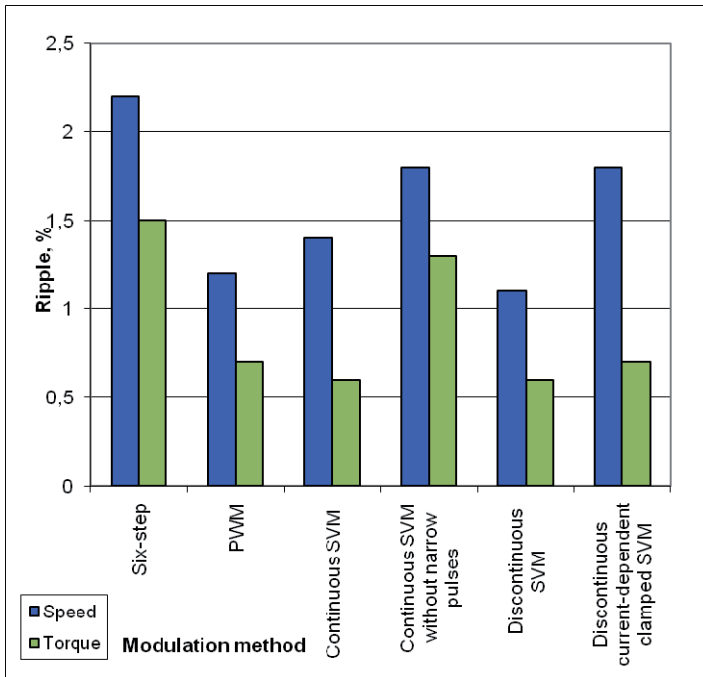


*Fig. 3.19 Speed and torque ripples of different modulation methods*

An analysis confirms that all the examined methods keep the ripples within the permissible 3 % range.

### **Resume of 3.4**

From the viewpoint of the current THD, all the techniques result in almost equal characteristics. At the same time, the discussed continuous SVM method with the elimination of short pulses results in less IGBT and motor losses than those of the PWM and continuous SVM, whereas the totally minimal losses within the allowed ripple range are provided by the discontinuous current-dependent clamping SVM designed in this chapter.

## **3.5 Conclusions**

1. The concept of load-dependent control for the supply inverter is grounded in this chapter. In compliance with this proposition, the motor parameters, such as inductances, resistances, and flux linkages, are to be taken into account in the design and tuning of an inverter. Mathematical and computer models for an induction motor were developed to implement this approach.

2. Current-dependent clamping of inverter legs decreases the losses and temperature of IGBT inverters. Performance simulation and experimental study of this technique demonstrates its benefits for open ended and close-loop ac motor drives fed by both the continuous and discontinuous SVM inverters.

3. The principle of the elimination of short pulses from the switching pattern is intended to reduce the number of IGBT commutations. This method opens a way to choose the optimal switching frequency in respect to the particular application performance. Both the developed algorithm and the implementation technique were confirmed by simulation and experimentation in the scope of an inverter-fed motor drive.

4. The comparative analysis of different modulation methods shows their particular benefits and drawbacks. From the viewpoint of the current THD, all the techniques result in almost equal characteristics. At the same time, the IGBT losses of the continuous SVM without short pulses are less than those of the PWM and the continuous SVM, whereas the totally minimal losses and heating within the allowable speed and torque ripples is provided by the discontinuous current-dependent clamping SVM.

## **4. COMPUTER AIDED DESIGN OF LOW-LOSS INVERTER-FED INDUCTION MOTOR DRIVES**

This chapter is devoted to the improvement of the computer aided design (CAD) technology for low-loss induction motor drives. As distinct from the known systems of such kind, in the enhanced CAD much attention is paid to the inverter as a significant part of a motor drive. Using the Matlab/Simulink models proposed in the foregoing chapters, a new toolbox was developed. In this software all the modulation methods were incorporated into a uniform computational environment and user interface. This improvement has resulted in the designed systems having high power economical performance. On the basis of the new toolkit, a future research scenario has been proposed.

### **4.1 Advancement in Motor Drive Design**

#### **4.1.1 Requirements to Motor Drive Designs**

Computer aided design (CAD) of motor drive, including selection of the right components for the application, is a complex task. Through a set of tasks meant for CAD systems related to motor drives, a designer practices the following:

- motor drive development, commissioning, and tuning;
- selection of electromechanical and electronic components;
- schematic elaboration and correctness verification;
- accounting of powers, voltages and currents;
- time and frequency response and waveform analysis;
- explanation, reporting, and documentation of results obtained.

The designer's foremost concern is to find which device composition is the most cost-effective in his application. To this aim, the designer has to deal with part numbers and technology curves from several suppliers. For a given voltage, package and application capability, there will be many possible candidates. Some are more efficient than others and, possibly, more expensive.

Design instruments are expected to be suitable to compare the calculated and experimental data and to generate documentation [72] which typically includes:

- component specifications and circuit diagrams;
- resulting, comparative, and dependency data tables;
- torque, speed, power, voltage and current traces;
- maintenance rules and requirements.

To provide an effective design, development tools should involve the following databases:

- electrical motors, loading mechanisms and sensors;
- different kinds of power converters;
- certain electronic modules built on the transistors, passive components and integral circuits;
- power sources of dc, ac, voltage-controlled, current-controlled, pulse, and clocking operation principles;
- measuring devices, oscilloscopes, and function generators.

In the light of the abovementioned features, the success of the selected CAD system increases proportionally to the number of the included features and possibilities. Also, other properties can be listed as follows:

- different input and output formats;
- computer tools for content development and management;
- database and XML support;
- compatibility with industrial and company standards;
- multiple language support;
- backup support;
- group work and debate forums;
- ease of system installation and minimum system requirements.

The flowchart of the discussed design algorithm is depicted in Fig. 4.1.

First, the mechanism travel diagram is developed and the drive load-carrying capacity is estimated, resulting in the mechanical torque, power, moment of inertia, and angular speed counting. If acceleration is restricted, the system dynamics is defined right away. Finally, a torque and power diagrams of the load are drawn.

After acquainting with the data sheets of gears and motors that correspond to the required drive type, the gear types with different output speeds are selected. Through these gears, the mechanical forces and speed found previously are converted to the equivalent values on the motor shaft.

For each gear, the particular motor is to be selected, meant for the converted forces and speed. Once the equipment framework is found, the optimum motor-gear combinations are searched. To find a solution, a designer should create appropriate criteria and sort them. It may be a criterion of minimum power, weight, or inertia, highest efficiency, rigidity, etc. Thus, the overall scale of the electromechanical and electronic properties is gathered, from which the choice is done on the basis of judgments about preferences of that or another criterion. Then, it is required to examine the dynamic overloading of the optimum motor-gear set. For cycling systems the equivalent load heating is estimated. For

induction motors, the periodic operation of which includes a standstill pause, the cyclic duration factor is calculated.

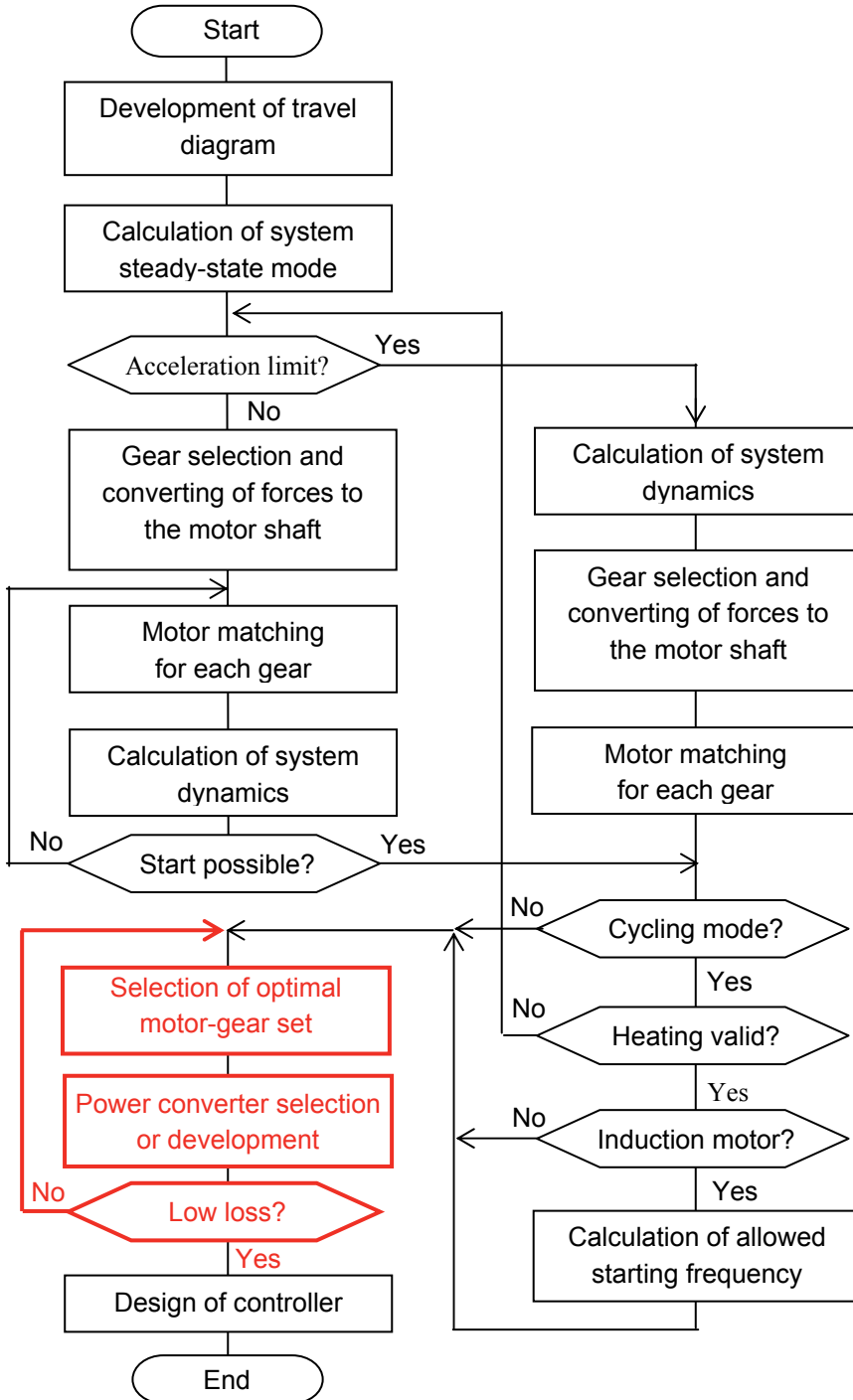


Fig. 4.1 Flowchart of motor drive design algorithm



A power converter which meets all the above mentioned requirements is selected to the motor-gear set. The design algorithm takes into account whether the marketable converter will be used or the original one is developed. The former way is more conventional due to the simplicity of the project. The latter one leads to higher power economical level but often results in a more expensive application.

Usually, a grid-connected motor is designed as small as possible to ensure that it is fully loaded and thereby operates with high efficiency. But the same is not the case for adjustable motors operated in the low-loss mode [41]. This is the reason why the choice of another motor-gear set may be needed to fulfil the power economical requirements. Thus, the discussed technology includes an additional loop in the design algorithm 4.1.

On the last stage, the controllers are designed, including the required regulators and sensors. Their transfer functions, gains, factors, and time constants are calculated to meet the standard settings. Then, the closed-loop system is tested and its optimization is conducted, if necessary.

#### **4.1.2 Review of Contemporary Motor Drive CAD Systems**

Looking back to earlier years of the drive, as technology advances and increases in complexity, the product offerings become more numerous and more tailored to one application or the other. Today, the choices are many, characteristics are different, materials costs have become critical and time-to-market factor has shortened. This boils down to a massive headache for the designer who has to select the right components for the application through a laborious iterative process. This process cannot be short-circuited but can be streamlined and rationalized with some helpful tools [29]. This, in turn, requires either a closer relationship between the manufacturer and the design engineer or specialized tools to support the designer. Fortunately, the new design tools become more and more available from manufacturers, thus supporting engineers in specifying the motor drive components.

To derive, choose, and tune driving equipment, many well-known companies have developed their own technologies. Examples are the guides and software of ABB, Siemens, Omron, Sew Eurodrive, Maxon Motors, Mitsubishi [73] [74] [75]. The cores of these toolboxes are composed on the preliminary worked-out corporative databases, the management systems of which help to find and optimize multiple electric drive combinations. Also, the designed systems are tuned in accordance with the corporative methods. Such approaches are conventional for the majority of firms that carry out project designs and have rich experience in decision making based on extensive computer databases, constituting numerous catalogue archives and "absorbing" their contents and structures [40] [76].

However, their main drawback is the technological restriction and data limitation within the particular corporative scope that deprive a designer of an

optimum way in the project. It is especially important at the beginning of a project work, when the most responsible decisions are taken.

Another problem lies in the restrictions of the design possibilities of the corporate toolboxes. Usually, they include the bounded volume of components (motors, gears, converters, sensors, controllers) having the limited number of regulated parameters. As a rule, an incorporation of extern components is prohibited or strictly protected.

The same concerns the input and output signals, references, and disturbances. Their number and configuration is restricted and is not subjected to changing. Particularly, no methods have been found to study new switching patterns and their influence on the motor torque and speed.

Finally, the design procedure itself is bounded by the technological requirements and company rules. Development methods and algorithms of a particular expert may not be implemented into the design due to these borders.

#### **4.1.3 eDrive Toolkit as the Core of CAD**

As the core of the proposed design technology, the toolkit *eDrive* from St. Petersburg Electrotechnical University has been chosen [77]. An object-oriented environment of this system offers solutions of the following project management motor drive problems:

- informational support in the automatic selection of electrical, mechanical, and electronic equipment;
- mathematical and computer simulation and computation in the standard database environment;
- testing and result verification in accordance with different criteria;
- control system development, tuning and optimization.

The software involves the following components:

- powerful database;
- models of motors, converters, sensors and mechanical actuators;
- kit of adjustable controller schemes;
- signal generator to produce the test reference and load signals as well as the nonlinear curves, noises, and filters;
- report generator and system analyzer;
- graphic package for the representation of the steady-state and dynamic simulated processes with automatic and manual scaling and preview facilities.

Compactness, high efficiency, and convenience are the significant features of *eDrive* program modules independent of additional simulation software. The main characteristics of *eDrive* are presented in Table 4.1.

Table 4.1 Simulation quantities of *eDrive*

Quantity	Number
<i>Simulation of the ready-to-service modules of power converters</i>	
Overall number of types of virtual converter simulators	3
incl. the number of virtual ac/dc converter simulators	1
incl. the number of virtual dc/ac converter simulators	1
incl. the number of virtual ac/ac converter simulators	1
incl. the number of virtual dc/dc converter simulators	1
Number of manufacturer's databases of power converters with the ready-to-service modules	17
<i>Simulation of induction squirrel-cage motors</i>	
Number of winding parameters	5
Number of other electrical parameters	4
Number of mechanical parameters	5
Number of manufacturer's databases of induction squirrel-cage motors	5
<i>Simulation of electrical drives besides induction squirrel-cage motors</i>	
Overall number of types of virtual motor simulators	3
Number of manufacturer's databases of motors besides induction squirrel-cage motors	10
Overall number of types of virtual gearbox simulators	4
Number of manufacturer's databases of gearboxes	5
Overall number of types of virtual loop controllers	3
Overall number of types of virtual sensors	3
Overall number of types of virtual filters	11
<i>Exploring and analyses</i>	
Overall number of types of virtual measuring devices	6
Overall number of types of virtual signal generators	9
Steady-state analysis	2
Transient analysis	3
Frequency analysis	0
Spectral analysis	0

This toolkit does not suit the problem of low-signal electronic design. On the other hand, *eDrive* proposes many possibilities to study electrical motors in different modes of driving operation and to design an electrical drive using the ready-to-service components from the industrial databases. The *Multisim* and *Spice* discussed above do not fit these requirements, whereas *PSIM* and *Simulink* are not so suitable for comparison and exploration of the driving applications of different vendors. As distinct from the companies, which process and propagate their production, an *eDrive* approach is addressed to the overall equipment selection, tuning, and optimization independent of the firm interests (Fig. 4.2). It transfers multiple data from the variety of databases into the uniform *eDrive* database with the specific data management system, which

provides the search and updating of the data using the open-access corporative databases.

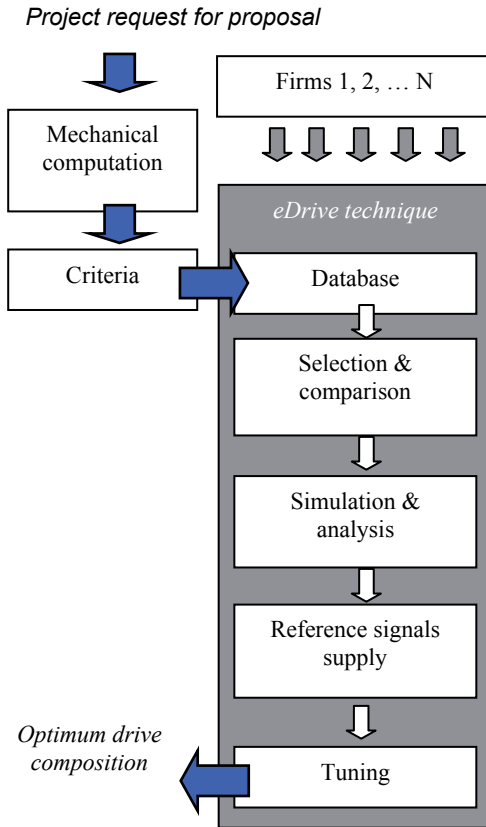


Fig. 4.2 Project mastering in eDrive

Here, designers have an opportunity to conduct their own step-by-step decomposition of a “decision tree”. The software provides automatic component optimization according to the taste and professional skills of a designer as shown in Fig. 4.1. Informational search of motors is carried out in a number of *eDrive* data tables: alternating current machines with a phase rotor, multi-speed and commonly used motors; dc high torque machines, low-inertia and commonly used ones; synchronous and step motors. To each of the machine found, a set of mechanical gears of six types (toothed, worm, ball screw, planetary) and power converters of three types (thyristor, transistor, stepping) can be brought to conformity. The database is open for external correction and updating. If necessary, the industrial catalogues, possessed by the designers earlier, can be transformed into the electronic directories and sorted on any field.

To find the best motor-converter-gear combinations, a designer creates appropriate criteria by use of which the system sorts the selected components.

Using the ready-to-service components from the industrial databases, the toolkit is suitable for the component selection and system tuning. It has the reach library of electromechanical models and proposes many possibilities to study electrical motors and gears in different modes of the driving operation. The signal generator of *eDrive* is destined for the required speed and path setting, reference and disturbance generating for the explored electric drives, examining the influence of distortions and disturbances on the behaviour of the drive components. To improve the system performance, the signal time and level offsets, and the filters and correctors are intended.

The main drawback is that *eDrive* does not meet the requirements of the electronic component design.

An example of ACS800 simulation executed by *eDrive* is given in Fig. 4.3. The results of simulations are in agreement with the experimental preconditions shown earlier in Fig. 2.4, thus allowing quantitative evaluation of the starting and steady-state situations.

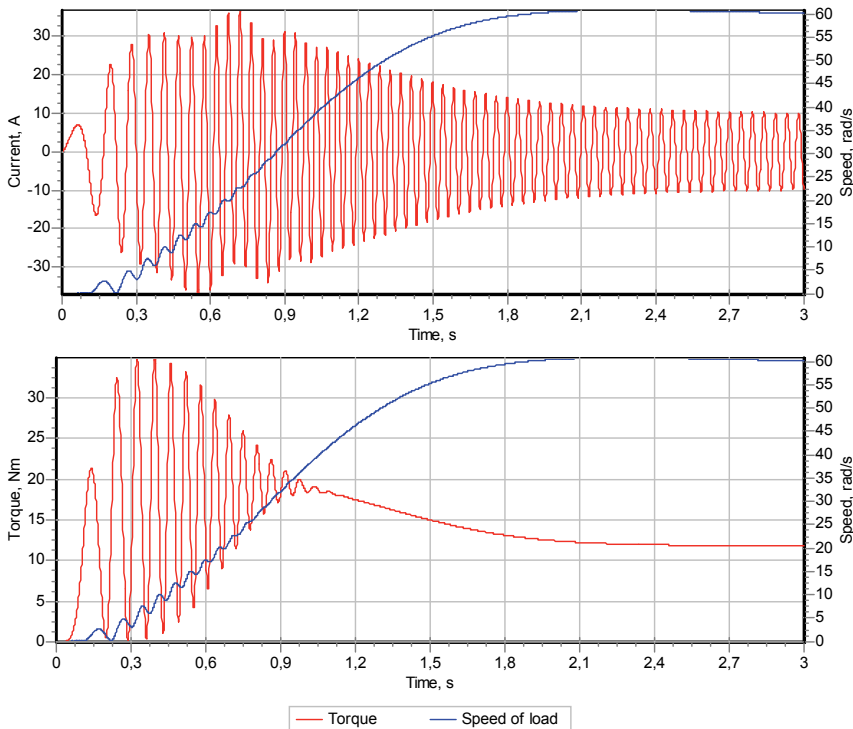


*Fig. 4.3 Speed-current and speed-torque traces of eDrive simulation of the direct start-up for the loading ACS800 drive*

An example of the TUT experimental setup simulation conducted by *eDrive* is presented in Fig. 4.4. The results of simulations are in agreement with the experimental preconditions shown earlier in Fig. 2.9, thus allowing quantitative evaluation of the starting and steady-state situations.

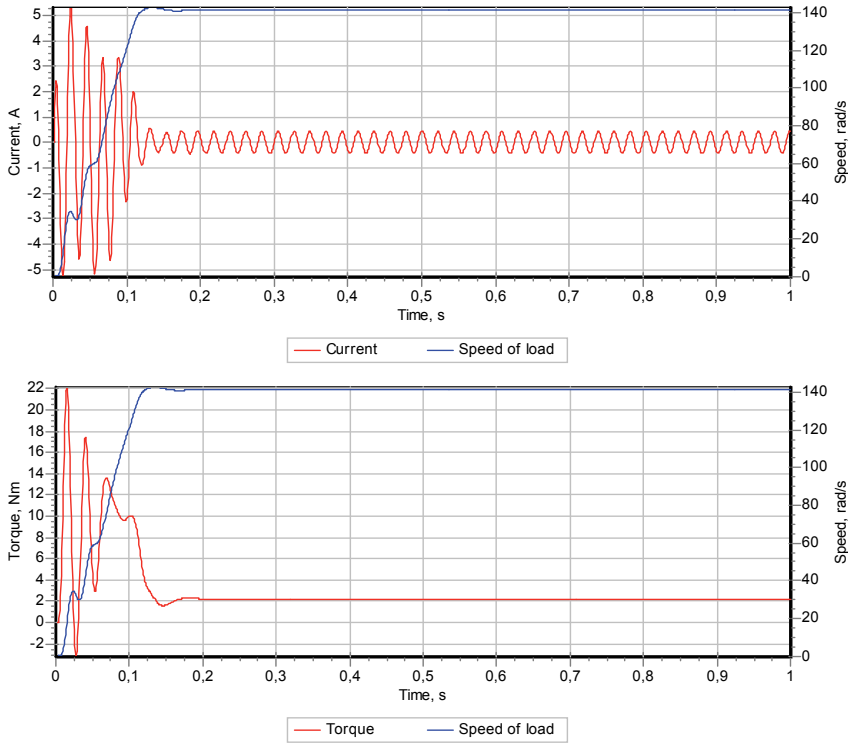


*Fig. 4.4 Speed-current and speed-torque traces of eDrive simulation of the direct start-up for the TUT experimental setup*

#### 4.1.4 Advanced Design Technology

In view of the above drawbacks of the contemporary motor drive CAD systems, an improved design technology is proposed in this work aiming to help a designer in the development of power economical motor drives. The improved technology flowchart is presented in Fig. 4.5. The process has a non-linear, multi-loop character because each step of the algorithm is completed by the validation of the obtained result. While the result does not satisfy the requirements specification, another choice was made and the corresponding branch of the flowchart is repeated.

Following the objective setting, problem statement, and requirements specification, the designer develops the mechanism travel diagram and estimates the load-carrying capacity, which results in the load torque, power, moment of inertia, and angular speed defining.

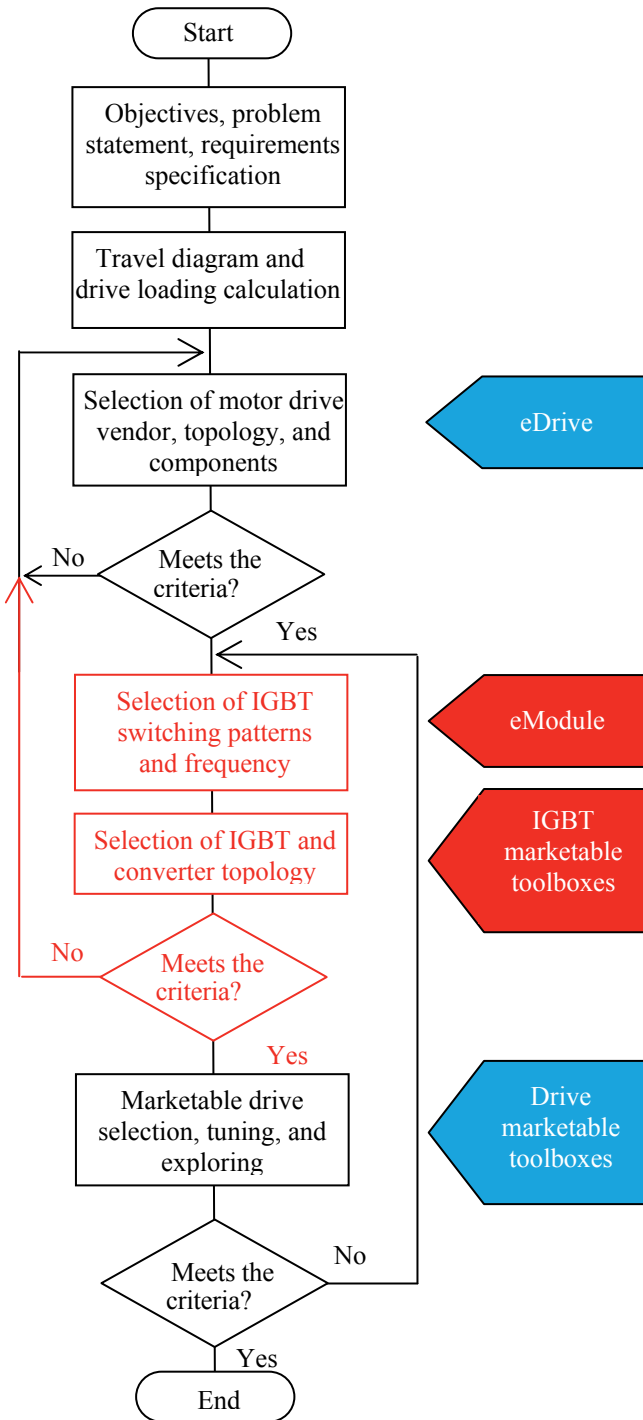


Fig. 4.5 Technological diagram of motor drive design

Next, the required motor drive components and the topology are selected and explored using *eDrive*. This toolkit provides the search of motors, gears, and

power converters as well as automatic component optimization. Each possible variant is explored within the library of the built-in models. Using the signal generator of *eDrive*, the required speeds and trajectories, references and disturbances for the electric drive are generated. The designer examines the influence of distortions and disturbances on the drive behavior and improves the system performance by the signal offsets, filters, and correctors. Then, the control system is designed. The library of *eDrive* includes all the required regulators and sensors. Their transfer functions, gains, factors, and time constants are calculated automatically to meet the standard settings. A designer tests the open-loop and closed-loop systems and conducts its optimization, if necessary.

An important stage of the described technology is to select and explore the switching patterns for power converters that supply a motor. An original toolkit called *eModule* has been developed to execute this operation. Its objective is to find the switching law, switching frequency, and switching pulse distribution to obtain the most power effective converter performance. The new software supplements such traditional toolkits as *PSIM* or *Matlab/Simulink* on the first design stage. Its organization and structure helps the designer to select, explore, and compare IGBT converters with different switching topologies along with the choice of the preferred vendor. In motor drive systems, the switching patterns govern the voltage and current harmonics, torque ripple, acoustic noise emitted from the motor as well as electromagnetic interference, therefore *eModule* serves as a helpful development stage for power electronic applications.

As neither *eDrive*, nor *eModule* provide the heating and power loss analysis of IGBT switches, the marketable toolkits of different IGBT vendors must be involved on the next design stage. They help a designer in choosing an IGBT and converter type, imposing restrictions, and estimating the results obtained. Using them, a designer can restructure a list of power modules and circuits and compose the optimum power system. One of the toolboxes from the semiconductor vendors is applied finally to select the particular IGBT and power converters along with the loss and temperature analysis.

At the same time, the three described design stages do not provide for exploration of such drive characteristics as torque and speed ripple, acoustic noise emitted from the motor, electromagnetic interference, etc. This is the reason why the next stage of the design must be inevitably supervised by the particular marketable motor drive toolboxes. ABB, Siemens, Omron, Sew Eurodrive, Maxon Motors, Mitsubishi Electric, etc. listed above are the typical candidates. Their methodologies are applied to check and recalculate the electrical and mechanical parameters of the drive, to select proper equipment, and to provide correct maintenance. On this stage, the standard drive is finally selected and explored. Also, the system designed is tuned in accordance with the corporative recommendations.



## **Resume of 4.1**

As it follows from the overview, there are no standard requirements to the CAD systems of the motor drive. Many companies have built their own design technology and provide a consumer with specific recommendations and design rules. The main drawback of this approach is the technological restriction and data limiting within the particular corporate scope that deprive a designer of an optimum way in the project. The technology proposed in this section involves five steps: preliminary calculation, search of a motor drive vendor using *eDrive* toolkit, selection of IGBT switching patterns and switching frequency using *eModule* toolbox, choice of IGBT and converter topology using IGBT marketable toolboxes, and a final drive selection, tuning, and exploring the use of drive marketable toolboxes. All the procedures are repetitive, being currently supervised by a designer.

## **4.2 New Toolbox for Switching Patterns Optimization**

### **4.2.1 Description of the Developed Toolbox**

Relying on the *Matlab/Simulink* models proposed in the previous chapters, a new toolbox has been developed. The aim of the *eModule* toolbox is to help in finding the switching patterns, including the switching law, switching frequency, and switching pulse distribution, which provide the most power effective converter performance in the scope of the required voltage and current THD values.

The package is enveloped into the modules, each performing different types of operations. For the best coherence, all the programs are united by the common computational environment written in C++ and user interface, which provides a uniform layout and functionality. Using the front panel, a design engineer can interact with the software to choose the required mode of performance and to set up new ranges and parameter values in algorithms.

The main features of the described soft tool that discern it from the models meant for the known toolboxes are:

- descriptiveness and compatibility of switching patterns;
- clearness of physical essence;
- suitability of report generation and format conversion;
- independence of particular vendors' interests;
- matching of the standards and design rules.

The toolbox opens broad possibilities to analyze and study three-phase bridge inverters offering the solution of the next project management problems:

- informational support in the selection of optimal switching patterns;
- mathematical and computer simulation along with overall computation;

- testing and result verifying in accordance with different criteria;
- comparison, tuning and optimization of control systems.

The technological diagram of *eModule* is shown in Fig. 4.6.

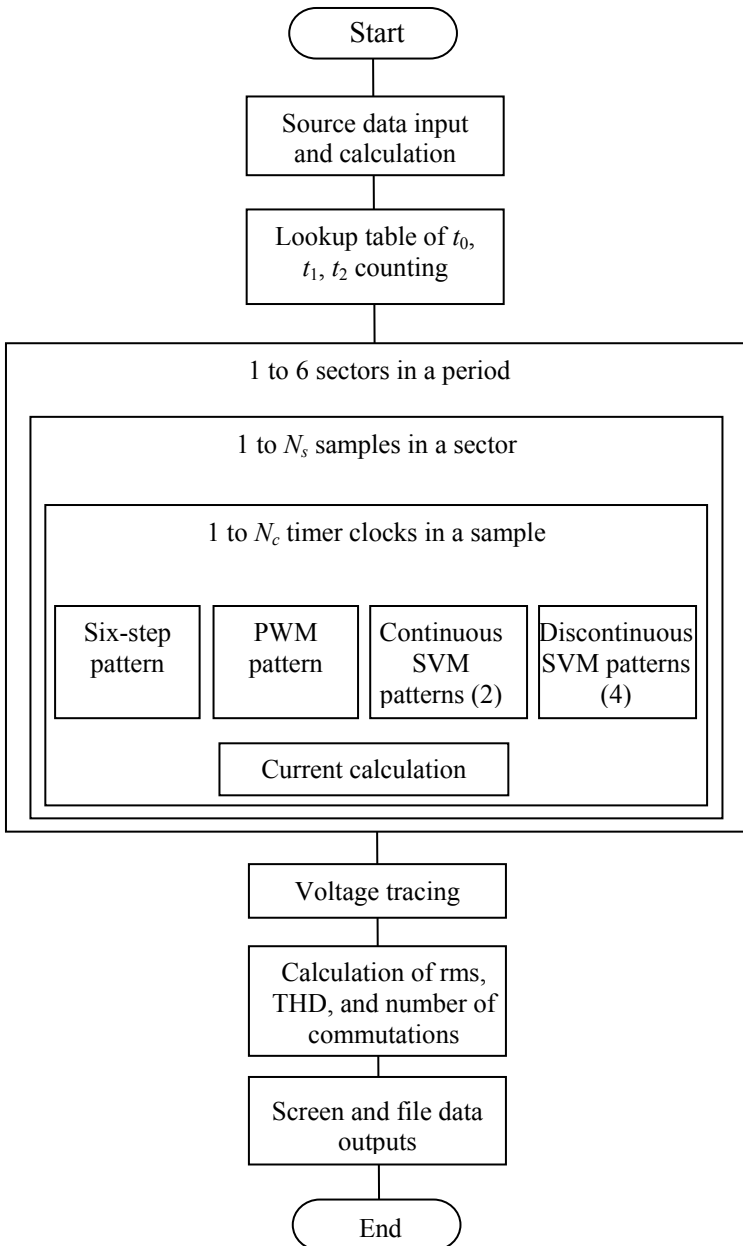


Fig. 4.6 Technological diagram of *eModule*

The toolbox involves the following components:

- body of adjustable controller schemes;

- model of an electromagnetic chain of the induction motor;
- signal generator to produce the test references;
- result analyzer to calculate voltage and current rms, average, extreme, and THD values;
- graphics package for the representation of the steady-state and dynamic simulated processes with automatic and manual scaling and preview facilities.

Three main modulation techniques are subjected to investigation by the toolbox - six-step modulation, PWM, and SVM. In the package described, the generic control method is based on the SVM approach. The list of SVM variants includes two continuous and four discontinuous patterns:

- continuous SVM;
- continuous SVM with the elimination of short pulses;
- discontinuous SVM with on-clamping;
- discontinuous SVM with off-clamping;
- discontinuous SVM with current-dependent clamping;
- discontinuous SVM with the elimination of short pulses.

PWM and six-step methods are considered here as the descendants of the generic SVM method. Such approach simplifies an analysis and comparison of different modulation techniques from the viewpoint of voltage and current profiles, ripples, and distortion. In the SVM mode of operation without short pulses the system provides an automatic search of optimal switching frequency. For each control method, an average IGBT switching frequency is counted.

Initial data for the switching patterns generation are as follows:

$F = 5$  to 55 Hz - user-defined referenced output frequency to specify the motor shaft speed of rotation;

$f_c = 1$  to 15 kHz - user-defined sampling frequency;

$k_{mod}$  - user-defined modulation index for PWM and SVM;

$T_e = 0$  to 9 ms - user-defined electromagnetic time constant of the motor;

$U_d$  - user-defined dc bus voltage;

$U/F$  - user-defined voltage-frequency control option for PWM and SVM;

$N_c = 32$  - number of timer clocks in a sample (timer frequencies 32 to 480 kHz, timer intervals 2 to 31  $\mu$ s);

$N_{s\ max} = 200$  - minimum number of samples in a sector;

$N_{max} = 36000$  - maximum number of timer clocks in a period;

$T_{min} = 18$  ms - shortest period of supply voltage obtainable at highest motor speed;

$T_{max} = 200$  ms - longest period of supply voltage at the lowest motor speed.

#### 4.2.2 Built-in Models of Inverter and Induction Motor

All the inverter models that accomplish *eModule* are considered as ideal components without losses and voltage drop in the power supply and in the load. To account for the real IGBT parameters, the vendors' software must be drawn after the switching pattern generation. Such approach allows gaining of analysis power along with the design development being suitable to explore the parameter influence on the system characteristics [17].

The voltage source inverter simulator makes it possible to connect each of the three motor phase coils to a positive or negative voltage of the ideal dc link source. To calculate the instant values of the phase-to-supply neutral, phase-to-load neutral and inner phase motor voltages, the model of an inverter proposed in 1.4 is applied in the toolbox.

The rms value of the phase voltage for the described operation depends on the dc link voltage  $U_d$  reaching  $\frac{U_d}{2}$  in the case of six-step modulation and  $\frac{k_{mod}U_d}{2}$  in the case of PWM and SVM control. The inverter leg phase voltages are obtained from 1.14 and 1.15. The line-to-line voltages are related to the phase voltages as given in 1.16.

To calculate the current values in the machine windings, an electromagnetic model of the induction motor is intended. A generic electrical machine description applied in the toolbox is based on a detailed motor model given in 3.1.1. Simultaneously, the voltage and current amplitude and rms values are counted using this model.

An induction motor fed from an inverter has harmonics in its voltage which give rise to harmonic current. As only the first harmonic of the supply voltage develops the motor torque, the phase voltages and currents of an inverter-fed motor must be expressed by the Fourier series. To find the THD data, the apparatus of the numerical spectral analysis was used. Using the fast Fourier transformation, the Fourier coefficients  $a_k$  and  $b_k$  of  $k^{th}$  harmonics, their amplitudes  $A_k$  and phases  $\phi_k$  are derived in respect to each  $i^{th}$  pulse of the given  $N$ -pulsing converter output signals having the sampling frequency  $f_c$ :

$$\begin{aligned}
 a_k &= \frac{2}{N} \sum_{i=0}^{N-1} y_i \cos(2\pi k f_c i dt), \\
 b_k &= \frac{2}{N} \sum_{i=0}^{N-1} y_i \sin(2\pi k f_c i dt), \\
 y_k &= \sum_{k=1}^i (a_k \cos(2\pi k f_c dt) + b_k \sin(2\pi k f_c dt)), \\
 A_k &= \sqrt{a_k^2 + b_k^2}, \quad \phi_k = -\arctan\left(\frac{b_k}{a_k}\right).
 \end{aligned} \tag{4.1}$$

THD yields as follows:

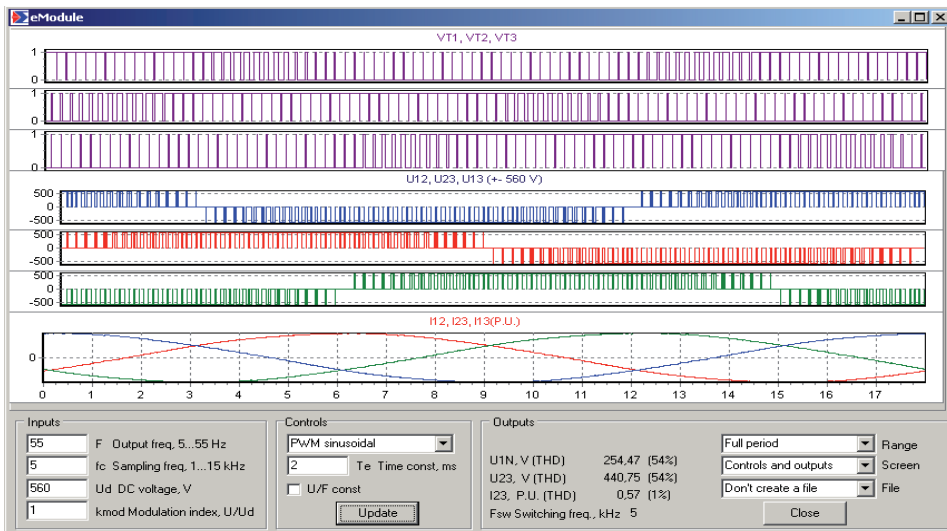
$$THD = \frac{\sqrt{\sum_{k=2}^{\infty} A_{(k)rms}^2}}{A_{(1)rms}} = \frac{\sqrt{A_{rms}^2 - A_{(1)rms}^2}}{A_{(1)rms}}. \quad (4.2)$$

These models are used in multiple simulation procedures conducted by a designer through the user interface.

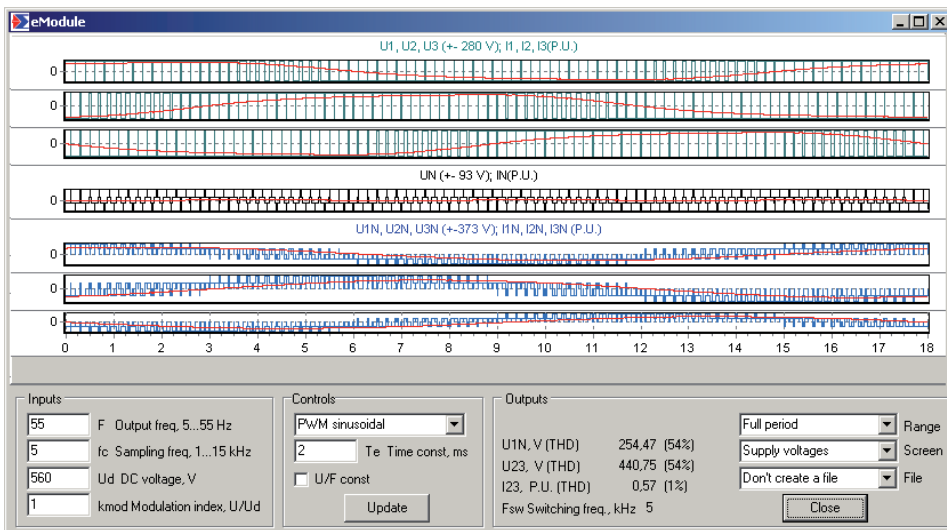
### 4.2.3 User Interface of the Toolbox

The main windows of the toolbox are shown in Fig. 4.7. Full information about the selected control method, load, and supply is accessible from the particular panes of the window. A researcher may try different variants of parameters, frequencies, loads, and tunings on these pages. The main window includes:

- diagram panel to display the gate, neutral, load phase (line-to-neutral) and line-to-line voltages and currents;
- panel *Inputs* to set such values as output and sampling frequencies, dc voltage, and modulation index;
- panel *Controls* for setting the following switching patterns: six-step, PWM, continuous and discontinuous SVM including the special SVM modes as well as an electromagnetic time constant, and the drive control mode;
- panel *Outputs* to display rms and THD values of voltages and currents as well as the switching frequency;
- selector of the displaying time intervals - the full-period or the particular sector;
- selector of the displaying traces and instruments for their scaling;
- report generator.



a.



b.

Fig. 4.7 Main windows of the toolbox: (a) control signals and line-to-line voltages; (b) load and inverter leg phase voltages

## Resume of 4.2

The toolbox *eModule* opens broad possibilities for the analysis and study of the multiple switching patterns of three-phase inverter-fed induction motor drives. It is suitable in the illustration of advantages and disadvantages of different steady-state and dynamic modes of the power converter performance in a number of applications. The proposed category of the simulation techniques can

be effectively applied in drives working in open loop voltage-frequency control modes. At the same time, it is proper for the vector and direct torque controlled drives. Using this software, new kinds of modulation algorithms and systems of motor drive inverters were developed.

### 4.3 Design Example of Inverter-Fed Motor Drive for a Vehicle Application

#### 4.3.1 Aim and Load Object

The aim of this section is to illustrate the motor drive design procedure for a vehicle supplied from the on-board battery source  $U_d = 400$  VDC. The types of the gear, motor, and power converter should meet the following drive composition:

- induction motor is supplied by an IGBT inverter with voltage/frequency control;
- worm-gear maximum total moved mass  $m$  is 3000 kg with axle radius  $r = 0.03$  m and wheel radius  $r_L = 0.25$  m;
- maximum traveling velocity  $v$  is equal 0.5 m/s;
- rolling friction of wheels  $\mu_r$  is 0.5 mm, sliding friction  $\mu = 0.02$ , inertia ratio  $\lambda_J = 100$ , and efficiency of the mechanical system  $\eta_L = 0.85$ .

The friction factor is determined as

$$\mu_{\Sigma} = \frac{\mu_r + \mu r}{r_L} = \frac{0.0005 + 0.020 \cdot 0.03}{0.25} = 0.0044. \quad (4.3)$$

The static power of the load

$$P_L = \frac{mg\mu_{\Sigma}v}{\eta_L} = \frac{3000 \cdot 9.81 \cdot 0.0044 \cdot 0.5}{0.85} = 76 \text{ W}. \quad (4.4)$$

The angular frequency of the wheel

$$\omega' = \frac{v}{r_L} = \frac{0.5}{0.25} = 2 \frac{\text{rad}}{\text{s}}. \quad (4.5)$$

The static load torque

$$M' = \frac{P_L}{\omega'} = \frac{76}{2} = 38 \text{ Nm}. \quad (4.6)$$

Moment of inertia of the driven wheels

$$J' = mr_L^2 = 3000 \cdot 0.25^2 = 187.5 \text{ kgm}^2 \quad (4.7)$$

### 4.3.2 Gear and Motor Selection

The three-phase bridge inverter is used in the drive. The phase supply voltage of an induction motor is limited by the inverter output value:

$$U_c = \frac{U_d \sqrt{2}}{3q_{\max}} - \frac{3U_F}{k} = \frac{400\sqrt{2}}{3 \cdot 0.95} - \frac{3 \cdot 2.5}{2} = 194 \text{ V}, \text{ (340 V line-to-line)} \quad (4.8)$$

where  $q_{\max}$  is the maximum duty ratio of the transistor switches,  $k$  is the number of current-conducted transistors,  $U_F$  is the mean IGBT voltage drop. A common-mode induction machine should operate at the frequency  $f_c$  proportional to the voltage level  $U_c$

$$f_c = \frac{f_M U_c}{U_M} = \frac{50 \cdot 194}{220} = 44 \text{ Hz}, \quad (4.9)$$

where  $f_M = 50 \text{ Hz}$  - rated motor frequency and  $U_M = 220 \text{ V}$  - rated motor phase voltage. The gears required should meet the restrictions:

$$M_G \geq M', \quad P_G \geq M' \omega' = 38 \cdot 2 = 76, \quad \text{and} \quad \frac{\omega_G}{i} \geq \omega' \cdot \frac{f_M}{f_c} = 2 \cdot \frac{50}{44} = 2.27 \quad (4.10)$$

Using *eDrive*, an SQL query is generated for searching the optimal motor-gear kit:

```
SELECT * FROM maABB, gp
WHERE Pg_W >= 38 * 2
AND ng_rpm / 10 / ig >= 2
AND Mg_Nm >= 38
AND P_W >= 38 * 2 * 100 / [%g]
AND P_W / n_rpm >= 38 * 10 / [%g] / ig
AND n_rpm / 10 >= 2 * ig
AND J_kgcm2 >= 187.5 / ig^2 / 100
ORDER BY Pg_W + P_W
```

This query provides the search from ABB induction motors database and warm gears to meet the calculated  $\omega'$ ,  $M'$ , and  $J$  values and criteria of minimal total motor-gear power. The result obtained includes the following motor-gear set:

- induction motor M3AA 90L,  $P_M = 550 \text{ W}$ ,  $\omega_M = 72 \text{ rad/s}$ ,  $M_M = 7.5 \text{ Nm}$ ,  $M_{\max} = 15.75 \text{ Nm}$ ,  $M_s = 12.75 \text{ Nm}$ ,  $J_M = 43 \text{ kgcm}^2$ ,  $I_M = 2.35 \text{ A}$ ,  $I_s = 7.05 \text{ A}$ ;
- warm gear 3P-25-1,  $i = 10$ ,  $M_G = 64 \text{ Nm}$ ,  $P_G = 750 \text{ W}$ ,  $\omega_G = 126 \text{ rad/s}$ ,  $\eta_G = 70 \%$ ;
- supply 194 V, 44 Hz.

Start-up open-loop current-speed and torque-speed timing diagrams from *eDrive* are shown in Fig. 4.8.



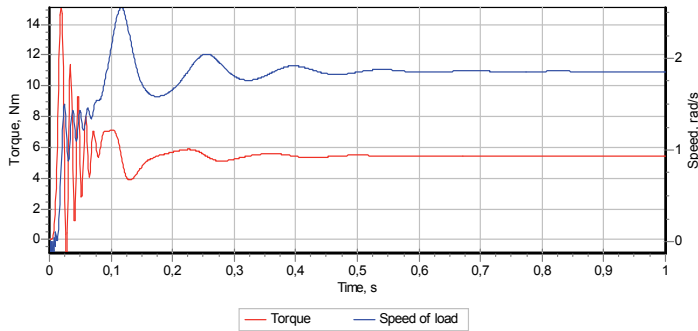
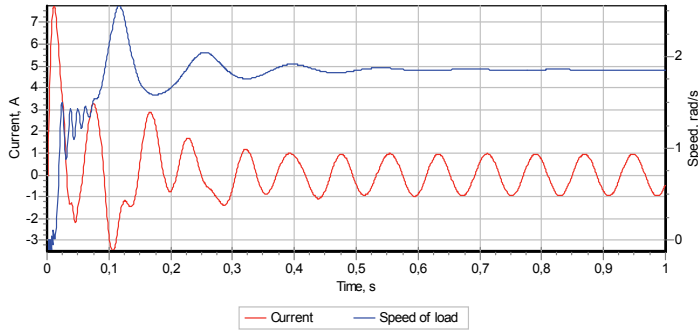
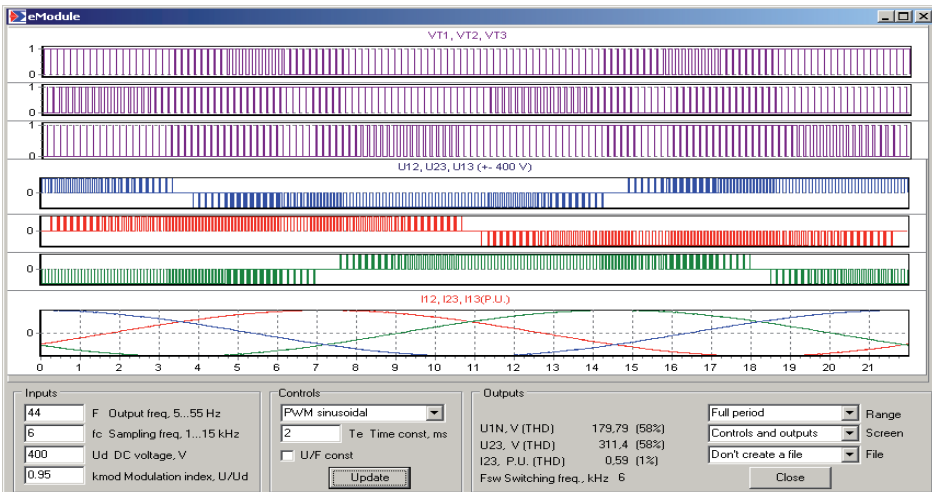


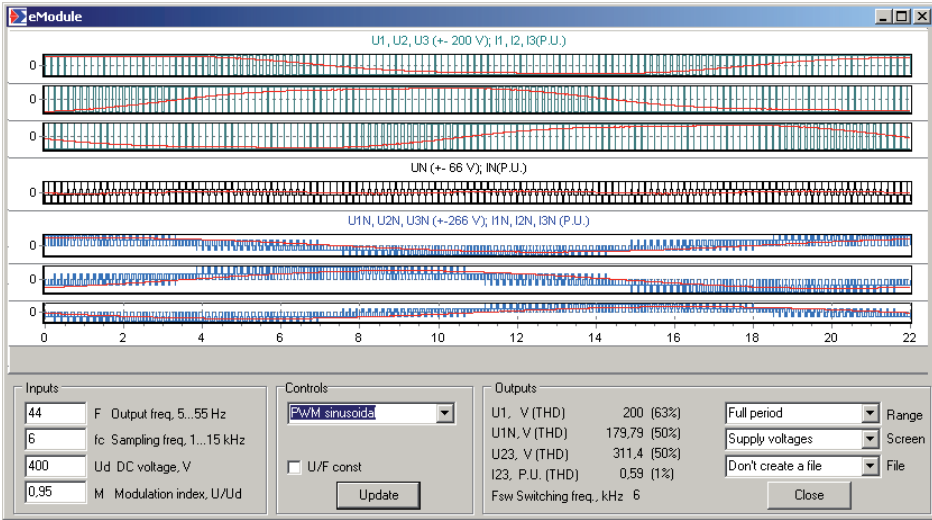
Fig. 4.8 Start-up current-speed and torque-speed diagrams of the open-ended desired systems

### 4.3.3 Inverter Design

Using *eModule* toolbox, inverter timing diagrams for possible modulation patterns and switching frequencies were obtained (Fig. 4.9 and 4.10).

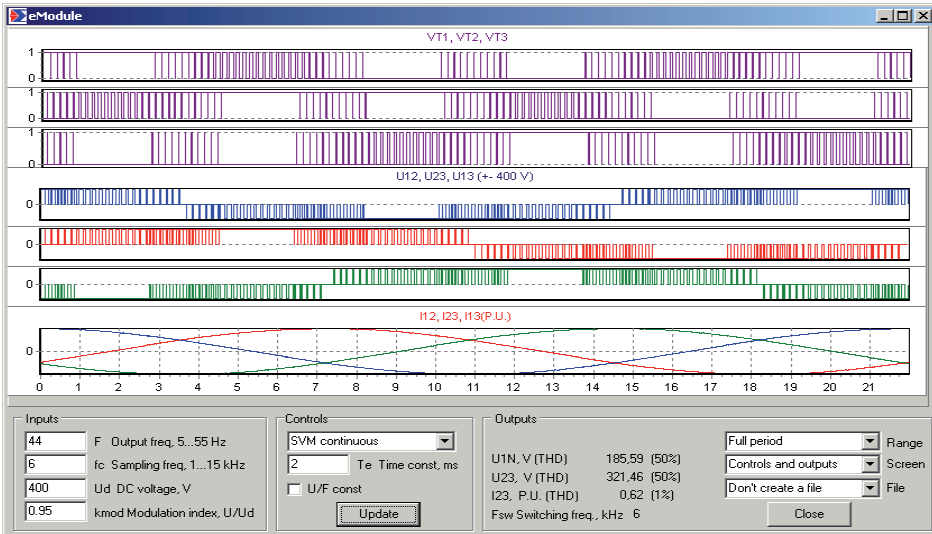


a.

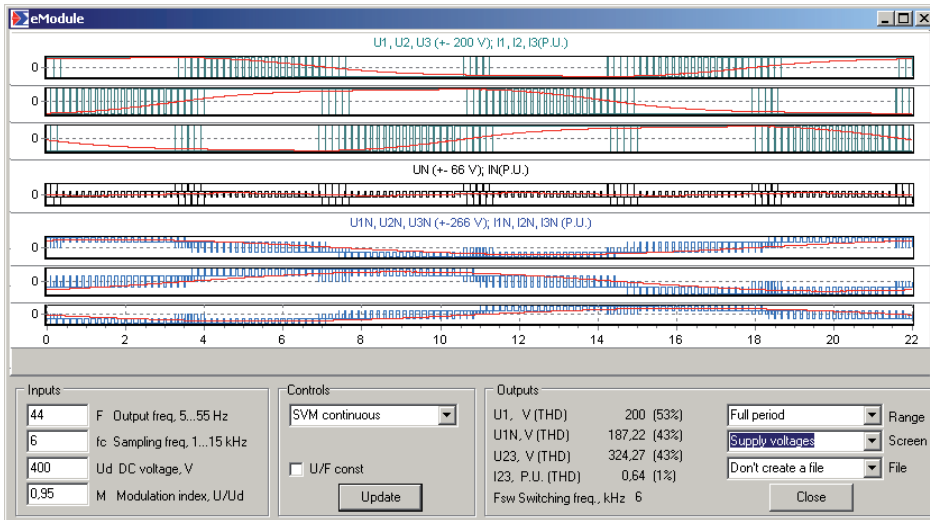


b.

Fig. 4.9 Screen dumps of PWM operation: (a) control signals and line-to-line voltages; (b) load and inverter leg phase voltages



a.



b.

Fig. 4.10 Screen dumps of continuous SVM operation: (a) control signals and line-to-line voltages; (b) load and inverter leg phase voltages

To evaluate and select power equipment, a *Semisel* toolbox was used. Three-phase bridge IGBT modules SKM 600GB066D of SEMITRANS line were selected with the following data:

$$U_d = 400 \text{ V}, U_c = 312 \text{ V}, I_c = 1.742 \text{ A}, P_c = 0.8 \text{ kW}, f_c = 44 \text{ Hz}, \cos \varphi = 0.85, f_{sw} = 6 \text{ kHz}, I_{cmax} = 17 \text{ A}, t_{overload} = 1 \text{ s}.$$

Results of heat calculation are presented in Tables 4.2 -4.4.

Table 4.2 Heating data from *Semisel*

Transistor	Diode
$E_{tr} = 37 \text{ mJ} (@300 \text{ V})$	$E_d = 25 \text{ mJ}$
$U_{CE.150} = 0.9 \text{ V}$	$U_{TO.150} = 0.9 \text{ V}$
$r_{c.150} = 2.025 \text{ mOhm}$	$r_{T.150} = 1.25 \text{ mOhm}$
$U_{CE.sat} = 2.12 \text{ V}$	$U_f = 1.65 \text{ V}$
$I_c = 600.00 \text{ A}$	$I_f = 600.00 \text{ A}$
$R_{th(i-e)} = 0.08 \text{ K/W}$	$R_{th(i-e)} = 0.125 \text{ K/W}$
$R_{th(c-s)} = 0.038 \text{ K/W}$	
* - soft turn-off in case of short circuit necessary	
Data set from 2008/01/22	

Table 4.3 Cooling data from *Semisel*

Ambient temperature	40°C
Number of switches per heat sink	6
Number of parallel devices on the same heat sink	1
Additional power source at this heat sink	0 W
Predefined SK-Heat Sink	P14 120
Correction factor	1
Natural air cooling, flow rate:	5m <sup>3</sup> /h
$R_{th(s-a)}$	0.727 K/W

Table 4.4 Calculated losses and temperatures with rated current, at overload and at  $f_{minout}$

	Rated current	Overload	$f_{min}$ and Overload
$P_{cond\ tr}$	0.71 W	7.35 W	4.44 W
$P_{sw\ tr}$	0.30 W	3.03 W	3.03 W
$P_{tr}$	1.02 W	10 W	7.47 W
$P_{cond\ d}$	0.06 W	0.58 W	3.45 W
$P_{sw\ d}$	0.82 W	3.32 W	3.34 W
$P_d$	0.88 W	3.90 W	6.79 W
$P_{tot}$	11 W	86 W	86 W
	Average Values	Average Values	Maximum Values
$T_h$	48 °C	48 °C	48 °C
$T_c$	48 °C	49 °C	49 °C
$T_{tr}$	48 °C	50 °C	51 °C
$T_d$	49 °C	49 °C	51 °C

Analysis confirms that for given operating conditions, the minimum temperature overheating of crystal is provided by SKM 600GB066D.

The wiring diagram of the ac drive built on the SKM 600GB066D is shown in Fig. 4.11. Here, the storage battery voltage from the power inputs V+, LeU, LeV, and LeW supplies the power inverter built on the IGBT switches VT1 - VT6 with freewheeling diodes. The associated triggering driver circuit supplied from 15 VDC switches the inverter's power transistors using high and low gate signals HinU...HinW, LinU...LinW so that a modulated voltage feeds the motor. The controller compares the set-points with actual values obtained from the phase current sensors VbU - VbW and generates the control signals that are routed to the gating circuits of the individual power transistors of the inverter through the gate current limiters Rg1 - Rg6. The desired waveform on the power outputs U, V, W is built up by switching the output transistors on and off at a fixed frequency. The modulated voltage produces a current in the motor. Heat and overload protection signals T/Itrip are also generated by the driver.

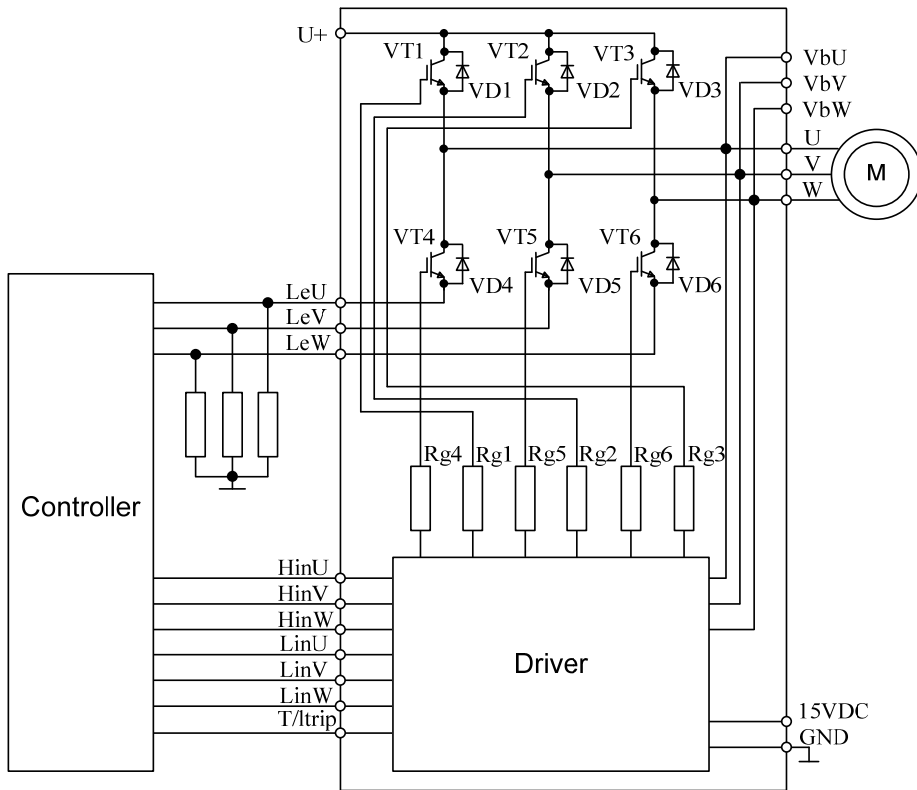


Fig. 4.11 Wiring diagram of designed system

### Resume of 4.3

The design example results in the energy effective motor drive built on the basis of the minimum power motor-gear kit and low-switching power inverter. The software tools used in the design procedure provide overall computation and simulation of electronic, electrical, and mechanical processes in the desired system.

## 4.4 Future Research Scenario

### 4.4.1 Involvement of a PWM Rectifier to Decrease Power Losses

One of the known drawbacks of IGBT inverters relates to the increase of THD along with the drop of the modulation index. Particularly, in Fig. 3.1 shown above, the current THD increases twofold since the modulation index decreases from 0.9 to 0.6. Fig. 4.12 illustrates a relationship between the voltage and current THD and the modulation index (dc bus voltage) keeping the stable line-to-line output voltage 100 V of an inverter.

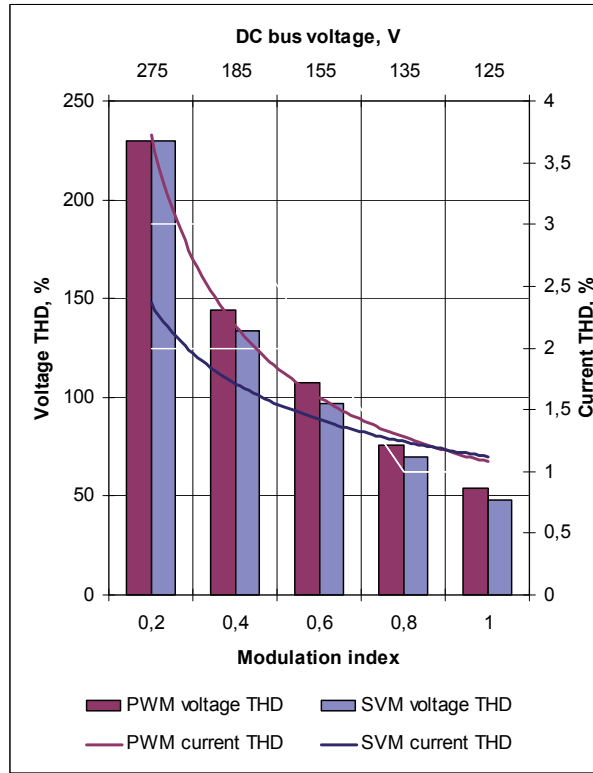


Fig. 4.12 Relationship between the voltage and current THD and the modulation index

These diagrams open the way to decrease the THD level by the control of the dc link voltage instead of the modulation index. In this way, the modulation index may be kept as high as 0.9 to 1.0 upon the low THD levels.

For this purpose, a PWM rectifier can be applied [30]. Today, energy consumers pay increasing attention to the energy quality since standard inverter applications create strong “polluting” phenomena for the energy distribution networks. As shown in 1.1.5, the majority of marketable inverters are produced with an input rectification stage that usually represents the simple diode bridge. However, this solution distorts the current and voltage of the power line with consequent line losses and interference due to the high harmonic content. Taking care of these problems, some manufacturers supply an inverter from a PWM rectifier, known also as an active front end, which exploits the peculiarities of an IGBT rectifier bridge rather than the diode classic bridge.

The operation principle of a PWM rectifier is described in [78] [79] [80]. An important benefit of the active front end circuits is the possibility to control the output dc voltage level.

The aim of the proposed operation consists in keeping the dc-link voltage at a desired reference value, using a feedback control loop as shown in Fig. 4.13. This reference value has to be high enough to keep the diodes of the rectifier

blocked. Once this condition is satisfied, the dc-link voltage is measured and compared with the reference. The error signal of this comparison is used to switch on and off the valves of the rectifier. In this way, power can come or return to the ac source according to the dc-link voltage value. When the dc load current is positive (rectifier operation), the capacitor is being discharged, and the error signal becomes positive. Under this condition, the control block takes power from the supply by generating the appropriate PWM signals for the six power transistor switches. In this way, current flows from the ac to the dc side, and the capacitor voltage is recovered. Inversely, when the inverter operation becomes negative, the capacitor is overcharged, and the error signal requests the control to discharge the capacitor returning power to the ac mains.

Evidently, using the regenerative active front-end instead of the typical drive configuration represents an expensive solution that can only be justified today in applications that truly need bidirectional power flow. However, thanks to well-known capabilities such as power regeneration, low harmonic input current, sinusoidal input current wave form, high total power factor, small filter, four-quadrant operation (bidirectional power transmission), the PWM rectifier with controlled dc-link voltage will become more popular in industry applications. Additional advantages can be summarized as follows:

- process energy is recovered from the power mains, eliminating the costs of resistive braking circuits;
- inverter absorbs a practically sinusoidal current from the power main at the unit power factor with low harmonic distortion;
- harmonic values generated by the inverter fall within the recommendations of IEEE 519;
- reactive energy is not derived from the power mains.

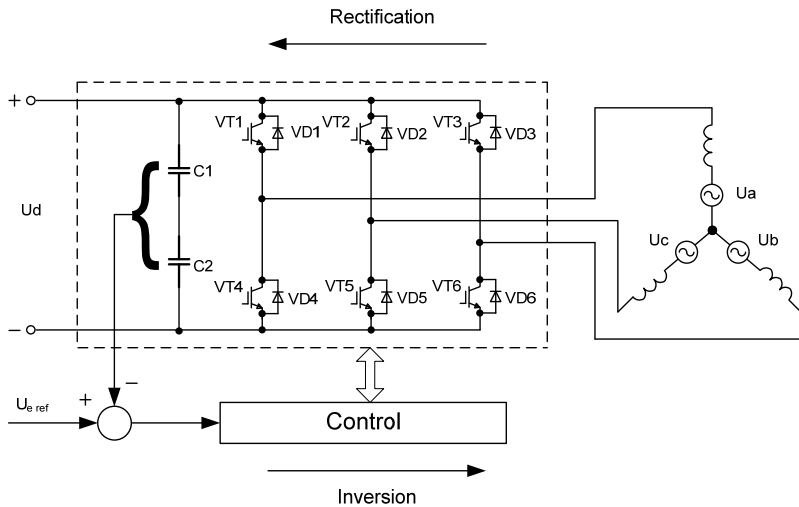


Fig. 4.13 Operation principle of a PWM rectifier with voltage control

#### 4.4.2 Adaptive SVM as a Universal Tool to Decrease Power Losses

An adaptive approach to modulation was initially proposed in [41] and [24]. The concept of adaptive SVM provides the use of the overall modulation range for maximal reduction of power losses by the selection of the optimal switching frequencies, currents and voltages in conjunction with the required motor drive operation.

To find the preferable modes of operation, the dependence was studied between the modulation index and the switching frequency for different modulation methods of the voltage-frequency controlled motor drive with 512 VDC inverter. The aim was to find the minimum sampling frequency sufficient for keeping the current THD in the 3 % range. Results of the study are shown in Fig. 4.14.

Using Fig. 4.14, two optimal modes of SVM can be recommended to achieve adaptation. These modes are distributed in the range of the modulation index as follows:

- $0 < k_{mod} \leq 0.5$  - continuous SVM with elimination of narrow pulses;
- $0.5 < k_{mod} \leq 1$  - discontinuous SVM with current-dependent clamping.

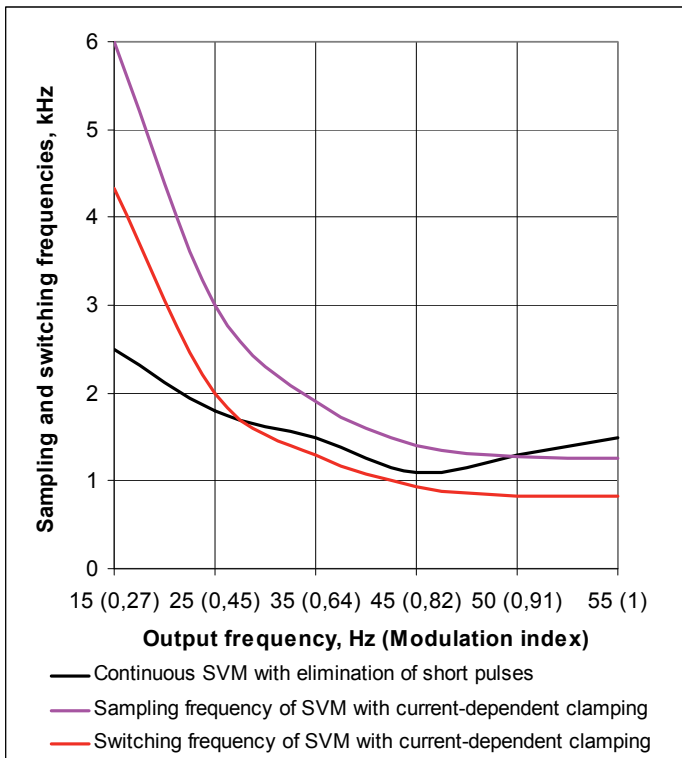


Fig. 4.14 Sampling and switching frequencies vs. output frequency for the voltage-frequency controlled motor drive



As distinct from [41] where four adaptive regions were suggested, and [24] where six and more regions were proposed, this study indicates that the two above methods can fully meet the demands of an adjustable motor drive with the voltage-frequency mode of operation. In the first region of low speeds (less than 30 Hz) and voltages (less than 300 V) the sampling frequency and switching frequencies may be reduced below 2.5 kHz or 4.5 kHz for the continuous SVM. In the second region of high speeds (30 to 55 Hz) and voltages (300 to 415 V) the peak of the load current should be located in the center of the clamped sectors for maximum reduction of switching losses. In this band, either online observation of the load current or application of the precomputed motor model is required.

#### **Resume of 4.4**

Two directions of the future research have been proposed and explored in this section. Replacing the traditional diode front-end by a PWM rectifier opens up new possibilities in power loss reduction. Simulation has shown the way to obtain the stable THD level by the control of the dc link voltage instead of the modulation index regulation. In this way, the modulation index may be kept as high as 0.8 to 1.0. An important drawback concerns the high cost of this approach in respect to the simple adjustable motor drives. Therefore, its application is restricted by high-effective closed-loop systems. In turn, an adaptive method of the power loss reduction proposed further in this section seems universal and therefore can be used in all drive applications.

#### **4.5 Conclusions**

1. The advanced motor drive design technology involves five steps: preliminary calculation, search of a motor drive vendor using *eDrive* toolkit, selection of IGBT switching patterns and frequency using *eModule* toolkit, choice of IGBT and converter topology using IGBT marketable toolboxes, and a final drive selection, tuning, and exploring by help of drive marketable toolboxes. All the procedures are multi-looped, being currently supervised by a designer.
2. The toolbox *eModule* is suitable for the analysis and study of multiple switching patterns of three-phase inverter-fed induction motor drives. It illustrates power converter performance taking into account the electromagnetic properties of the load. This software enables new kinds of modulation algorithms and systems of motor drive inverters to be developed.
3. The presented example illustrates the procedure of an energy economical motor drive design. The software tools used in the design procedure provide overall computation and simulation of electronic, electrical, and mechanical processes in the desired system.
4. Two directions of the future research have been proposed and explored. Replacing the traditional diode front-end by a PWM rectifier opens up new possibilities in power loss reduction. An important drawback concerns the high cost of this approach in respect to the simple adjustable motor drives. In turn, an adaptive method of the power loss reduction seems universal and therefore can be used in all drive applications.

## CONCLUSIONS

In this thesis new control methods for inverters that supply variable-speed induction motors of asynchronous drives were developed and studied. The proposed switching patterns govern the voltage and current harmonics, torque ripple, acoustic noise emitted from the motor as well as electromagnetic interference. A significant feature of the new technique is its focus on the load parameter variation and disturbance. As a final result, an enhanced computer aided design methodology for variable-speed induction motor drives suitable from the viewpoint of power economical inverter and motor combined performance was developed. Other results that provide valuable information, particularly for practical engineers, are listed below.

1. As power economic requirements grow along with increasing consumption and diminishing resources of power energy, the new prospective ways were suggested in the development of economic power converters.
2. To evaluate the influence of power losses on the efficiency, size, cost, power consumption, and other motor drive characteristics, an output power density was proposed as an effective figure of merit, instead of efficiency.
3. As a result of regimentation of the control systems, new possibilities for effective load-dependent power control were exposed. Among them, the real-time load tracking, the preliminary calculated modulation schemes, and the ahead counted evolution of the current were selected as the prospective research directions. In the basic partition of the control system, switching control layer that enables power electronics to behave as an adaptive system was found of primary importance from the viewpoint of power economical performance.
4. Careful analysis of switching patterns for IGBT inverters revealed the role of different modulation schemes in motor drive applications. Therefore, the problem of the synthesis of the new switching patterns, which can provide power economical performance for IGBT inverters of induction motor drives, was formulated.
5. A set of recommendations was drawn, including the peculiarities of different toolkits for the power converter design and exploration, which are to be taken into account in modelling and simulation.
6. Benefits and drawbacks of different control methods, such as six-step modulation, PWM, and SVM were illustrated in the steady-state and dynamic modes of the converter performance in ac drive applications.
7. Computer description of an induction motor has been elaborated to implement the concept of the load-dependent control.
8. New models and experimental methodology of the current-dependent clamping of inverter legs demonstrate their benefits for induction motor drives fed by both the continuous and discontinuous SVM inverters.

9. The developed algorithm and implementation technique of the elimination of short pulses from the switching patterns and the methodology of choosing the optimal switching frequency were confirmed by simulation and experimentation in the scope of an inverter-fed motor drive.

10. All the procedures of the new motor drive design methodology are explained in detail - preliminary calculation, selection of a motor drive vendor, topology, and components using *eDrive* toolkit, selection of IGBT switching patterns and frequency of using *eModule* toolkit, selection of IGBT and converter topology using IGBT marketable toolboxes, and a final drive selection, tuning, and exploration using the drive marketable toolboxes.

11. The toolbox *eModule* illustrates power converter performance taking in account the electromagnetic properties of the load. Using this software, new kinds of modulation algorithms and systems of motor drive inverters may be developed.

12. Two directions of the future research have been proposed and explored using *eModule*. Replacing the traditional diode front-end by a PWM rectifier opens up new possibilities in power loss reduction. A universal adaptive method of power loss reduction may be recommended for all adjustable drive applications.

## REFERENCES

- [1] Kerkman, R. J., Skibinski, G. L. and Schlegel, D. W., AC drives: Year 2000 (Y2K) and beyond, *14<sup>th</sup> Annual Applied Power Electronics Conference and Exposition APEC'99*, Dallas, TX, 1999, v. 1, pp. 28-39.
- [2] Jahnz, T. M. and Blasko, V., Recent advances in power electronics technology for industrial and traction machine drives, *Proceedings of the IEEE*, v. 89, no. 6, 2001, pp. 963-975.
- [3] Lorenz, R. D., Future motor drive technology issues and their evolution, *12<sup>th</sup> International Power Electronics and Motion Control Conference EPE-PEMC'06*, Portoroz, Slovenia, 2006, pp. 18-24.
- [4] Bocker, J., State of the art of induction motor control, *Electric Machines & Drives Conference IEMDC'07*, Antalya, Turkey, 2007, pp. 1459-1464.
- [5] Peng, F. Z., Recent advances and applications of power electronics and motor drives, *8<sup>th</sup> International Conference on Power Converters*, 2008, pp. 30-33.
- [6] Bose, B. K., Power electronics and motor drives recent progress and perspective, *IEEE Transactions on Industrial Electronics*, v. 56, no. 2, 2009, pp. 581-588.
- [7] Kazmierkowski, M. P. and Tunia, H., *Automatic Control of Converter-Fed Drives*, Amsterdam; NY, Elsevier; Warszawa, PWN, Polish Scientific Publishers, 1994, 559 p.
- [8] Krishnan, R., *Electric Motor Drives: Modeling, Analysis, and Control*, NY, Prentice Hall, 1996.
- [9] Novotny, D. W. and Lipo, T. A. *Vector Control and Dynamics of AC Drives*, NY, Oxford University Press, 1996, 440 p.
- [10] Leonhard, W., *Control of Electric Drives*, NY, Springer-Verlag, 1996, 420 p.
- [11] Грузов, В. Л., Вентильные преобразователи, Вологда, ВоГТУ, 2002, 92 с.
- [12] Соколовский, Г. Г., Электроприводы переменного тока с частотным управлением, Москва, Академия, 2006, 272 с.
- [13] Vodovozov, V. and Vinnikov, D., *Electronics Systems of Motor Drive*, Tallinn, TTU, 2008, 248 p.
- [14] Brown, M., *Practical Switching Power Supply Design*, NY, Academic Press, 1990, 240 p.
- [15] Vithayathil, J., *Power Electronics: Principles and Applications*, NY, McGraw-Hill, 1995, 632 p.

- [16] Joller, J., *Jõuelektronika*, Tallinn, TTU, 1996, 216 p.
- [17] Зиновьев, Г. С., *Основы силовой электроники*, Новосибирск, НЭТИ, 2000, 411 с.
- [18] Erickson, R. W. and Maksimovic, D. *Fundamentals of Power Electronics*, NY, Springer, 2001, 883 p.
- [19] Agrawal, J. P, *Power Electronic Systems: Theory and Design*, NJ, Prentice Hall, 2001, 562 p.
- [20] Mohan, N., Undeland, T. M. and Robbins, W. P, *Power Electronics: Converters, Applications, and Design*, NJ, John Wiley & Sons, 2003, 802 p.
- [21] Ang, S. and Oliva, A., *Power Switching Converters*, NY, Taylor & Francis, 2005, 540 p.
- [22] Ohashi, H., Power electronics innovation with next generation advanced power devices, The 25<sup>th</sup> International Telecommunications Energy Conference INTELEC'03, Pacifo, Yokohama, 2003, pp. 9-12.
- [23] Van Wyk, J. D., Lee, F. C., Boroyevich, D., Zhenxian L. and Kaiwei, Y., A future approach to integration in power electronics systems, *The 29<sup>th</sup> Annual IEEE Industrial Electronics Society Conference, IECON'03*, Richmond, Virginia, 2003, p. 1008.
- [24] Neacsu, D. O., *Power Switching Converters*, NY, Tailor & Fransis, 2006, 365 p.
- [25] Strzelecki, R. and Benysek, G. (Eds), *Power Electronics in Smart Electrical Energy Networks*, London, Springer-Verlag, 2008, 414 p.
- [26] Hingorani, N., Ginn, H., Sullivan, J., Control/protection architecture for power electronic converters, *57<sup>th</sup> Annual Petroleum and Chemical Industry Conference PCIC'10*, San Antonio, TX, 2010, Record of Conference Papers Industry Applications Society.
- [27] Vobecky, J., Future trends in high power devices, *27<sup>th</sup> International Conference on Microelectronics MEL'10*, NIS, Serbia, 2010, pp. 67-72.
- [28] Neacsu, D. O., Space vector modulation - An introduction, *The 27<sup>th</sup> Annual Conference of the IEEE Industrial Electronics Society, IECON'01*, Colorado, USA, 2001, pp. 1583 - 1592.
- [29] Kuang, S., Williams, B. W. and Finney, S. J., A review of IGBT models, *IEEE Transactions on Power Electronics*, v. 15, no. 6, 2005, pp. 1250-1266.
- [30] Kazmierkowski, M. P., Control strategies for PWM rectifier / inverter-fed induction motors, *IEEE International Symposium on Industrial Electronics ISIE'00*, Cholula, Puebla, Mexico, 2000, pp. TU15 = TU23.

- [31] Reddy, T. B., Amarnath, J. and Rayudu, D. S., New hybrid SVPWM methods for direct torque controlled induction motor drive for reduced current ripple, *IEEE Power Electronics, Drives and Energy systems for Industrial Growth Conference PEDES'06*, New Delhi, India, 2006, paper 3B-20.
- [32] Massobrio, G., *Semiconductor Device Modelling with Spice*, New Jersey, McGraw-Hill, 1993, 479 p.
- [33] Ramshaw, R. and Schuurman, D., *PSpice Simulation of Power Electronic Circuits: An Introductory Guide*, NY, Chapman & Hall, 1996, 400 p.
- [34] Usher, J. M., A tutorial and review of object-oriented design of manufacturing software systems, *Computers and Industrial Engineering*, v. 30, no. 4, 1996, pp. 781-798.
- [35] Hefner, A., Jr. and Bouche, S., Automated parameter extraction software for advanced IGBT modelling, The 7<sup>th</sup> IEEE Workshop on Computers in Power Electronics COMPEL'02, Puerto Rico, 2002, pp. 10-18.
- [36] Attia, J. O., *PSpice and Matlab for Electronics: An Integrated Approach*, Boca Raton, CRC Press, 2002, 338 p.
- [37] Dabney, J. B. and Harman, T. L., *Mastering Simulink*, NJ, Prentice Hall, 2004, 345 p.
- [38] Colgren, R., *Basic MATLAB, Simulink and Stateflow*, CA, AIAA, 2007, 485 p.
- [39] Spice, Available at: <http://en.wikipedia.org/wiki/SPICE>
- [40] Cetinkunt, S., Optimal design issues in high-speed high-precision motion servo systems, *Mechatronics*, v.1, no. 2, 1991, pp. 187-201.
- [41] Kazmierkowski, M. P., Krishnan, R. and Blaabjerg, F. (Eds.) *Control in Power Electronics*, Amsterdam, etc., Academic Press, 2002, 581 p.
- [42] Vodovozov, V. and Laugis, J., Object-oriented electric drive development technology, *IEEE International Electric Machines and Drives Conference IEMDC'07*, Antalya, Turkey, 2007, paper AF000434.
- [43] Браславский, И. Я., *Энергосберегающий асинхронный электропривод* Москва, Академия, 2004, 300 с.
- [44] Dolny, G. M., High-voltage semiconductor devices: Status and trends, *Bipolar/BiCMOS Circuits and Technology Meeting*, 2005, pp. 78-85.
- [45] Egorov, M., Vinnikov, D., Strzelecki, R. and Adamowicz, M. Impedance-source inverter-based high-power dc/dc converter for fuel cell applications, *8<sup>th</sup> IEEE International Conference on Environment and Electrical Engineering*, Karpacz, Poland, 2009, pp. 1-4.

- [46] Seguiet, G. and Labrique, F. Developments in power converters, *Mediterranean Conference "Integrating Research, Industry and Education in Energy and Communication Engineering" MELECON'89*, Lisbon, Portugal, 1989, pp. 59-64.
- [47] Колпаков, А., Melcosim? Iposim? Semisel?, *Силовая электроника*, 1, 2005.
- [48] Egorov, M., Vinnikov, D., Strzelecki, R. and Adamowicz, M., Comparison of three-phase isolated dc/dc converters with z- and quasi-z source inverters, *7<sup>th</sup> International Symposium "Topical Problems in the Field of Electrical and Power Engineering"*, Narva-Jõesuu, Estonia, 2009, pp. 9 – 14.
- [49] Egorov, M., Vinnikov, D. and Vodovozov, . Analysis of state of the art and development trends in soft-switched half-bridge dc/dc converters, *6<sup>th</sup> International Symposium "Topical Problems in the Field of Electrical and Power Engineering"*, Kuressaare, Estonia, 2009, pp. 49-54.
- [50] Ribeiro, P.F., Steurer, M. and Islam, M., Re-evaluating electric power system harmonic distortion limits for shipboard systems, *11<sup>th</sup> International Conference on Harmonics and Quality of Power*, 2004., pp. 706-711.
- [51] International Standard IEC 60034-2-1 "Rotating electrical machines – Part 2-1: Standard methods for determining losses and efficiency from tests; excluding machines for traction vehicles", 2008.
- [52] Gubia-Villabona, E., Sanchis-Gurpide, P., Alonso-Sadaba, O., Lumbreras-Azanza, A. and Marroyo-Palomo, L., Simplified high-frequency model for AC drives, *28<sup>th</sup> Annual Conference of the Industrial Electronics Society IECON'02*, Sevilla, Spain, 2002, v.2, pp. 1144-1149.
- [53] Kumar, A. Direct torque control of induction motor using imaginary switching times with 0-1-2-7 and 0-1-2 switching sequences: A comparative study, *The 30<sup>th</sup> Annual Conference of the IEEE IES'04*, 2004, pp. 1492-1497.
- [54] *NEC Application note 78K0. An Introduction to Space Vector Modulation using NEC's 8-bit Motor Control Microcontrollers*. Available at: [http://www2.renesas.eu/\\_pdf/U16699EE1V1AN00.pdf](http://www2.renesas.eu/_pdf/U16699EE1V1AN00.pdf).
- [55] Microhip Application notes, VF Control of 3-Phase Induction Motors using Space Vector Modulation. Available at: <http://ww1.microchip.com/downloads/en/AppNotes/00955a.pdf>.
- [56] *Texas Instr. Appl. Report, Space-Vector PWM with TMS320C24x/F24x using Hardware and Software Determined Switching Patterns*. Available at: <http://focus.ti.com/lit/an/spra524/spra524.pdf>.

- [57] Xing, K., Lee, F. C., Borojevic, D., Ye, Z. and Mazumder, S., Interleaved PWM with discontinuous space-vector modulation, *IEEE Transactions on Power Electronics*, v. 14, no.5, 1999, pp. 906-917.
- [58] Vodovozov, V. and Loparev, A., Simulation tool for design and testing of electric drives, *11<sup>th</sup> International Power Electronics and motion Control Conference EPE-PEMC'04*, Riga, Latvia, 2004, paper DS 7.16.
- [59] Vodovozov, V. and Raud, Z., Model-based learning in electric drive design, *The 2008 European Simulation and Modelling Conference ESM'08*, Le Harve, France, 2008, pp.355-359.
- [60] Egorov, M., Comparative analysis of toolboxes to explore power converters of electrical drives, *9<sup>th</sup> International Symposium "Topical Problems in the Field of Electrical and Power Engineering"*, Pärnu, Estonia, 2010, pp. 193-199.
- [61] Vodovozov, V., Raud, Z., and Egorov, M., A toolbox to design and study electric drives, *14<sup>th</sup> International Power Electronics and Motion Control Conference EPE-PEMC'10*, Ohrid, Macedonia, 2010, pp. T5-142 – T5-148.
- [62] National Instruments Multisim, Available at: <http://www.ni.com/multisim/>
- [63] PSIM Simulation Software. Available at: <http://www.psim-europe.com/>
- [64] *Simulink - Simulation and Model-Based Design*, Available at: <http://www.mathworks.com/products/simulink/>
- [65] Jalakas, T., Vinnikov, D., Roasto, I., Raud, Z. And Egorov, M., Versatile laboratory tools for advanced course of power electronics, *11<sup>th</sup> Biennial Baltic Electronics Conference BEC'08*, Tallinn, Estonia, 2008, pp.277-280.
- [66] Vodovozov, V., *Introduction to Power Electronics*, Copenhagen, Ventus Publishing, 2010, 118 p.
- [67] *Melcosim IGBT Loss Simulator*. Available at: [http://www.pwr.com/pwr/app/melcosim\\_app\\_note.pdf](http://www.pwr.com/pwr/app/melcosim_app_note.pdf).
- [68] *Semisel - Semikron Simulation Software*. Available at: <http://semisel.semikron.com/circuit.asp>
- [69] Egorov, M. and Vodovozov, V., Space vector modulation with reduced switching losses for motor drive inverters, *7<sup>th</sup> IEEE Conference-Workshop "Compatibility and Power Electronics" CPE'11*, Tallinn, Estonia, 2011, pp. 388 – 393.
- [70] *SemiSel*. Available at: [http://www.semikron.com/skcompub/de/SID-04CC6C59-44633F97/AN-8004\\_SemiSel\\_Version-3-1\\_final.pdf](http://www.semikron.com/skcompub/de/SID-04CC6C59-44633F97/AN-8004_SemiSel_Version-3-1_final.pdf)



- [71] *Mitsubishi Electric Power Module Loss Simulator*. Available at: [http://www3.mitsubishichips.com/dm/binu\\_als\\_form\\_e.pl](http://www3.mitsubishichips.com/dm/binu_als_form_e.pl)
- [72] *New Webtools Speed-up*, Available at: <http://powerelectronics.com/images/Semiconductors211.pdf>
- [73] Vodovozov, V., The educational resources of mechatronics, *Mechatronic*, v. 5, no.1, 1995, pp. 15-24.
- [74] *Drive engineering - Practical implementation. Volume 1. Drive Arrangements with SEW Geared Motors. Calculation Methods and Examples*, SEW Eurodrive, 1998.
- [75] *Siemens Standard Drives.Application Handbook*, Congleton, Siemens, 1997.
- [76] Roos, F., Johansson, H. and Wikander, J., Optimum selection of motor and gearhead in mechatronic applications, *Mechatronics*, v. 16, no. 1, 2006, pp. 16-24.
- [77] *eDrive - Toolbox to Design Electric Drives*, Available at: <http://edrive.narod.ru>
- [78] Rodríguez J. R., Dixon, J. W., Espinoza J. R., Pontt, J. and Lezana, P., PWM regenerative rectifiers: State of the art, *IEEE Transactions On Industrial Electronics*, v. 52, no. 1, 2005, pp. 5 – 22.
- [79] Marques, G.D., A PWM rectifier control system with dc current control based on the space vector modulation and stabilization, *7<sup>th</sup> International Conference on Power Electronics and Variable Speed Drives*, 1998, 1998, pp. 74 - 79.
- [80] Malinowski, M., Kazmierkowski, M. P. and Tryznadlowski, A., Direct power control with virtual flux estimation for three-phase PWM rectifiers, *IEEE International Symposium on Industrial Electronics ISIE'00*, Cholula, Puebla, Mexico, 2000, v. 2, pp. 442 – 447.

## ABSTRACT

This thesis is devoted to the development of control methods for low-loss IGBT inverter-fed induction motor drives. The area of research covers the variable-speed induction motor drive supplied from an IGBT inverter with dc link. Major attention is paid to the control methods, mainly to the switching layer of the control system with voltage-frequency operation. To evaluate the proposed technical solutions, mathematical models, simulations and experimental devices were used. Two effective IGBT control principles are proposed for use: current-dependent clamping of inverter legs which decreases the losses and temperature of inverter-fed drive components and the principle of the elimination of short pulses from the switching patterns which opens a way to choose the optimal switching frequency in respect to the particular application performance.

Development and study of control methods are analyzed in the first part of the thesis. The problem is significant because IGBT control governs the voltage and current harmonics, torque ripple, acoustic noise, and electromagnetic interference. An essential feature of the proposed technique is the adaptation of the inverter control to the load parameters.

Improvements in the methodology of computer aided motor drive design based on the new IGBT switching patterns are introduced in the second part of the thesis. The proposed approach focuses on the converter composition that provides minimization of the drive power losses. The main research tasks were solved:

- Development of simulation and experimental tools to study the major techniques of inverter control in induction drive applications
- Exploring the IGBT modulation methods from the viewpoint of loss reduction
- Proposition, examination, and implementation of the new switching patterns for the modulation systems of motor drive inverters
- Improvement in the methodology of computer aided motor drive design based on the new IGBT switching patterns

The thesis consists of four chapters. Chapter 1 is devoted to the state of the art of the research and recent advances in power electronics technology for induction motor drives. Chapter 2 introduces the simulation study of IGBT inverters for induction motor drives. For this purpose different modulation methods were implemented in the Matlab/Simulink environment. Chapter 3 covers the implementation and evaluation of new load-dependent IGBT switching patterns. The last chapter opens the new possibilities in computer aided design of inverter-fed induction motor drives.

## KOKKUVÕTE

Doktoritöö arendatakse välja kõrge efektiivsusega IGBT-põhiste pingetoiteliste vaheldite juhtimismeetodid. Antud vaheldid on mõeldud asünkroonajamite kiiruse ja momendi reguleerimiseks. Väitekirja põhitähelepanu on suunatud vaheldi lülitusmeetoditele. Doktoritöö käigus väljaarendatud juhtimis põhiõhõtete paikapidavust kontrolliti nii matemaatiliste mudelite, raalsimulatsioonide kui ka ehitatud katsemaketi abil. IGBT-de juhtimiseks pakutakse välja kaks lülitusmeetodit: voolust sõltuvat vaheldi õlgade õntimist ja liigluhikeste impulsside elimineerimist lülitustabelist. Esimene meetod vähendab kadusid ja komponentide töötemperatuuri, teine meetod võimaldab valida optimaalset lülitussagedust vastavalt konkreetsele rakendusele.

Väitekirja esimeses osas uuritakse ja töötatakse analüütiliselt välja juhtimismeetodid. Teema tähtsust rõhutab fakt, et IGBTde juhtimisviisis sõltuvad mitmed faktorid: voolu ja pinge harmoonilised, momendi pulsatsioon, müratase ja elektromagnetilised häired. Väljapakutud meetodi üheks oluliseks omaduseks on vaheldi juhtimisviisi kohandamine koormuse iseloomuga. Esimeses osas väljatöötatud meetodeid täiustati töö teises osas. Täideti järgnevad eesmärgid:

- arvutimudelite koostamine ja katsestendi ehitamine vaheldi juhtimismeetodite eksperimentaalseks uurimiseks asünkroonajamites;
- IGBT modulatsioonimeetodite uurimine eesmärgiga vähendada kadusid;
- uue elektriajami vaheldile mõeldud modulatsiooniviisi väljatöötamine, uurimine ja rakendamine;
- IGBT lülitusviisidele baseeruva elektriajami raalprojekteerimismeetodi täiustamine.

Doktoritöö koosneb neljast peatükist. Esimeses peatükis tuuakse ära elektriajamite muundurite tehnika tase. Teises peatükis uuritakse IGBT vaheldeid Matlab/Simulink keskkonnas loodud arvutisimulatsioonide abil. Väljatöötatud, koormuse iseloomu arvestavate modulatsioonimeetodite rakendamist käsitleb kolmas peatükk. Viimases ehk neljandas peatükis on ära toodud uued võimalused vahelditoiteliste asünkroonajamite raalprojekteerimiseks.

## AUTHOR'S MAIN PUBLICATIONS

1. Egorov, M. and Vodovozov, V., Space vector modulation with reduced switching losses for motor drive inverters, 7<sup>th</sup> IEEE Conference-Workshop "Compatibility and Power Electronics" CPE'11, Tallinn, Estonia, 2011, pp. 388 - 393.
2. Vodovozov, V. and Egorov, M., Discontinuous space vector modulation technique for motor supply, International IEEE Conference EUROCON'11, Lisbon, Portugal, 2011, paper 259.
3. Egorov, M., Simulation study of inverter-fed motor drives, 10<sup>th</sup> International Symposium "Topical Problems in the Field of Electrical and Power Engineering" and Doctoral School of Energy and Geotechnology II, Pärnu, Estonia, 2011, pp. 165 - 168.
4. Vodovozov, V., Raud, Z., and Egorov, M., A toolbox to design and study electric drives, 14<sup>th</sup> International Power Electronics and Motion Control Conference EPE-PEMC'10, Ohrid, Macedonia, 2010, pp. T5-142 - T5-148.
5. Egorov, M., Comparative analysis of toolboxes to explore power converters of electrical drives, 9<sup>th</sup> International Symposium "Topical Problems in the Field of Electrical and Power Engineering", Pärnu, Estonia, 2010, pp. 193 - 199.
6. Andrijanoviš, A., Egorov, M., Lehtla, M. and Vinnikov, D., New method for stabilization of wind power generation using an energy storage technology, Agronomy Research, 2010, 8(S1), pp. 12 - 24.
7. Andrijanoviš, A., Egorov, M., Lehtla, M. and Vinnikov, D., A hydrogen technology as buffer for stabilization of wind power generation, 8<sup>th</sup> International Symposium "Topical Problems in the Field of Electrical and Power Engineering". Doctoral School of Energy and Geotechnology II, Pärnu, Estonia, 2010, pp. 62 - 70.
8. Vinnikov, D., Hõimoja, H., Rosin, A. and Egorov, M., Load leveling and loss minimization in tram systems - Possibilities and challenges, Техническая электродинамика. Тематический выпуск, Киев, 2009, pp. 83 - 88.
9. Egorov, M., Vinnikov, D., Strzelecki, R. and Adamowicz, M., Comparison of three-phase isolated dc/dc converters with z- and quasi-z source inverters, 7<sup>th</sup> International Symposium "Topical Problems in the Field of Electrical and Power Engineering", Narva-Jõesuu, Estonia, 2009, pp. 9 - 14.
10. Vinnikov, D., Egorov, M. and Strzelecki, R., Evaluative analysis of 2- and 3-level dc/dc converters for high-voltage high-power applications,

- 6<sup>th</sup> IEEE Conference-Workshop "Compatibility and Power Electronics" CPE'09, Badajoz, Spain, 2009, pp. 432 - 437.
11. Egorov, M., Vinnikov, D., Strzelecki, R. and Adamowicz, M. Impedance-source inverter-based high-power dc/dc converter for fuel cell applications, 8<sup>th</sup> IEEE International Conference on Environment and Electrical Engineering, Karpacz, Poland, 2009, pp. 1 - 4.
  12. Egorov, M., Vinnikov, D. and Vodovozov, V., Analysis of state of the art and development trends in soft-switched half-bridge dc/dc converters, 6<sup>th</sup> International Symposium "Topical Problems in the Field of Electrical and Power Engineering", Kuressaare, Estonia, 2009, pp. 49 - 54.
  13. Egorov, M.; Vinnikov, D.; Vodovozov, V. Электролиз как способ аккумуляции избыточной энергии ветроэнергетических установок, Техническая электродинамика. Тематический выпуск, Киев, 2008, pp. 42 - 47.
  14. Винников, Д., Лаугис, Ю., Лехтла, Т. и Егоров, М., О результатах многолетнего сотрудничества Института электропривода и силовой электроники ТТУ с Таллинским трамвайно-троллейбусным объединением, International Education and Science Cooperation IESC'08, С.-Петербург, Россия, 2008, с. 271 - 279.
  15. Vinnikov, D., Laugis, J., Strzelecki, R. and Egorov, M., 6.5 kV IGBT switch realization possibilities and their feasibility study for high-power applications, 6<sup>th</sup> International Conference on Electrical Engineering ICEENG'08, Cairo, Egypt., 2008, p. 9.
  16. Vinnikov, D., Jalakas, T. and Egorov, M., Feasibility study of half- and full-bridge isolated dc/dc converters in high-voltage high-power applications, 13<sup>th</sup> International Power Electronics and Motion Control Conference EPE-PEMC'08, Poznan, Poland, 2008, pp. 1272 - 1277.
  17. Jalakas, T., Mölder, H. and Egorov, M., EMI reduction problems in power converters with 6.5 kV IGBTs, The 6<sup>th</sup> International Conference "2008 Power Quality and Supply Reliability" PQ'08, Pärnu, 2008, pp. 229 - 233.
  18. Jalakas, T.; Vinnikov, D.; Roasto, I.; Raud, Z.; Egorov, M. (2008). Versatile Laboratory Tools for Advanced Course of Power Electronics. In: BEC 2008 : 2008 International Biennial Baltic Electronics Conference : Proceedings: 11th Biennial Baltic Electronics Conference, Tallinn University of Technology, 6-8 Oct. 2008, pp. 277 - 280.
  19. Egorov, M., Vinnikov, D. and Vodovozov, V., Feed drive of a lathe, 5<sup>th</sup> International Symposium "Topical Problems in the Field of Electrical and Power Engineering", Kuressaare, Estonia, 2008, pp. 163 - 169.

## LISA 1 / ANNEX 1

### ELULOOKIRJELDUS

#### 1. Isikuandmed

Ees- ja perekonnanimi: Mikhail Egorov  
Sünniaeg ja -koht: 17.01.1983, Saint-Petersburg  
Kodakondsus: Vene  
Perekonnaseis: vallaline  
Lapsed: -

#### 2. Kontaktandmed

Aadress: Akadeemia tee 5, Tallinn 12611  
Telefon: (+372) 53244168  
E-posti aadress: mikhail.egorov@ttu.ee

#### 3. Hariduskäik

<b>Õppeasutus (nimetus lõpetamise ajal)</b>	<b>Lõpetamise aeg</b>	<b>Haridus (eriala/kraad)</b>
Saint-Petersburgi Riiklik Tehnikainstituut	2007	Dipl. Ins.
Saint-Petersburgi Elektrotehnika Kolledž	2002	tehnika
Saint-Petersburgi Keskool	1998	keskharidus

#### 4. Keelteoskus (alg-, kesk- või kõrgtase)

<b>Keel</b>	<b>Tase</b>
vene	emakeel
inglise	kesktase
eesti	algtase

#### 5. Teenistuskäik

<b>Töötamise aeg</b>	<b>Ülikooli, teadusasutuse või muu organisatsiooni nimetus</b>	<b>Ametikoht</b>
2009	Gdynia Maritime ülikool, Poola	staseerimine
2007 -	Tallinna Tehnikaülikool	doktorant

## 6. Teadustegevus

2011-2016	SF0140016s11 Aktiivsete elektri jaotusvõrkude muundurite topoloogiad ja juhtimismeetodid
2011-2014	ETF8538 Kvaasi-impedantsallikaga alalis- ja vahelduvpingemuundurid
2009-2012	ETF8020 Võimsate IGBT muundurite innovatiivsete juhtimis- ja diagnoostikasüsteemide uurimine
2008-2010	ETF7425 Kõrgepingeliste IGBT transistoride lülitusomaduste uurimine

## 7. Kaitstud lõputööd

- “Treipingi etteandeam” (Dipl. Ins., 2007, Saint-Petersburgi Riiklik Tehnikainstituut)

## 8. Teadustöö põhisuunad

- Väikeste kadudega ja muudetava kiirusega asünkronajamite taitvate inverterite juhtimismeetodite valjatöötamine ja uurimine

Kuupäev: 25.07.11.

## LISA 2 / ANNEX 2

### CURRICULUM VITAE

#### 1. Personal information

Name: Mikhail Egorov

Date and place of birth: 17.01.1983, Saint-Petersburg

Citizenship: Russian

Marital status: single

Children: no

#### 2. Contact information

Address: Akadeemia tee 5, Tallinn 12611

Telephone: (+372) 53244168

E-mail: mikhail.egorov@ttu.ee

#### 3. Education

<b>Institution</b>	<b>Graduation year</b>	<b>Education</b>
Saint-Petersburg State Engineering Institute	2007	Dipl. Eng.
Saint-Petersburg Electrotechnical College	2003	Technician
Saint-Petersburg School	1998	Basic

#### 4. Languages

<b>Language</b>	<b>Level</b>
Russian	Native
English	Middle
Estonian	Basic

#### 5. Professional Employment

<b>Date</b>	<b>Organization</b>	<b>Position</b>
2009	Gdynia Maritime University, Poland	study course
2007 -	Tallinn University of Technology	doctoral student



#### 6. Scientific work

2011-2016	SF0140016s11 New converter topologies and control methods for electronic power distribution networks
2011-2014	ETF8538 Quasi-impedance source DC/DC and AC/AC converters
2009-2012	ETF8020 Research of advanced control and diagnostics systems for the high-power IGBT converters
2008-2010	ETF7425 Research of dynamic performance of high-voltage IGBTs

#### 7. Defended theses

- “Feed Drive of a Lathe” (Dipl. Eng, 2007, Saint-Petersburg State Engineering Institute)

#### 8. Main areas of scientific work

- Development and explore the control methods for inverters that supply low-loss variable-speed induction motor drives.

Date: 25.07.11.

**DISSERTATIONS DEFENDED AT  
TALLINN UNIVERSITY OF TECHNOLOGY ON  
*POWER ENGINEERING, ELECTRICAL ENGINEERING,  
MINING ENGINEERING***

1. **Jaan Tehver**. Boiling on Porous Surface. 1992.
3. **Endel Risthein**. Electricity Supply of Industrial Plants. 1993.
4. **Tõnu Trump**. Some New Aspects of Digital Filtering. 1993.
5. **Vello Sarv**. Synthesis and Design of Power Converters with Reduced Distortions Using Optimal Energy Exchange Control. 1994.
6. **Ivan Klevtsov**. Strained Condition Diagnosis and Fatigue Life Prediction for Metals under Cyclic Temperature Oscillations. 1994.
7. **Ants Meister**. Some Phase-Sensitive and Spectral Methods in Biomedical Engineering. 1994.
8. **Mati Meldorf**. Steady-State Monitoring of Power System. 1995.
9. **Jüri-Rivaldo Pastarus**. Large Cavern Stability in the Maardu Granite Deposit. 1996.
10. **Enn Velmre**. Modeling and Simulation of Bipolar Semiconductor Devices. 1996.
11. **Kalju Meigas**. Coherent Photodetection with a Laser. 1997.
12. **Andres Udal**. Development of Numerical Semiconductor Device Models and Their Application in Device Theory and Design. 1998.
13. **Kuno Janson**. Paralleel- ja järjestikresonantsi parameetrilise vaheldumisega võrgusageduslik resonantsmuundur ja tema rakendamine. 2001.
14. **Jüri Joller**. Research and Development of Energy Saving Traction Drives for Trams. 2001.
15. **Ingo Valgma**. Geographical Information System for Oil Shale Mining – MGIS. 2002.
16. **Raik Jansikene**. Research, Design and Application of Magnetohydrodynamical (MHD) Devices for Automation of Casting Industry. 2003.
17. **Oleg Nikitin**. Optimization of the Room-and-Pillar Mining Technology for Oil-Shale Mines. 2003.
18. **Viktor Bolgov**. Load Current Stabilization and Suppression of Flicker in AC Arc Furnace Power Supply by Series-Connected Saturable Reactor. 2004.

19. **Raine Pajo.** Power System Stability Monitoring – an Approach of Electrical Load Modelling. 2004.
20. **Jelena Shuvalova.** Optimal Approximation of Input-Output Characteristics of Power Units and Plants. 2004.
21. **Nikolai Dorovatovski.** Thermographic Diagnostics of Electrical Equipment of Eesti Energia Ltd. 2004.
22. **Katrin Erg.** Groundwater Sulphate Content Changes in Estonian Underground Oil Shale Mines. 2005.
23. **Argo Rosin.** Control, Supervision and Operation Diagnostics of Light Rail Electric Transport. 2005.
24. **Dmitri Vinnikov.** Research, Design and Implementation of Auxiliary Power Supplies for the Light Rail Vehicles. 2005.
25. **Madis Lehtla.** Microprocessor Control Systems of Light Rail Vehicle Traction Drives. 2006.
26. **Jevgeni Šklovski.** LC Circuit with Parallel and Series Resonance Alternation in Switch-Mode Converters. 2007.
27. **Sten Suuroja.** Comparative Morphological Analysis of the Early Paleozoic Marine Impact Structures Kärkla and Neugrund, Estonia. 2007.
28. **Sergei Sabanov.** Risk Assessment Methods in Estonian Oil Shale Mining Industry. 2008.
29. **Vitali Boiko.** Development and Research of the Traction Asynchronous Multimotor Drive. 2008.
30. **Tauno Tammeoja.** Economic Model of Oil Shale Flows and Cost. 2008.
31. **Jelena Armas.** Quality Criterion of road Lighting Measurement and Exploring. 2008.
32. **Olavi Tammemäe.** Basics for Geotechnical Engineering Explorations Considering Needed Legal Changes. 2008.
33. **Mart Landsberg.** Long-Term Capacity Planning and Feasibility of Nuclear Power in Estonia under Certain Conditions. 2008.
34. **Hardi Torn.** Engineering-Geological Modelling of the Sillamäe Radioactive Tailings Pond Area. 2008.
35. **Aleksander Kilk.** Paljupooluseline püsomagnetitega sünkroongeneraator tuuleagregaatidele. 2008.
36. **Olga Ruban.** Analysis and Development of the PLC Control System with the Distributed I/Os. 2008.
37. **Jako Kilter.** Monitoring of Electrical Distribution Network Operation. 2009.
38. **Ivo Palu.** Impact of Wind Parks on Power System Containing Thermal Power Plants. 2009.

39. **Hannes Agabus**. Large-Scale Integration of Wind Energy into the Power System Considering the Uncertainty Information. 2009.
40. **Kalle Kilk**. Variations of Power Demand and Wind Power Generation and Their Influence to the Operation of Power Systems. 2009.
41. **Indrek Roasto**. Research and Development of Digital Control Systems and Algorithms for High Power, High Voltage Isolated DC/DC Converters. 2009.
42. **Hardi Hõimoja**. Energiatõhususe hindamise ja energiasalvestite arvutuse meetoodika linna elektertranspordile. 2009.
43. **Tanel Jalakas**. Research and Development of High-Power High-Voltage DC/dC Converters. 2010.
44. **Helena Lind**. Groundwater Flow Model of the Western Part of the Estonian Oil Shale Deposit. 2010.
45. **Arvi Hamburg**. Analysis of Energy Development Perspectives. 2010.
46. **Mall Orru**. Dependence of Estonian Peat Deposit Properties on Landscape Types and Feeding Conditions. 2010.
47. **Erik Väli**. Best Available Technology for the Environmentally Friendly Mining with Surface Miner. 2011.
48. **Tarmo Tohver**. Utilization of Waste Rock from Oil Shale Mining. 2011.